

THE UNIVERSITY OF CALGARY

Kinetics of Gas Hydrate Formation: Particle Size Measurements

by

Saurabh Sharma

A THESIS

SUBMITTED TO THE FACULTY OF GRADUATE STUDIES

IN PARTIAL FULFILMENT OF THE REQUIREMENTS FOR THE
DEGREE OF MASTER OF SCIENCE IN CHEMICAL ENGINEERING

DEPARTMENT OF CHEMICAL AND PETROLEUM ENGINEERING

CALGARY, ALBERTA

AUGUST, 1996

© Saurabh Sharma 1996

THE UNIVERSITY OF CALGARY
FACULTY OF GRADUATE STUDIES

The undersigned certify that they have read, and recommend to the Faculty of Graduate Studies for acceptance, a thesis entitled "Kinetics of Gas Hydrate Formation: Particle Size Measurements" submitted by Saurabh Sharma in partial fulfilment of the requirements for the degree of Master of Science in Chemical Engineering.



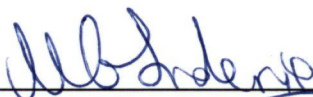
Dr. P.R. Bishnoi, Supervisor/Committee Chairperson

Department of Chemical and Petroleum Engineering



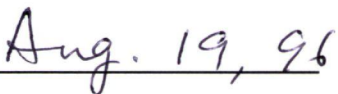
Dr. A.K. Mehrotra

Department of Chemical and Petroleum Engineering



Dr. M.G. Sideris

Department of Geomatics Engineering



Date

ABSTRACT

Natural gas hydrates present a huge future hydrocarbon resource which can be commercially exploited under right economic environment. Development of new technologies based on hydrates, requires comprehensive understanding of hydrate formation and decomposition kinetics. A high pressure experimental apparatus, which incorporates a laser particle analyzer, was designed and used for particle size measurements of ethane and methane gas hydrates. The data are reported at temperatures ranging from 274 to 278 K and pressures up to 4.93 MPa. Particle size distributions were found to be log-normal, with the minimum particle size well below 600 μm . The Englezos et al. (1987) model for hydrate formation kinetics is adopted and the combined rate parameter, K^* , is determined using experimentally obtained data on particle size distribution. For ethane and methane hydrates, the experimentally determined values of K^* are 0.2 and 0.1 ($\text{mol}/\text{m}^2 \cdot \text{s} \cdot \text{MPa}$), respectively.

ACKNOWLEDGEMENTS

The author wishes to express his gratitude to Dr. P.R. Bishnoi for his supervision, guidance, and support throughout the course of this project.

The author wishes to thank Dr. A.K. Mehrotra for many helpful comments and suggestions and Mahendra Malegaonkar for unflagging support.

Financial support from NSERC and the Department of Chemical & Petroleum Engineering is greatly appreciated.

The assistance in preparing the experimental apparatus, provided by Mr. Derek Verhegge is appreciated.

This work is dedicated to Dr. P. Khastgir and
my father, mother, brother and bhabhi.

TABLE OF CONTENTS

Approval Page	ii
Abstract	iii
Acknowledgements	iv
Dedication	v
Table of Contents	vi
List of Tables	ix
List of Figures	x
Nomenclature	xvi
Chapter 1 Introduction	1
1.1 Gas Hydrates	1
1.2 Scope of the Work	9
Chapter 2 Experimental Apparatus and Procedure	11
2.1 The Reactor Setup	11
2.2 The Laser Particle Analyzer	13
2.3 The Particle Size Analyzer Circuit	16
2.4 The High Pressure Microflow Cell	18
2.5 Procedure	18
2.6 Ruska Pump Experiment	23
Chapter 3 The Englezos et al. (1987) Model	25

Chapter 4 Experimental Results	33
4.1 Experiments Conducted	33
4.2 The Gas Consumption Curve	38
4.3 Laser Particle Analyzer Results	40
4.3.1 Particle Number Density	40
4.3.2 Particle Area Density	41
4.3.3 Particle Volume Density	41
4.3.4 Distribution of Number Density	41
4.3.5 Distribution of Area Density	51
4.3.6 Distribution of Volume Density	51
4.3.7 Second Moment of Particle Size Distribution	65
4.3.8 Gas Consumption in Hydrate Formation	66
4.3.9 Median Particle Size	66
 Chapter 5 Discussion of Results	 72
5.1 Particle Size and Hydrodynamics	72
5.2 Extrapolation of Data	73
5.3 Mole Balance and Shape Factor	82
5.4 Least Squares Estimation of K^*	98
 Chapter 6 Conclusions and Recommendations	 108
6.1 Conclusions	108

6.2 Recommendations	109
Bibliography	110
Appendix A	115
Appendix B	124
Appendix C	149
Appendix D	157
Appendix E	169

LIST OF TABLES

Table 1.1 Physical Properties of Hydrate Lattices	3
Table 4.1 List of Experiments Conducted for Ethane at 274 K	34
Table 4.2 List of Experiments Conducted for Ethane at 276 K	34
Table 4.3 List of Experiments Conducted for Ethane at 278 K	35
Table 4.4 List of Experiments Conducted for Methane at 278 K	36
Table 4.5 List of Experiments Conducted for Methane at 276 K	36
Table 4.6 List of Experiments Conducted for Methane at 274 K	37
Table 5.1 Particle Number, Area and Volume Density (%), (E007)	91
Table 5.2 Particle Number, Area and Volume Density (%), (E009)	92
Table 5.3 Particle Number, Area and Volume Density (%), (M014)	93
Table 5.4 Particle Number, Area and Volume Density (%), (M015)	94
Table 5.5 Kinetic Parameter (K^*) for Ethane Hydrate Formation & Sensitivity Analysis	102
Table 5.6 Kinetic Parameter (K^*) for Methane Hydrate Formation & Sensitivity Analysis	102
Table 5.7 Kinetic Parameter (K^*) for Ethane Hydrate Formation & Error Analysis	104
Table 5.8 Kinetic Parameter (K^*) for Methane Hydrate Formation & Error Analysis	104
Table 5.9 Average (K^*) for Ethane and Methane Hydrate Formation	106
Table 5.10 K^* (Englezos) for Ethane Hydrate Formation	107
Table 5.11 K^* (Englezos) for Methane Hydrate Formation	107
Table B1 Second Moment, μ_2 (cm ² /mL), as a Function of Time, t, (min)	148

LIST OF FIGURES

Figure 1.1	Structures of Gas Hydrates	2
Figure 1.2	Phase Diagram for Single Gas Hydrate Formation.	4
Figure 2.1	Experimental Setup.	12
Figure 2.2	Laser Particle Analyzer.	15
Figure 2.3	Particle Analyzer Circuit.	17
Figure 2.4	High Pressure Microflow Cell.	19
Figure 2.5	Partial Three Phase (Gas-Liquid Water-Solid Hydrate) Equilibrium Diagrams for: (a) Ethane-Water (b) Methane-Water Systems.	20
Figure 4.1	Gas Consumption Curve for Ethane.	39
Figure 4.2	Particle Number Density, $N(\#/m^3)$, vs Time (min).	42
Figure 4.3	Particle Area Density, $A(m^2/m^3)$, vs Time (min).	43
Figure 4.4	Particle Volume Density, $V(m^3/m^3)$, vs Time (min).	44
Figure 4.5	Distribution of Particle Number Density, $N(\#/m^3)$, with Size (μm).	45
Figure 4.6	Distribution of Particle Number Density, $N(\#/m^3)$, with Size (μm).	46
Figure 4.7	Distribution of Particle Number Density, $N(\#/m^3)$, with Size (μm).	47
Figure 4.8	Distribution of Particle Number Density, $N(\#/m^3)$, with Size (μm).	48
Figure 4.9	Distribution of Particle Number Density, $N(\#/m^3)$, with Size (μm).	49

Figure 4.10	Distribution of Particle Number Density, $N(\#/m^3)$, with Size (μm).	50
Figure 4.11	Log-Normal Fit through the Distribution of Particle Number Density, $N(\#/m^3)$, with Size (μm) ("dots" indicate raw data obtained at time=33 min).	52
Figure 4.12	Distribution of Particle Area Density, $A(m^2/m^3)$, with Size (μm).	53
Figure 4.13	Distribution of Particle Area Density, $A(m^2/m^3)$, with Size (μm).	54
Figure 4.14	Distribution of Particle Area Density, $A(m^2/m^3)$, with Size (μm).	55
Figure 4.15	Distribution of Particle Area Density, $A(m^2/m^3)$, with Size (μm).	56
Figure 4.16	Distribution of Particle Area Density, $A(m^2/m^3)$, with Size (μm).	57
Figure 4.17	Distribution of Particle Area Density, $A(m^2/m^3)$, with Size (μm).	58
Figure 4.18	Distribution of Particle Volume Density, $V(m^3/m^3)$, with Size (μm).	59
Figure 4.19	Distribution of Particle Volume Density, $V(m^3/m^3)$, with Size (μm).	60
Figure 4.20	Distribution of Particle Volume Density, $V(m^3/m^3)$, with Size (μm).	61
Figure 4.21	Distribution of Particle Volume Density, $V(m^3/m^3)$, with Size (μm).	62
Figure 4.22	Distribution of Particle Volume Density, $V(m^3/m^3)$, with Size (μm).	63
Figure 4.23	Distribution of Particle Volume Density, $V(m^3/m^3)$, with Size (μm).	64

Figure 4.24	Second Moment of Particle Size Distribution, μ_2 (m^2/m^3), vs Time (min).	67
Figure 4.25	Gas Moles Consumed for Hydrate Formation vs Time (min) ("dots" indicate data points. A straight line is regressed through the data).	68
Figure 4.26	Gas Moles Consumed for Hydrate Formation vs Time (min) ("D": DORIC and "P": Analyzer. "Dots" indicate data points).	69
Figure 4.27	Median Particle Size or Diameter (μm) vs Time (min).	70
Figure 5.1	Cumulative Number Density Oversize ($\#/\text{m}^3$) vs Size (μm)	76
Figure 5.2	Cumulative Number Density Oversize ($\#/\text{m}^3$) vs Size (μm).	77
Figure 5.3	Distribution of Particle Number Density, N (%), with Size (μm).	78
Figure 5.4	Distribution of Particle Number Density, N (%), with Size (μm).	79
Figure 5.5	Distribution of Particle Number Density, N (%), with Size (μm).	80
Figure 5.6	Distribution of Particle Number Density, N (%), with Size (μm).	81
Figure 5.7	Distribution of Particle Area Density, A (%), with Size (μm).	83
Figure 5.8	Distribution of Particle Area Density, A (%), with Size (μm).	84
Figure 5.9	Distribution of Particle Area Density, A (%), with Size (μm).	85
Figure 5.10	Distribution of Particle Area Density, A (%), with Size (μm).	86
Figure 5.11	Distribution of Particle Volume Density, V (%), with Size (μm).	87

Figure 5.12	Distribution of Particle Volume Density, V (%), with Size (μm).	88
Figure 5.13	Distribution of Particle Volume Density, V (%), with Size (μm).	89
Figure 5.14	Distribution of Particle Volume Density, V (%), with Size (μm).	90
Figure 5.15	Gas Moles Consumed for Hydrate Formation, M (mol), vs Time (min) ("bold": DORIC; "dots": Analyzer) (Expt. E007-a, E009-b, E011-c, E016-d, E019-e).	96
Figure 5.16	Gas Moles Consumed for Hydrate Formation, M (mol), vs Time (min) ("bold": DORIC; "dots": Analyzer) (Expt. M014-a, M015-b, M011-c, M012-d, M004-e, M005-f).	97
Figure 5.17	Gas Moles Consumed for Hydrate Formation, n (mol), vs Time (min) ("bold": Experimental; "dots": Predicted) (Expt. E007-a, E009-b, E011-c, E016-d, E019-e).	99
Figure 5.18	Gas Moles Consumed for Hydrate Formation, n (mol), vs Time (min) ("bold": Experimental; "dots": Predicted) (Expt. M014-a, M015-b, M011-c, M012-d , M004-e, M005-f).	100
Figure 5.19	Sensitivity Analysis of K^* .	103
Figure A-1	Gas Moles Consumed, n (mol), vs Time (min) (Expt. E006-a, E008-b, E014-c, E018-d, E020-e, E021-f).	118
Figure A-2	Gas Moles Consumed, n (mol), vs Time (min) (Expt. M016-a, M017-b, M010-c, M013-d, M007-e, M008-f).	119
Figure A-3	Gas Moles Consumed, n (mol), vs Time (min) (Expt. E007-a, E009-b, E011-c, E016-d, E019-e).	120
Figure A-4	Gas Moles Consumed, n (mol), vs Time (min) (Expt. M014-a, M015-b, M011-c, M012-d, M004-e, M005-f).	121
Figure B-1	Experiment E009.	126
Figure B-2	Experiment E011.	127

Figure B-3	Experiment E016.	128
Figure B-4	Experiment E019.	129
Figure B-5	Experiment M004.	130
Figure B-6	Experiment M005.	131
Figure B-7	Experiment M011.	132
Figure B-8	Experiment M012.	133
Figure B-9	Experiment M014.	134
Figure B-10	Experiment M015.	135
Figure B-11	Distribution of Particle Number Density, N (%), with Size (μm).	136
Figure B-12	Distribution of Particle Number Density, N (%), with Size (μm).	137
Figure B-13	Distribution of Particle Number Density, N (%), with Size (μm).	138
Figure B-14	Distribution of Particle Number Density, N (%), with Size (μm).	139
Figure B-15	Distribution of Particle Area Density, A (%), with Size (μm).	140
Figure B-16	Distribution of Particle Area Density, A (%), with Size (μm).	141
Figure B-17	Distribution of Particle Area Density, A (%), with Size (μm).	142
Figure B-18	Distribution of Particle Area Density, A (%), with Size (μm).	143
Figure B-19	Distribution of Particle Volume Density, V (%), with Size (μm).	144

Figure B-20	Distribution of Particle Volume Density, V (%), with Size (μm).	145
Figure B-21	Distribution of Particle Volume Density, V (%), with Size (μm).	146
Figure B-22	Distribution of Particle Volume Density, V (%), with Size (μm).	147
Figure C-1	Cumulative Number Density Undersize Plot Y axis: Cumulative Number Smaller than Stated Size, % X axis: Particle Diameter or Size.	152
Figure C-2	Cumulative Number Density Oversize Plot Y axis: Cumulative Number Larger than Stated Size, % X axis: Particle Diameter or Size.	153
Figure C-3	Number Density Distribution Plot Y axis: Number Per cent per Micron X axis: Particle Diameter or Size.	154

NOMENCLATURE

$a=$	Interfacial Area per unit of Liquid Volume (m^2/m^3)
$A=$	Particle Area Density (m^2/m^3)
$A_{(g-l)}=$	Gas-Liquid Interfacial Area (m^2)
$A_p=$	Surface Area of a Particle (m^2)
$c=$	Concentration Gas in Liquid Water (mol/m^3)
$c_{w0}=$	Initial Concentration of Water Molecules (mol/m^3)
$D=$	Diffusivity of the Gas (m^2/s)
$f=$	Gas Fugacity (MPa)
$H=$	Henry's Constant (MPa)
$J=$	Molar Flux ($\text{mol}/\text{m}^2.\text{s}$)
$k_d=$	Mass Transfer Coefficient Around a Particle ($\text{mol}/\text{m}^2.\text{s.MPa}$)
$k_L=$	Liquid Phase Mass Transfer Coefficient (m/s)
$k_r=$	"Reaction" rate constant ($\text{mol}/\text{m}^2.\text{s.MPa}$)
$K=$	$\pi \mu_2 K^*$
$K^*=$	Combined Rate Parameter ($\text{mol}/\text{m}^2.\text{s.MPa}$)
$L=$	Distance between Interface and bottom of Reactor (m)
$M=$	Gas Moles Hydrated (mol)
$M_w=$	Molar Mass of Hydrate (gm)
$n=$	Moles of Gas Consumed (mol)
$n_{eq}=$	Moles of Gas Dissolved at Three Phase Equilibrium (mol)
$n^*=$	Solubility of Gas in Liquid Water (mol)

n_{tb} = Moles of Gas Dissolved at Turbidity Point (mol)

n_w = Moles of Water per Gas Molecule (mol)

n_{mw} = Moles of Water

N = Particle Number Density ($\#/m^3$)

P = Pressure (MPa)

PSD= Particle Size Distribution

r = Particle Radius (m)

r_{cr} = Critical Radius of Nucleus (m)

R = Universal Gas Constant (MPa.m³/mol.K)

$R_y(t)$ = Global Reaction Rate (mol/m³.s)

SM= Second Moment $,(\mu_2),(m^2/m^3)$

T = Temperature (K)

t = Time (s)

v_m = Molar Volume of Hydrate (m³/mol)

v_w = Molar Volume of Water (m³/mol)

V = Particle Volume Density (m³/m³)

V_L = Volume of Liquid Phase (m³)

V_P = Volume of a Particle (m³)

V_R = Gas Phase Volume of Reactor (m³)

V_S = Supply Reservoir Volume (m³)

x = Particle Size ,(diameter),(μm)

x_m = Mole Fraction of Gas in Liquid

y = Distance from Gas-Liquid Interface (m)

y_L = Film Thickness (m)

z = Compressibility Factor

Greek Symbols

ΔG = Free Energy (J)

ΔG_V = Free Energy Change Due to Formation of a New Phase (J)

ΔG_S = Free Energy Change Due to Formation of a Boundary (J)

Δg = Free Energy Change per unit Volume of Product (J/m³)

Δf = Driving Force (MPa)

$\phi(x)$ = Number Distribution Function (#/m⁴)

$\phi(x,t)$ =Number Distribution Function with Time (#/m⁴)

μ_n = n^{th} Moment of the Particle Size Distribution

μ_2 = Second Moment of Particle Size Distribution, (SM), (m²/m³)

α = Volume Shape Factor

β = Surface Shape Factor

γ = Hatta Number

ρ = Hydrate Density (Kg/m³)

σ = Surface Energy for the System Hydrate-Water (J/m²)

Subscripts

a = Initial Equilibrium State for the Ruska Pump Experiment

avg= Average
b= Liquid Phase Bulk
cr= Critical
d= Diffusion
e= Final Equilibrium State for Ruska Pump Experiment
eq= Three Phase Equilibrium Condition
exp= Experimental Conditions
g= Gas Phase
i= Particle Solution Interface
j= Gaseous Component
0= Time,0
t= Time,t
p= Particle
r= "Reaction"
R= Reactor
S= Supply Reservoir
w= Water

1.0 INTRODUCTION

1.1 Gas Hydrates

Gas hydrates are crystalline compounds which belong to a group of solids called clathrate. They are formed from mixtures of water and low molar mass gases at high pressures and low temperatures. Through hydrogen bonding, water molecules form a framework containing relatively large cavities which can be occupied by certain gas molecules with molecular diameters less than the diameter of the cavity. The framework, by itself thermodynamically unstable, is stabilized by the inclusion of the gaseous component. In the 1940's and 1950's, von Stackelberg and co-workers performed X-ray diffraction experiments on hydrates. The interpretation of these diffraction experiments (von Stackelberg and Muller, 1949, 1951 a,b) led to the determination of two hydrate Structures, I and II. Recently, a new structure, Structure H, has been discovered (Ripmeester et al., 1987, 1990; Hutz^a and Englezos, 1996).

Both Structures I and II have cubic unit cells. Structure I has a unit crystal structure of a body-centred cubic while Structure II is a diamond lattice (Figure 1.1). Ethane, methane and their mixtures are known to form Structure I hydrates. The number and size of the cavities differ for the two structures; however, in both cases, the water molecules are tetrahedrally coordinated as in ordinary ice, and the hydrate forming gases are linked to the water lattice by van der Waals forces. Table 1.1 (Holder et al., 1988) provides the general properties of the hydrate lattices. Detailed information on the structure of gas hydrates can be found in the literature (Holder, 1988; Sloan, 1991a). Figure 1.2 is a schematic of the partial phase diagram for a condensable single gas hydrate former and water system.

Formation of gas hydrates can cause plugging of gas transportation lines, jeopardize the foundation of deepwater platforms and pipelines, foul process heat exchangers, valves, expanders, plug blowout preventers, etc. and, therefore, can cause major problems in the oil and gas industry. Prevention of the formation, as well as proper design of the production and

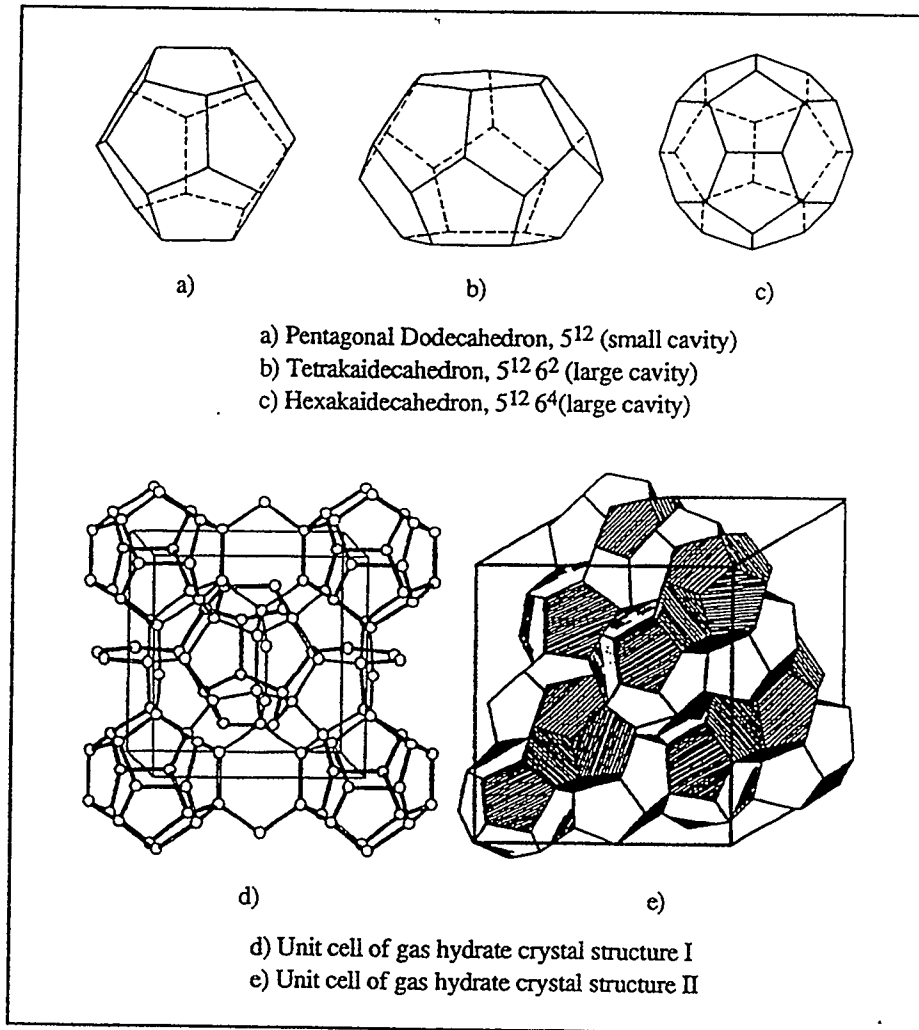


Figure 1.1 Structures of Gas Hydrates
 (von Stackelberg and Muller, 1949, 1951a,b).

	Structure 1	Structure 2
Unit Cell Size (Å)	12.03	17.31
Number of Cavities per Unit Cell	2 Small Cavities 6 Large Cavities	16 Small Cavities 8 Large Cavities
Diameter of Cavities (Å)		
Small	7.88	7.82
Large	8.60	9.46
Number of Molecules of Water per Unit Cell	46	136
Typical Hydrate Forming Gases	Methane, Ethane, Ethylene, Carbon Dioxide	Propane, Propylene, I-Butane

Table 1.1 Physical Properties of Hydrate Lattices

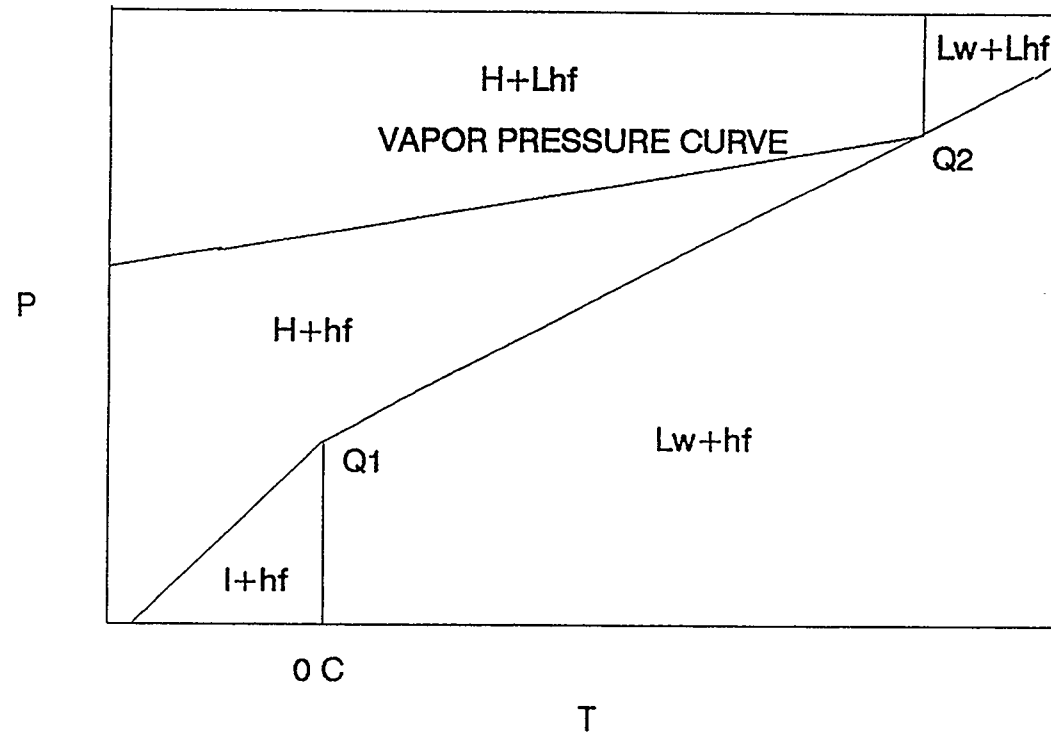


Figure 1.2 Partial Phase Equilibrium Diagram for a Condensable Single Gas Hydrate Former (Excess) and Water (Q1 & Q2: Quadruple Points; Lw: Liquid Water; I: Ice; hf: Hydrate Former (Gas); Lhf: Hydrate Former (Liquid); H: Hydrate).

processing facilities in the oil and gas industry, requires a comprehensive understanding of the formation and decomposition kinetics of hydrates. Such information can also be useful in possible future industrial applications, such as manufacture of pharmaceuticals, water desalination, gas separation, gas storage, etc.

Apart from this, natural gas hydrates present a huge future hydrocarbon resource which can be commercially exploited given the right economic environment. Conservative estimates indicate that there is twice as much energy in hydrated form as in all other hydrocarbon sources combined (1 m³ of hydrates may contain as much as 184 m³ (STP) of gas) (Sloan,1991b).

Thermodynamic analysis of the behaviour of gas hydrates has been done extensively by several researchers. van der Waals and Platteeuw (1959) were the first to use the Langmuir type adsorption theory for the prediction of gas hydrate equilibria. A numerical procedure based on their model to calculate hydrate formation conditions from gaseous mixtures, was proposed by Parrish and Prausnitz (1972). This procedure was improved by Ng and Robinson (1976) and later by John and Holder (1985). Extensive work for predicting gas hydrate equilibrium has been done by Holder et al. (1980) and Bishnoi et al. (1989) and summarized by Makogan (1981) and Sloan (1991a). Extensive work has also been done for predicting hydrate equilibrium in presence of inhibitors such as methanol (Englezos et al.,1991; Anderson and Prausnitz,1986) and electrolytes (Dholabhai et al.,1991,1994; Englezos and Bishnoi,1988; Tse and Bishnoi,1994).

Although the thermodynamics of gas hydrates have been studied extensively for several decades, the kinetics of the formation have only recently been investigated.

A few models have been proposed in the literature for the kinetics of gas hydrate formation. Some of these are described below.

(a) Vysniauskas and Bishnoi model

Vysniauskas and Bishnoi (1983) performed experimental studies of the kinetics of methane hydrate formation and proposed a semi-empirical model to correlate the experimental data. They postulated that the gas hydrate formation from liquid water undergoes a three body addition process (gas and water molecules and cluster) yielding an overall third-order effect of pressure on the reaction rate. Their model consists of three steps: an initial clustering process, formation of a critical cluster (nucleus), and growth of the hydrate crystal around the stable nucleus. The model is based on the assumption that the hydrate formation starts with nucleation at the gas-water interface and subsequent growth of the hydrate crystal around the formed nucleus. Vysniauskas and Bishnoi considered the reaction rate to depend on the concentrations of the critical size clusters and monomers of water and methane at the gas-water interface, and the total area of the water-gas interface.

(b) Englezos et al. model

Based on crystallization and two-film theory, Englezos et al. (1987) developed a mechanistic model for the kinetics of the formation of methane and ethane gas hydrates. In the model, the nucleation and growth processes are coupled with the transport processes in order to describe the over-all reaction. Experimental data were used to determine an adjustable parameter in the model. Englezos and co-workers' model for the growth of hydrate crystals is based on the assumption that the hydrate particle is surrounded by a laminar diffusion layer. Gas dissolved in the bulk of the solution diffuses to the crystal-liquid interface of the hydrate particle through this boundary layer and is incorporated into the framework of the structured water at the interface, thus stabilizing the hydrate lattice.

(c) Sloan et al. model for hydrate nucleation from ice

Sloan and Fleyfel proposed a new hypothesis to describe the molecular mechanism for gas

hydrate nucleation from ice (Sloan, 1990; Sloan and Fleyfel, 1991). The model consists of the following four steps:

- (i) Initially the ice and gas phases are separated by a thin film of water. Through molecular transitions the basic hydrate cavity (5^{12}) is formed within the liquid film at the ice interface.
- (ii) Cavities may link either through vertices to form hydrate of Structure I or through face-sharing to form hydrate of Structure II.
- (iii) Unit crystals of either structure are formed which combine with other unit crystals.
- (iv) Crystals with sizes larger than the critical size are formed. Once the crystals have grown beyond the critical size the primary nucleation period ends with the start of monotonic growth of the crystals.

(d) Muller-Bongartz model for hydrate nucleation from water

In 1992 a hypothesis for the primary nucleation of gas hydrates from water on a molecular level was developed by Muller-Bongartz et al. (1992). The hypothesis is an extension of that proposed by Sloan and Fleyfel (1991) for the formation of hydrate from ice.

(e) Lekvam and Ruoff model

One of the most recent kinetic models is that of Lekvam and Ruoff (1993). They proposed that the formation and growth of methane hydrate could be described as an autocatalytic process. Their model is divided into 5 pseudo-elementary processes with the following three dynamic elements.

- (i) Dissolution of methane gas into the water phase,
- (ii) the build-up of a precursor of methane hydrate, and
- (iii) growth of methane hydrate by an auto-catalytic process.

(f) Christiansen and Sloan model

Christiansen and Sloan (1993) have recently proposed a molecular mechanism for hydrate formation based on the following four components:

- (i) Labile clusters exist around dissolved apolar molecules;
- (ii) hydrate formation consists of joining these clusters together;
- (iii) clusters can transform from one coordination number to another upon joining;
- (iv) while cubic structure I has no distinguishing alternatives for joining hexagonal faces, cubic structure II has two alternatives, which leads to competing structures and slows hydrate nucleation and growth.

(g) Parent and Bishnoi model

Parent and Bishnoi (1996) studied hydrate nucleation by conducting a series of light scattering experiments. From their results they concluded that the "Thermal History of Water" and "Agitation Effects" were two other factors that influenced the nucleation phenomenon.

(h) Natarajan and Bishnoi model

Natarajan and Bishnoi (1996) focussed on the various perspectives of the kinetic processes at a conceptual level. They viewed hydrate nucleation as an intrinsically stochastic process that involves the formation and growth of gas-water clusters to critical sized, stable hydrate nuclei. Hydrate growth process involves the growth of stable hydrate nuclei as solid hydrates.

All models have their limitations. The Vysniauskas-Bishnoi model is semi-empirical in

nature. The Sloan, the Muller-Bongartz and the Christiansen and Sloan models propose a molecular mechanism of the hydrate nucleation process. The available information on hydrate nucleation is at a macroscopic level and very little is known experimentally about the sub-critical nuclei in solution. In order to accomplish modelling at a molecular level, the mechanism of hydrate nucleation needs to be experimentally studied and understood first. The Lekvam and Ruoff model does not impose the stability of the hydrate nuclei. It is well known (Makogan, 1981) that gas hydrate formation is a crystallization phenomenon. The mechanistic model of Englezos et al. views hydrate formation and growth as a crystallization process. These authors have successfully applied the model to ethane and methane gas hydrate formation as well as to their mixtures. Recently, the model has been extended by Dholabhai et al. (1993) to electrolyte solutions as well. Monford and Nzihou (1993) have adopted the Englezos et al. model for studying propane gas hydrate kinetics. Thus, this model has proved to be the most widely accepted and versatile in describing the kinetics of gas hydrate formation.

1.2 Scope of the Work

In this work experiments have been performed with ethane and methane and the collected data are used to evaluate K^* , the rate constant for hydrate growth in the Englezos et al. (1987) model for the kinetics of gas hydrate formation. The model employs the Kane et al. (1974) model for crystal growth to estimate μ_2 , the second moment of particle size distribution. Second moment of the distribution is a measure of the surface area of the hydrate particles. The authors suggest that experimental data for particle size distribution should be obtained in future for the estimation of K^* . In this work, experimental data for μ_2 has been obtained using a Helium-Neon laser particle size analyzer. The experimental data are then used for evaluating K^* , the rate constant for hydrate particle growth.

Experiments for ethane as well as methane were performed at 274, 276 and 278 K and at pressures approximately five bars for ethane and ten bars for methane above their three

phase equilibrium pressures. The experimental data were collected under isothermal and isobaric conditions at a stirring rate of 400 rpm. The data have been collected by contacting the gases with liquid water in a semi-batch stirred tank reactor. An experimental setup consisting of the laser analyzer, a microflow cell, a reciprocating pump and a concentric tube cooling system was designed and integrated with the modified (Englezos et al., 1987) experimental apparatus of Vysniauskas and Bishnoi (1983). The high pressure microflow cell of Nielsen (1993) was used in the analyzer in this work. The cell required additional focussing.

2.0 EXPERIMENTAL APPARATUS AND PROCEDURE

2.1 The Reactor Setup

A short description of the modified (Englezos et al. 1987) apparatus of Vysniauskas (1983) is given below.

The schematic of the reactor equipment setup is shown in Figure 2.1. It consists of a semi-batch stirred tank reactor with a temperature and pressure control system, a variable volume reservoir R1 which supplies gas to the reactor, and the equipment for data acquisition. Another reservoir, R2, is used as a reference reservoir in order to have accurate pressure measurements of the reservoir R1.

Both the reservoirs and the reactor are immersed in an insulated glycol bath. Cooling of the reactor and the reservoirs is provided by circulating refrigerant glycol from a 0.189 m³ temperature controlled bath. Agitation of the water in the reactor is accomplished by coupling a magnetic stir bar within the reactor with a rotating magnet mounted outside. The magnet is driven by a DC motor whose speed is regulated by an rpm controller. Stainless steel baffles are installed within the reactor in order to avoid the formation of vortices. A micro computer is used for direct data acquisition of the process temperatures and pressures, and to perform on line calculations of the gas consumption during an experiment. The Trebble-Bishnoi equation of state is used for the calculations of gas moles consumed.

Ultra-high purity grade methane and high purity ethane gases, supplied by Praxair, were used. The water was deionized and double-distilled.

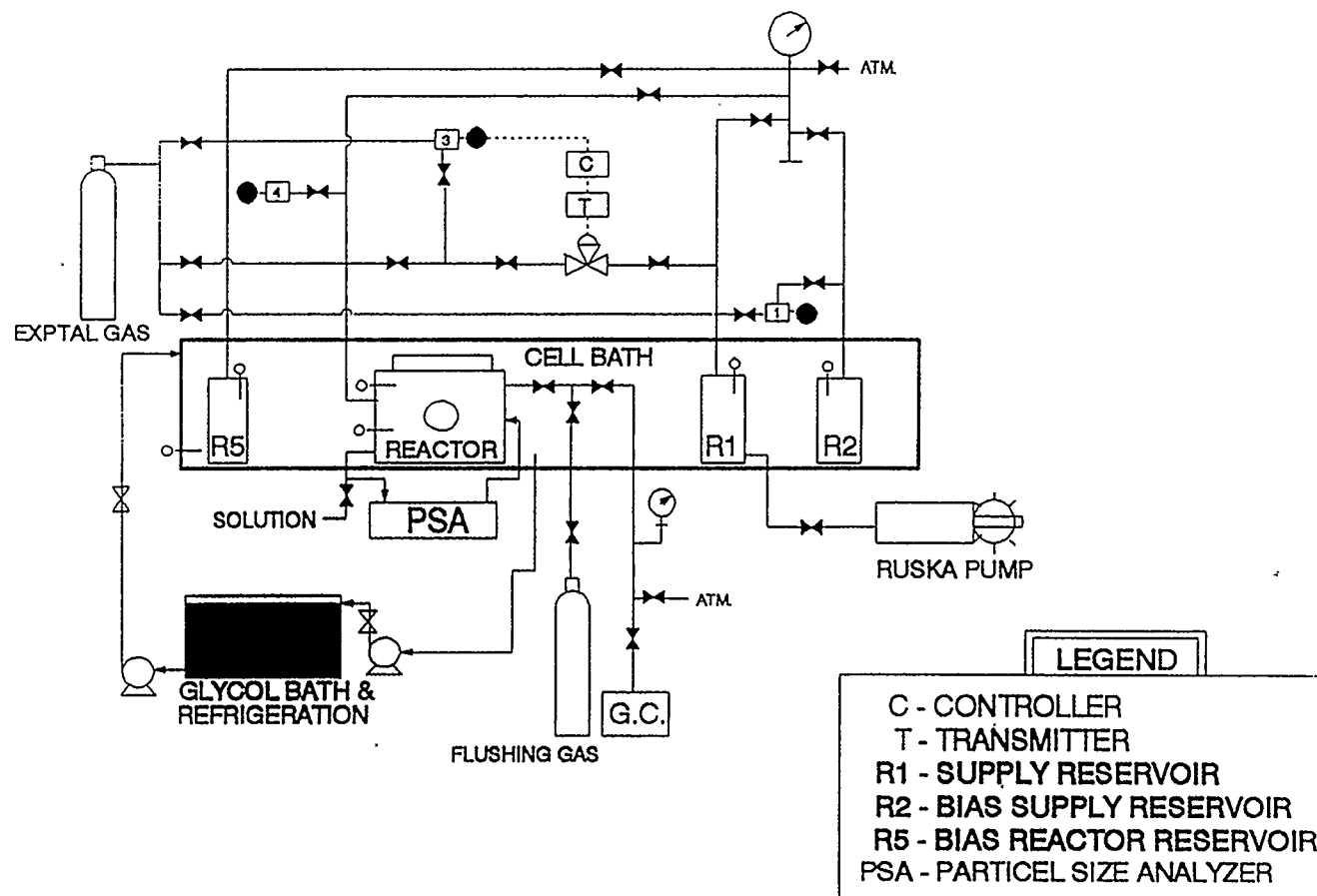


Figure 2.1 Experimental Setup

The errors in the pressure readings of the differential pressure transducers are 0.25% of the span which results in 0.0125 bar error. The error in the Heise pressure gauge is 0.25 bar and the error in all temperature readings is less than 0.1 °C.

2.2 The Laser Particle Analyzer

The heart of the experimental apparatus for this study is a Brinkmann (Galai) 2010 laser particle analyzer. The analyzer is driven by a micro computer that executes the software and controls the collection of data. The basic concepts behind the operation of the analyzer are as follows.

A fine, low-energy red beam is emitted by a Helium/Neon laser and focussed through a series of objectives to a rotating wedge prism. The prism spins the laser into a circular, optically defined path and is focused thereafter to a spot smaller than one micron inside the analytical cell. The beam diverges after the cell onto a photodiode, registering a potential measured in millivolts (Karasikov, 1987).

As the scanning radius of the circular path is defined and the rate of rotation of the prism is precisely monitored, the peripheral velocity of the beam may be determined. The basis of the measurement is the measured potential in the photodiode versus time. As the beam hits the first interface of a particle, a discrete, sharp decay of the potential occurs and a lower level is maintained during the transition period. At the second interface, the potential recovers upwards to the initial value, producing a time-based square pulse. The period of this pulse multiplied by the velocity of the beam gives the diameter of the measured particle. It is important to note that the velocity of the beam is easily calculated as both the scanning radius of the circular path of the beam and the rotation of the prism are precisely monitored. Also, the speed of the particle through the sampling region is negligible as compared to the high velocity of the spinning beam (Karasikov, 1987).

After the collection of data for each particle, a proprietary software package supplied by the manufacturer is employed to determine if accurate measurements were made. The laser beam may pass through the diameter of the particle or through a chord. While the former would produce a perfect square pulse, the latter would have a less discreet decay and recovery of the background potential. If this rise and fall is greater than a criterion set in the apparatus, the pulse is edited and the particle ignored from the total sample.

In this apparatus no calibration is required. This is obviously advantageous as both calibration time and possible operational errors are eliminated. However, in order to verify the measuring accuracy of the particle size analyzer, tests were performed in this work on standard polystyrene spheres of diameters 9.64, 19.81, 22.4 and 43.78 μm supplied by Coulter Electronics, Florida, USA. The analyzer results were in good agreement with the suppliers specifications. Figure 2.2 is a schematic of the sampling area where the focussed laser interacts with the particles and is then collected by the photodiode. The Galai Particle Size Analyzer is used to measure particles in the size range 5-600 μm .

Thus, the raw data acquired by the Galai Particle Analyzer is particle size and particle number density ($\#/ \text{mL}$) of each particle size. The particle size and number density together constitute a "Distribution of Particle Number Density with Size". Distributions of particle area and volume density are computed by the software making use of the above raw data (Refer Appendix C). The laser particle analysis measures a mean spherical diameter regardless of shape.

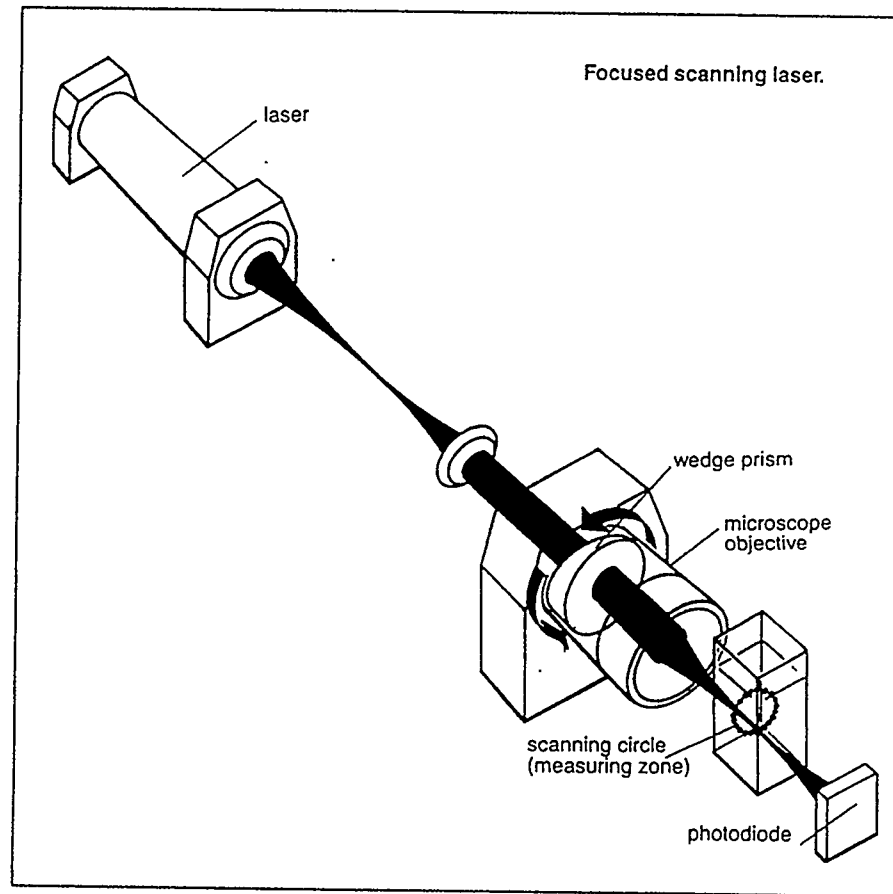


Figure 2.2 Laser Particle Analyzer

2.3 The Particle Size Analyzer Circuit

Figure 2.3 shows the analyzer circuit designed and fabricated in this work. The circuit volume is 19 cm^3 . The slurry of hydrates in liquid water is circulated through the high pressure microflow cell in the analyzer by means of a Gilson 303 reciprocating pump at the rate of 22.5 mL/min . Therefore, the residence time of a particle in the circuit is 50.7 s . The analyzer is located approximately 1 m from the reactor, the entire length of the circuit being about 5 m . Therefore, the time taken by a particle to reach the analyzer from the reactor is one-fifth of the total residence time, i.e, approximately 10 s .

The slurry, as it flows out of the reactor and through the circuit, would gain heat from the ambient causing the hydrates to decompose. To prevent the thermal decomposition of hydrates, the entire circuit is chilled by circulating cooling glycol from the reactor bath through an annular tube cooling arrangement. The hydrate-water slurry flows through the inner tube and the cooling glycol through the outer tube. The reciprocating pump circulating the hydrate-water slurry in the analyzer circuit would cause a pressure drop which if below the three phase equilibrium conditions would cause the hydrates to decompose. Gas bubble formation was observed in the microflow cell for experiments performed very close to the three phase equilibrium conditions. To overcome the decomposition of hydrates, kinetic experiments for ethane were performed approximately 7 bars above the three phase equilibrium conditions and for methane approximately 12 bars above the three phase equilibrium. No gas bubble formation was observed in the microflow cell anymore. Therefore, the thermal and pressure decomposition of hydrates was prevented.

Stainless steel $1/8"$ (OD) tubing was used in the analyzer circuit with an internal diameter of approximately $2200 \text{ }\mu\text{m}$. The magnetic stirring bar in the reactor provided stirring at the rate of 400 rpm which corresponds to approximately $\text{Re}=12,100$ assuming viscosity of hydrate-water slurry as that of water. The turbulence in the reactor can be expected to

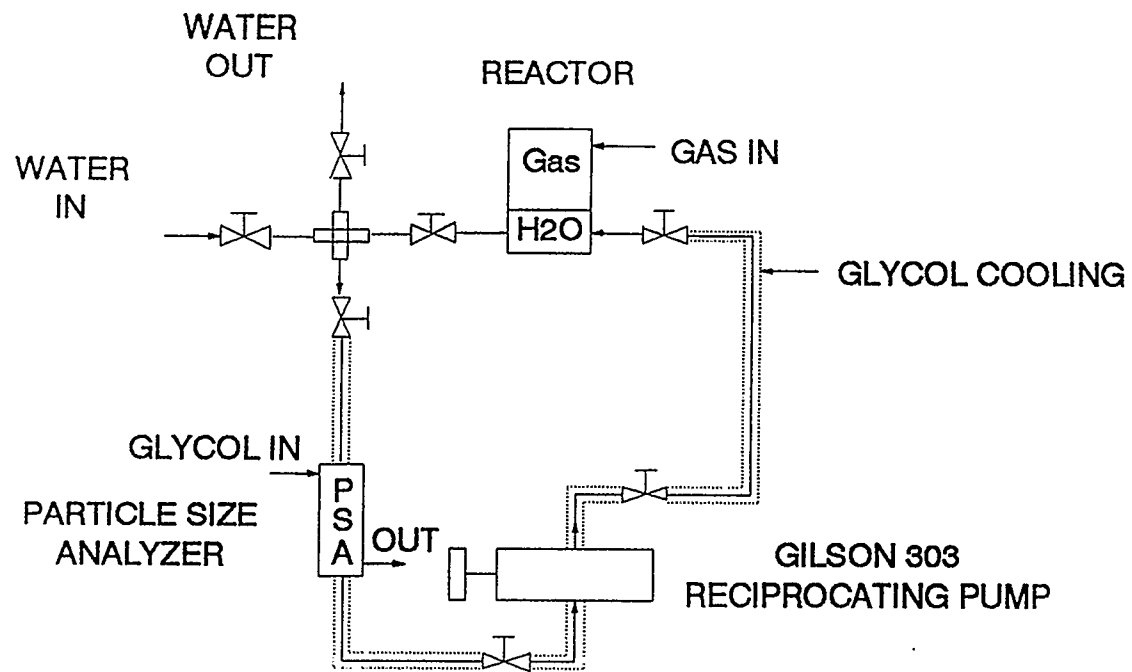


Figure 2.3 Particle Analyzer Circuit

result in an almost uniform hydrate-water concentration in the bulk. Throughout our kinetic experiments for ethane as well as methane, the largest particle size has been well below 600 μm , the maximum measuring ability of the analyzer. Therefore, it can be concluded that the internal diameter of tubing (2200 μm) is sufficient to draw a representative sample of the hydrate-water slurry in the reactor keeping in mind that the largest particles in the slurry are less than 600 μm in size.

2.4 The High Pressure Microflow Cell

The high pressure microflow cell of Neilson (1993) is shown in Figure 2.4. The cell's design pressure is 6 MPa and the material of construction is aluminium. Thick optical quality quartz lenses allow the laser beam to pass through while maintaining the high pressure. The size of the cell necessitated an additional focussing lens to converge the laser beam onto the photodiode. An internal passage in the body of the cell allows a glycol stream to maintain the desired temperature.

2.5 Procedure

Partial phase diagrams for the ethane-water and methane-water systems were computed using a proprietary software (MEGHA). Figure 2.5 shows the diagrams for the systems. All formation experiments were conducted above the three phase equilibrium line. Each experiment corresponds to a particular point on the P-T diagram.

The procedure for a typical experiment is described below and is similar to that followed by Englezos et al. (1987). The reactor and the analyzer circuit are charged with 319 cm^3 of deionized double-distilled water. The reference reservoirs R2 & R5 are pressurized with the hydrate forming gas to a pressure roughly equal to the experimental pressure. The supply reservoir R1 is then pressurized to a pressure of about 5 bars above that in the reference reservoir R2. The temperatures in the reactor and the reservoirs are allowed to

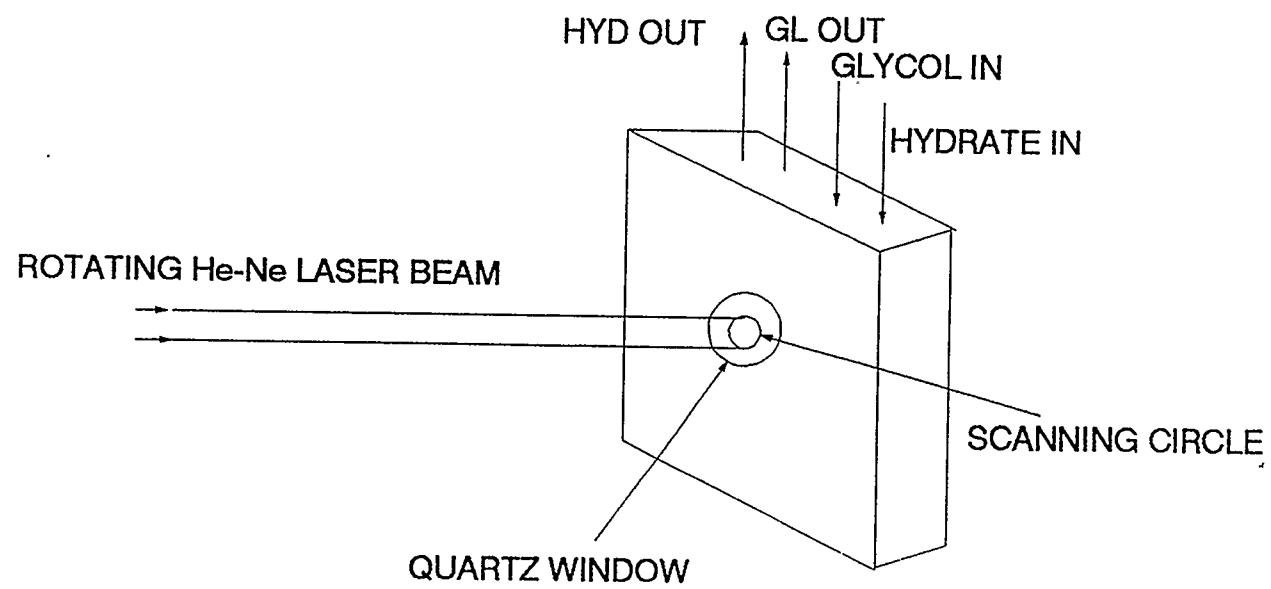


Figure 2.4 High Pressure Microflow Cell.

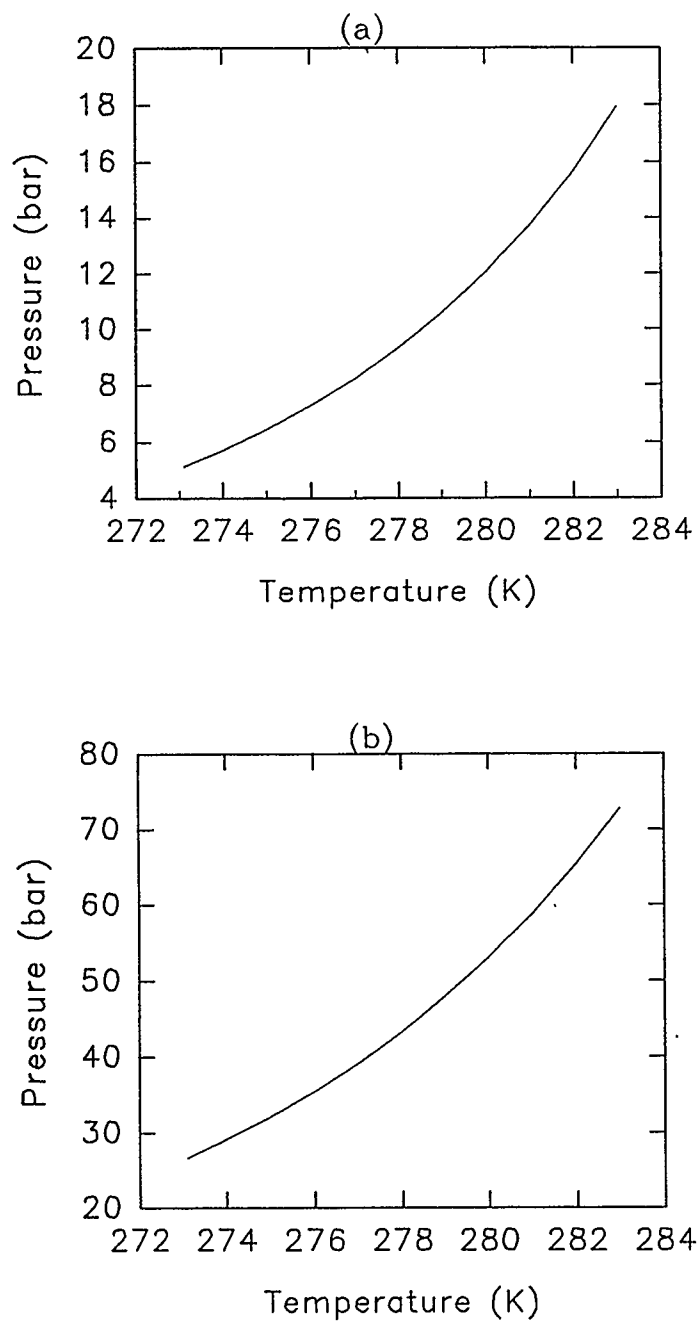


Figure 2.5 Partial Three Phase (Gas-Liquid Water-Solid Hydrate) Equilibrium Diagrams for:
(a) Ethane-Water
(b) Methane-Water Systems.

stabilize and then the reactor is pressurized to the experimental pressure with the gas from the cylinder. After the temperatures have stabilized the reactor is put on automatic control, the stirrer is started and the data acquisition is commenced. As the gas in the reactor is consumed for hydrate formation, additional gas is automatically supplied from reservoir R1 to maintain a constant pressure in the reactor. The reactor contents are watched constantly for the appearance of turbidity in the liquid phase. The turbidity is said to have appeared when the liquid phase becomes translucent due to the emergence of hydrate particles. The time taken to reach the turbidity was typically 30 to 60 minutes. The hydrate formation is continued until about 40 minutes after turbidity.

The major change in the procedure is due to the particle analyzer. The analyzer circuit is charged with fresh deionized double-distilled water before commencing an experiment. The laser gun is powered and the analyzer data acquisition software loaded and set on "automatic time based" data acquisition mode. In the setup above, once the temperatures have stabilized, the reactor is placed on automatic control and the stirrer and the Gilson 303 pump are started. Reactor liquid phase now flows through the laser analyzer. Upon onset of turbidity, the analyzer "automatic time based" data acquisition is commenced, where it continues to acquire particle size data at intervals of two minutes till the end of the experiment.

In addition to the formation experiments, for each isotherm two solubility runs were carried out, using the same procedure, at a pressure slightly below the three phase equilibrium pressure corresponding to that temperature. By measuring the rate at which the gas is being dissolved into the liquid water, we can estimate the liquid mass transfer coefficient (k_{La}) and the Henry's constant (H) of the dissolved gas in equilibrium with the gas at the gas-liquid interface.

The gas moles experimental data were used to determine the unknown parameters by minimizing the difference between the predicted and the measured moles of the gas

consumed during the solubility experiment (Appendix A). The resulting non-linear least squares problem was solved iteratively using the Gauss-Levenberg method (Englezos, 1986). The governing equations are given below.

$$\frac{dn}{dt} = (k_L a)(n^* - n) \quad 2.1$$

$$f = Hx_m^* \quad 2.2$$

$$x_m^* = \frac{n^*}{n_{mw} + n^*} \quad 2.3$$

where,

- n = Moles of Gas Consumed
- n^* = Solubility of Gas in Water
- n_{mw} = Moles of Water
- f = Gas Phase Fugacity of Dissolving Gas

During an experiment the DORIC data acquisition system scans the pressures and temperatures of the reactor and the reservoirs every 6 seconds. A personal computer running a data acquisition program computes the amount of free gas present in the reactor and the supply reservoir at a pre-determined interval using the Trebble-Bishnoi equation of state. This interval is set at 15 seconds. At any point in time the number of moles of the gas that have been consumed so far, are the difference between the number of moles of the free gas at time $t=0$ (start of stirring) and the number of moles of the free gas at time t present in the reactor and the supply cell. Namely,

$$n = (N_{R,0} + N_{S,0}) - (N_{R,t} + N_{S,t}) \quad 2.4$$

$$n = V_R \left(\frac{P}{zRT} \right)_{R,0} + V_S \left(\frac{P}{zRT} \right)_{S,0} - V_R \left(\frac{P}{zRT} \right)_{R,t} - V_S \left(\frac{P}{zRT} \right)_{S,t} \quad 2.5$$

where V_R is the volume of the gas phase of the reactor including the tubing and the analyzer circuit and V_S is the volume of the supply reservoir.

2.6 Ruska Pump Experiment

The volume of the supply reservoir is determined by performing a "Ruska Pump" experiment whereby a known volume of mercury is pumped into the reservoir and the pressure is measured before and after the mercury is pumped in. During the Ruska pump experiment the temperature and the number of moles remain constant, hence we have,

$$P_a V_{S,a} = N_S z_a RT \quad 2.6$$

$$P_e V_{S,e} = N_S z_e RT \quad 2.7$$

where subscripts a and e denote the equilibrium state before and after the mercury is pumped into the reservoir. The compressibility factors are calculated using the Trebble-Bishnoi equation of state. From the above equations after a simple manipulation we obtain,

$$V_S = V_{S,e} = \delta V_S \left(\frac{P_e z_a}{P_a z_e} - 1 \right)^{-1} \quad 2.8$$

where

$$\delta V_S = V_{S,a} - V_{S,e} \quad 2.9$$

Therefore, knowing δV_S , the volume V_S is obtained. The experimental error involved in the measurement of δV_S is less than 0.01 cm^3 .

3.0 THE ENGLEZOS ET AL. MODEL

Englezos et al. (1987) proposed a mechanistic model with only one adjustable parameter which represents the rate constant for the growth of the hydrate particles.

Their model has been followed in this work. For easy reference, a brief description of the model is given below.

An intrinsic kinetic model with only one adjustable parameter was proposed for the formation of ethane and methane gas hydrates. The kinetic model is based on the crystallization theory, while the two-film theory model is adopted for the interfacial mass transfer.

The study revealed that the formation rate is proportional to the difference in the fugacity of the dissolved gas and the three phase equilibrium fugacity at the experimental temperature. This difference defines the driving force which incorporates the pressure effects. The gas consumption rate is also proportional to the second moment of the particle size distribution.

Nucleation and driving force

The formation of gas hydrates is a phase transformation which requires a supersaturated environment in order to occur. It is a crystallization process. Gas molecules dissolve in liquid water build the supersaturated environment, throughout the liquid phase or locally

near the interface. At some point during the dissolution (turbidity point), the precursors to the hydrate phase (nuclei) appear. The nuclei subsequently grow if sufficient gas is present in the structured water environment.

The particulate nature of the process implies that two distinct kinetic processes (nucleation and growth) are involved and they have to be coupled with the transport processes to describe the overall phenomenon.

Hydrate formation is not restricted to a thin layer close to the gas-liquid interface but it can occur everywhere in the liquid water if supersaturation exists as a result of the dissolution process. The probability of nuclei formation in the water saturated gas phase is very small since the molar volume of vapour water is very large and hence there is very little possibility that the water molecules will group together in a manner corresponding to that of the hydrate structure.

It is assumed that the type of nucleation that characterizes this system is primary or spontaneous homogenous (absence of foreign particles) nucleation.

For modelling the data, it is assumed that the nuclei are formed instantaneously and the primary nucleation ceases after turbidity because the energy barrier to form a new nucleus is greater than that of the enclathration of gas into existing nucleation centres.

Since, the three-phase equilibrium fugacity represents the minimum fugacity at which hydrates can exist, we propose that the overall driving force for the crystallization process be given by the difference in the fugacity of the dissolved gas and the three-phase equilibrium fugacity at the experimental temperature, namely,

$$\Delta f = f - f_{eq} \quad 3.1$$

f = Gas Fugacity

f_{eq} = Gas Fugacity at the Three Phase Equilibrium Conditions

It should be noted that the driving force is not determined by the magnitude of the experimental pressure but rather by the deviation from equilibrium conditions.

Crystal growth rate

Following the modelling approach by Karpinski (1980) for crystal growth from a solution, they proposed the following two consecutive steps for the hydrate particle growth.

Step 1: Diffusion of the dissolved gas from the bulk of solution to the crystal-liquid interface through the laminar diffusion layer around a particle.

Step 2: "Reaction" at the interface, which is an adsorption process describing the incorporation of the gas molecules into the water molecules and the subsequent stabilization of the framework of the structured water.

Since no accumulation is allowed in the diffusion layer around the particle, the above two rates are equal. Hence, the rate of growth per particle in terms of the overall driving force is obtained:

$$\left(\frac{dn}{dt}\right)_p = K^* A_p (f - f_{eq}) \quad 3.2$$

K^* = Combined Rate Parameter

A_p = Surface Area of Particle

where,

$$\frac{1}{K^*} = \frac{1}{k_r} + \frac{1}{k_d} \quad 3.3$$

k_r ="Reaction" Rate Constant

k_d =Mass Transfer Coefficient Around Particle

Here, it is assumed that the outside surface of the surrounding layer is equal to the inside one, which is the surface of the particle. It is also assumed that the particles are spherical.

Homogeneous global "reaction" rate

In order to formulate a global reaction rate for all the particles, they integrated the rate per particle for all particles of any size, namely

$$R_y(t) = \int_0^\infty \left(\frac{dn}{dt} \right)_p \phi(x,t) dx \quad 3.4$$

where,

x =Particle Size or Diameter

$\phi(x,t)$ =Number Distribution Function

$$R_y(t) = \int_0^\infty K^* A_p (f - f_{eq}) \phi(x,t) dx \quad 3.5$$

$$R_y(t) = \pi K^* \mu_2 (f - f_{eq}) \quad 3.6$$

where μ_2 is the second moment of particle size distribution (PSD) and is given by

$$\mu_2 = \int_0^\infty x^2 \phi(x,t) dx \quad 3.7$$

Therefore, the global reaction rate can be written in the form

$$R_y(t) = K(f - f_{eq}) \quad 3.8$$

where,

$$K = \pi K^* \mu_2$$

The rate of crystallization process taking place in the liquid phase is thus described by the overall rate given by Equation 3.8, i.e. a pseudo-first order irreversible homogeneous reaction.

Two-film theory

The two film theory was adopted for the system. Assuming quasi-steady-state conditions, the accumulation term in the liquid film can be neglected and hence the mass balance for the gas in the film in a slice of thickness dy and unit cross section area yields

$$D \frac{d^2 c}{dy^2} = K(f - f_{eq}) \quad 3.9$$

where,

D = Diffusivity of Gas

c = Concentration of Gas in Liquid Water

Since the concentration of the gas can be written in terms of its fugacity, assuming that the number of moles of the water remain practically constant, we have

$$c = \frac{c_{w0}f}{H} \quad 3.10$$

where,

c_{w0} =Initial Concentration of Water Molecules

H =Henry's Constant

Thus, Equation 3.9 can be written as

$$D^* \frac{d^2 Y}{dy^2} = KY \quad 3.11$$

where

$$Y = f - f_{eq}, D^* = \frac{Dc_{w0}}{H} \quad 3.12$$

Equation 3.11 satisfies the following boundary conditions:

$$y=0, Y=f_g - f_{eq} \quad 3.13$$

$$y=y_L, Y=f_b - f_{eq} \quad 3.14$$

where,

y =Distance From Gas-Liquid Interface

Here, it is assumed that the gas-phase resistance is negligible since the partial pressure of water in the gas phase is very small. Analytical solution of Equation 3.11 with the above boundary conditions yields the fugacity profile of the gas in the liquid phase film:

$$f = f_{eq} + ((f_g - f_{eq}) \sinh(\gamma(1 - \frac{y}{y_L})) + (f_b - f_{eq}) \sinh(\gamma \frac{y}{y_L})) (\frac{1}{\sinh \gamma}) \quad 3.15$$

where gamma is the Hatta number, which indicates how rapidly the reaction proceeds compared with the diffusion rate through the film. The Hatta number is given by

$$\gamma = y_L \sqrt{(4\pi K^* \mu_2 / D^*)} \quad 3.16$$

The flux at the interface can then be obtained from

$$(J)_{y=0} = -D \left(\frac{dc}{dy} \right)_{y=0} = -D^* \left(\frac{df}{dy} \right)_{y=0} \quad 3.17$$

The rate with which the gas is being transported to the liquid phase and either is dissolved or forms hydrates is related to the flux at the interface by the equation

$$(J)_{y=0} A_{g-l} = \frac{dn}{dt} \quad 3.18$$

Substitution of Equation 3.15 into Equation 3.17 and the resulting expression for $(J)_{y=0}$ into Equation 3.18 yields

$$\frac{dn}{dt} = \left(\frac{D^* \gamma A_{g-l}}{y_L} \right) \frac{((f_g - f_{eq}) \cosh \gamma - (f_b - f_{eq}))}{\sinh \gamma} \quad 3.19$$

The number of moles of gas that have already been dissolved into the liquid phase at the turbidity point are measured for each experiment and define the initial condition for equation 3.19. In order to determine f_b as a function of time, we do a mass balance in the bulk which, when coupled with the equation 3.15, yields

$$\frac{df_b}{dt} = \frac{HD^* \gamma a}{c_{w0} y_L \sinh \gamma} ((f_g - f_{eq}) - (f_b - f_{eq}) \cosh \gamma) - \frac{\pi K^* \mu_2 H(f_b - f_{eq})}{c_{w0}} \quad 3.20$$

At the turbidity point, we have $f_b = f_{eq}$ (minimum fugacity for the hydrate to exist). It is implied here that the excess gas beyond the three-phase equilibrium concentration is consumed "instantaneously" to form the hydrate nuclei.

Population balance

The Englezos model employs the Kane et al. (1974) model to estimate μ_2 with time. They, however, felt the necessity to obtain experimental data for the same. Therefore, the model has been modified here and experimentally obtained data for the second moment (μ_2) of particle size distribution are supplied.

Parameters such as the film thickness, y_L , $k_L a$ and Henry's constant are obtained from solubility experiments. The critical size, of the nucleus is calculated assuming primary homogenous nucleation.

4.0 EXPERIMENTAL RESULTS

4.1 Experiments Conducted

Tables 4.1, 4.2, and 4.3 list all the experiments conducted for ethane and Tables 4.4, 4.5 and 4.6 list all the experiments conducted for methane. For both the gases, two kinetic and two solubility experiments were performed at three isotherms each (274, 276 and 278 K). The tables list the experiments as "Kinetic" or "Solubility". Solubility experiments were performed to estimate the liquid phase mass transfer coefficient, $k_L a$, and the Henry's constant, H (Refer Chapter 2, Section 2.5 and Appendix A), both of which were required for the evaluation of K^* , the overall reaction rate constant for hydrate formation in the Englezos et al. model. The estimated $k_L a$ and H values were compared with values reported by Lekvam and Bishnoi (1995). Deviation from their values of $k_L a$ was less than 5 % and for H less than 18 %. Kinetic experiments provided the gas mole consumption data for estimation of K^* .

Tables 4.1 to 4.6 list certain experiments as either "trial runs" or "failed". It has been observed (Englezos et al., 1987) that the turbidity point in a hydrate kinetic experiment can appear very soon if the experimental pressure is well above the three phase equilibrium pressure, at that isotherm. (Turbidity point is defined as that point in time from the start of the experiment, when the hydrates first appear in the liquid phase, turning it from a clear to a turbid liquid. Turbidity point will be discussed in detail in section 4.3). This is due to the local supersaturation of the liquid phase at the gas-liquid interface and the hydrate formation in this local region of supersaturation.

Englezos et al. reported that at moderate experimental pressures and good mixing of the liquid phase, nucleation could be achieved *throughout* the liquid phase due to almost uniform concentration of the hydrate forming gas in the bulk liquid phase. Closer the

TEMPERATURE= 274 K

RUN #	SOLUBILITY	KINETIC	PRESSURE (BAR)	ACCEPTED(A)/ TRIAL(T)/ FAILED(F)
E001		*		T
E002	*			T
E003		*		T
E004		*		T
E005		*		T
E006	*		4.8	A
E007		*	9.7	A
E008	*		4.8	A
E009		*	7.2	A

Table 4.1 List of Experiments Conducted for Ethane at 274 K.

TEMPERATURE= 276 K

RUN #	SOLUBILITY	KINETIC	PRESSURE (BAR)	ACCEPTED(A)/ TRIAL(T)/ FAILED(F)
E010		*		T
E011		*	10.7	A
E012	*			F
E013				F
E014	*		6.0	A
E015		*		F
E016		*	10.7	A
E017		*		F
E018	*		6.0	A

Table 4.2 List of Experiments Conducted for Ethane at 276 K.

TEMPERATURE=278 K

RUN #	SOLUBILITY	KINETIC	PRESSURE (BAR)	ACCEPTED(A)/ TRIAL(T)/FAILED(F)
E019		*	12.5	A
E020	*		7.7	A
E021	*		7.7	A
E022		*		F
E023		*		F
E024		*		T
E025		*		T

Table 4.3 List of Experiments Conducted for Ethane at 278 K.

TEMPERATURE= 278 K

RUN #	SOLUBILITY	KINETIC	PRESSURE (BAR)	ACCEPTED(A)/ TRIAL(T)/ FAILED(F)
M001		*		T
M002		*		T
M003		*		T
M004		*	49.3	A
M005		*	49.2	A
M006	*			F
M007	*		35.2	A
M008	*		35.1	A

Table 4.4 List of Experiments Conducted for Methane at 278 K.

TEMPERATURE= 276 K

RUN #	SOLUBILITY	KINETIC	PRESSURE (BAR)	ACCEPTED(A)/ TRIAL(T)/ FAILED(F)
M009		*		T
M010	*		28.3	A
M011		*	42.4	A
M012		*	42.5	A
M013	*		28.3	A

Table 4.5 List of Experiments Conducted for Methane at 276 K.

TEMPERATURE=274 K

RUN #	SOLUBILITY	KINETIC	PRESSURE (BAR)	ACCEPTED(A)/ TRIAL(T)/ FAILED(F)
M014		*	37.2	A
M015		*	37.2	A
M016	*		23.1	A
M017	*		23.1	A

Table 4.6 List of Experiments Conducted for Methane at 274 K.

experimental pressure is to the three phase equilibrium pressure at a temperature, closer is the nucleation to being a bulk phenomenon. At the same time, for an experiment being performed at a pressure very close to the three phase equilibrium, turbidity might not occur for as long as 24 hours or even more. Trial runs were therefore performed to get a rough estimate on what lowest pressures the experiments could be performed so as to have the turbidity point appear within 2 hours from the start of the experiment. Thus, a large number of trial runs were performed.

It can be seen from the tables that the number of trial runs decreased as we went to the next higher isotherm for ethane and reduced further for methane, the order being chronological. This can be attributed to the fact that we became more experienced with the phenomenon. "Failed" runs refer to experiments that had to be abandoned due to equipment problems.

For ease of understanding, only one kinetic experiment E007 for ethane will be discussed in detail in this chapter. Gas consumption curves for all other kinetic and solubility experiments for both the gases can be found in Appendix A. Particle size analyzer results for kinetic experiments other than E007 can be found in Appendix B.

It must be emphasized here that the following discussion is relevant to all other experiments as well. This is due to the fact that for both, the gas consumption curves and the particle analyzer data, the nature of the data is very similar for all experiments. Thus, discussion on the data of experiment E007 applies to all the other experiments.

4.2 The Gas Consumption Curve

The number of moles of gas that have been consumed due to dissolution or hydrate formation at any point in time are calculated online (Refer Chapter 2, Section 2.5). Figure 4.1 shows the gas consumption curve for the kinetic experiment E007. Plotting the

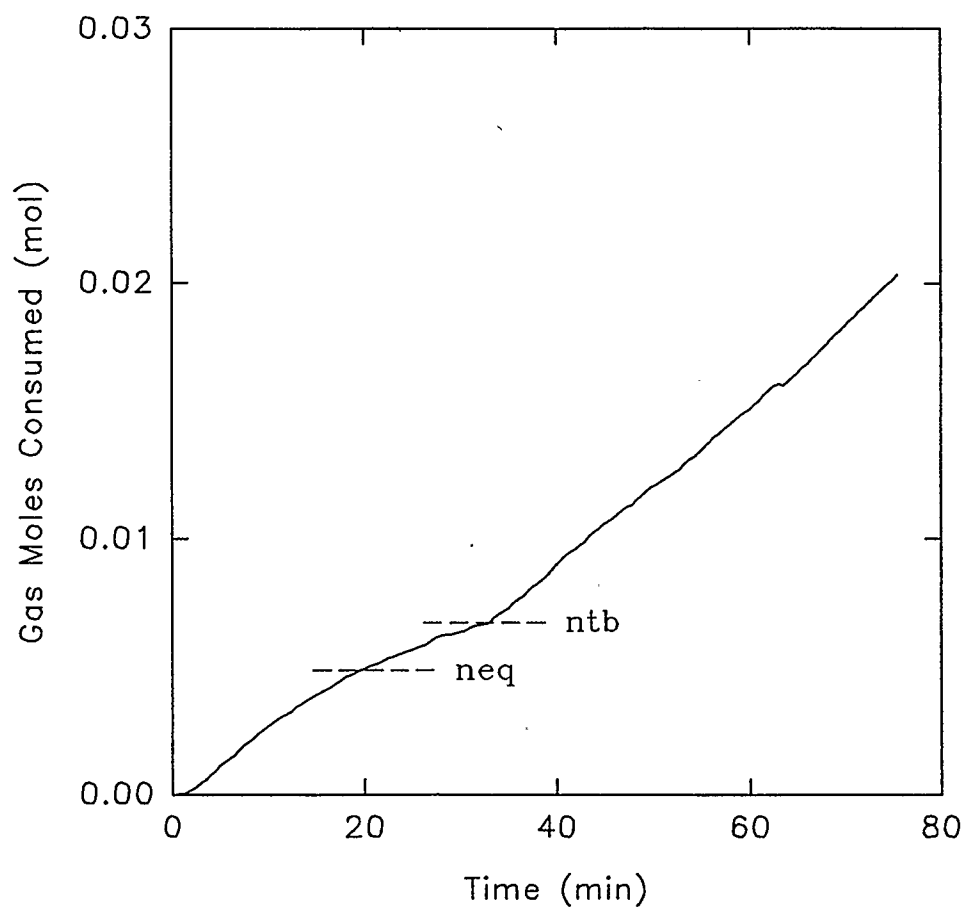


Figure 4.1 Gas Consumption Curve for Ethane.

number of moles of the consumed gas vs. time yields the experimental gas consumption curve for experiment E007. Turbidity point is indicated by " n_{tb} " while " n_{eq} " is the moles of gas dissolved at three phase equilibrium conditions. From the beginning of the experiment until the turbidity point, the process is simply physical absorption of the gas and represents the induction period. The growth period starts at the turbidity point and it is this part of the experimental data that is modelled in the Englezos et al. model, which is being followed in this work. The difference " $n_{tb}-n_{eq}$ " represents the average supersaturation.

Hydrate particle data in terms of number, area, volume and size of particles were acquired from the turbidity point till the end of the experiment, at two minute intervals. Thus, particle data have been monitored at intervals of 2 minutes from the onset of turbidity, till the end of the experiment and is discussed in the following sections. While the particle number, area, volume and size are available from the analyzer data acquisition software, the second moment of particle size distribution and the moles of gas in hydrate form had to be computed from the analyzer data.

4.3 Laser Particle Analyzer Results

The laser particle analyzer acquired data at 2 minute intervals from the onset of turbidity till the end of the experiment. Each data acquisition provided information on the number, surface area, volume and sizes of particles in a unit volume of the hydrate-water slurry. Refer Appendix C for more information on particle size analysis.

4.3.1 Particle Number Density

Particle number density is the total number of particles of all sizes present per unit volume of the hydrate-water slurry. For every data acquisition at two minute intervals, the analyzer measures the particle number density (#/mL) of the sample as a sum of the

number of particles of all sizes present in one mL of sample. Please see Appendix C for more details. Figure 4.2 is a plot of the particle number density from the onset of turbidity till the experiment end. As can be seen there is almost a five fold increase in the number density from the turbidity point to the end of the experiment.

4.3.2 Particle Area Density

Particle area density is the total surface area of particles of all sizes present per unit volume of hydrate-water slurry. It is calculated by the analyzer software from the particle number density data (Refer Appendix C). Figure 4.3 is a plot of the particle area density from the onset of turbidity till the experiment end and shows approximately a five fold increase.

4.3.3 Particle Volume Density

Particle volume density is the total volume of particles of all sizes present per unit volume of hydrate-water slurry. It is calculated by the analyzer software from the particle number density data (Refer Appendix C). Figure 4.4 is a plot of the particle volume density from the onset of turbidity till the experiment end.

4.3.4 Distribution of Number Density

The distribution of number density is a plot of the contribution of each particle size range to the total particle number density. Figures 4.5 to 4.10 are the distributions of number density at times 33, 39, 48, 53, 60 and 63 minutes corresponding to times 33, 39, 48, 53, 60 and 63 minutes, i.e. the same time on Figure 4.1.

Due to the limitation in the measuring range of the analyzer we could measure particles only in the range 5-600 μm . The distributions of particle number density clearly indicate

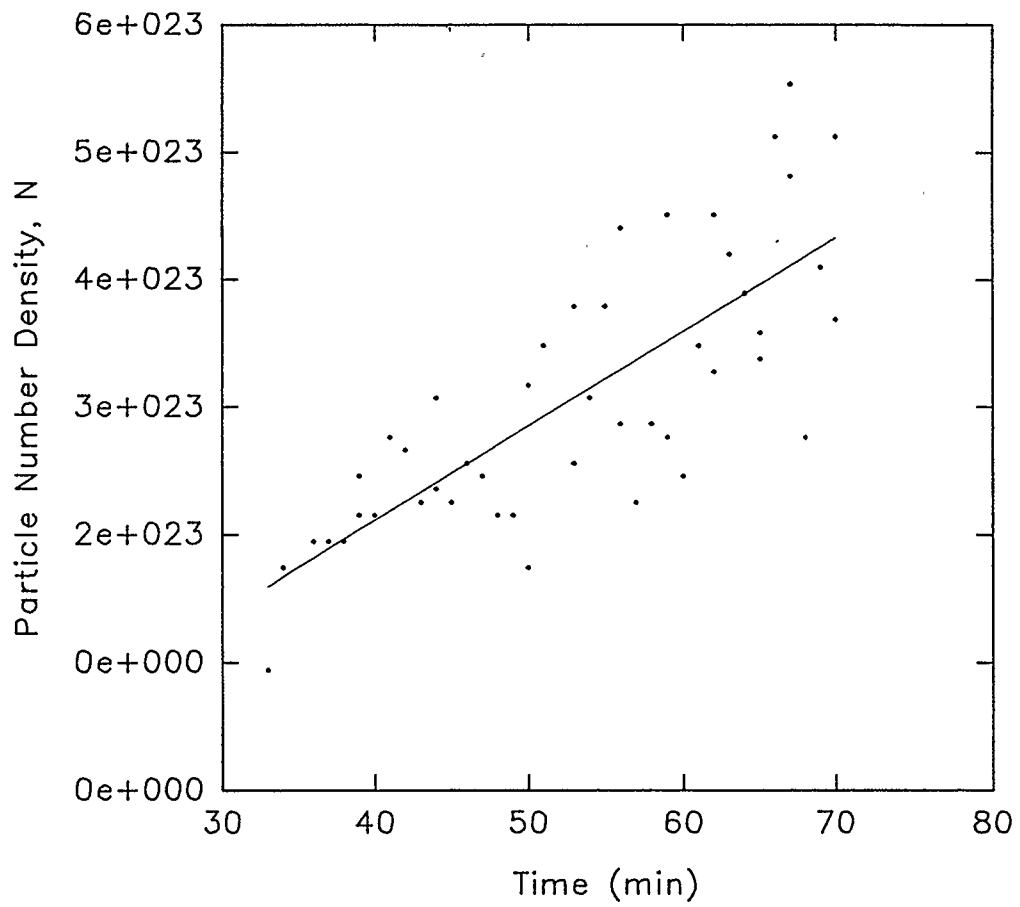


Figure 4.2 Particle Number Density, $N(\text{\#}/\text{m}^3)$, vs Time (min).

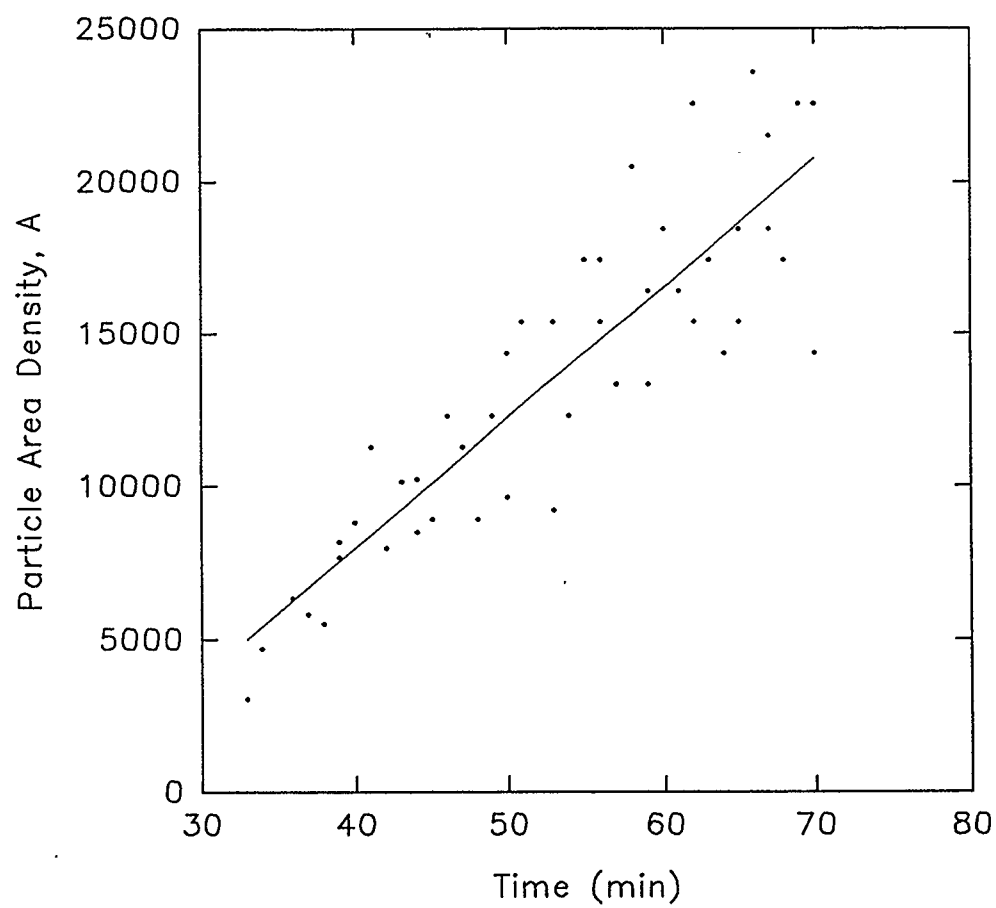


Figure 4.3 Particle Area Density, A (m^2/m^3), vs Time (min).

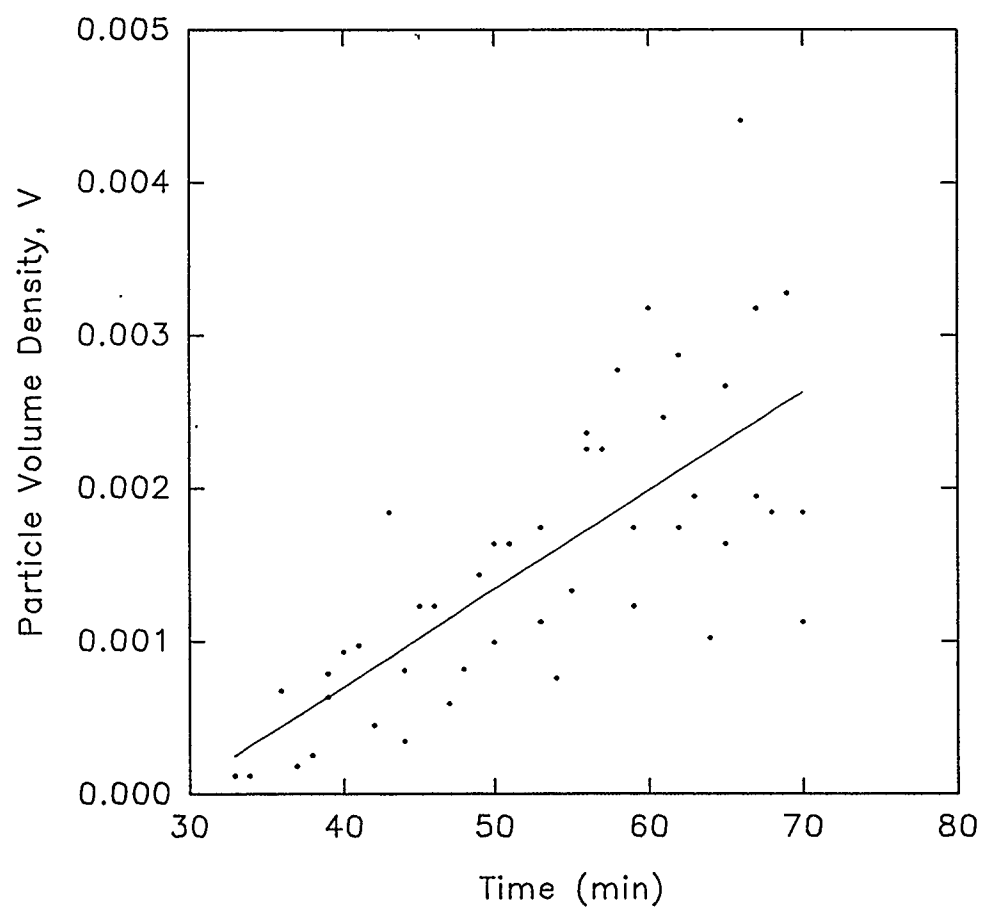


Figure 4.4 Particle Volume Density, V (m^3/m^3), vs Time (min).

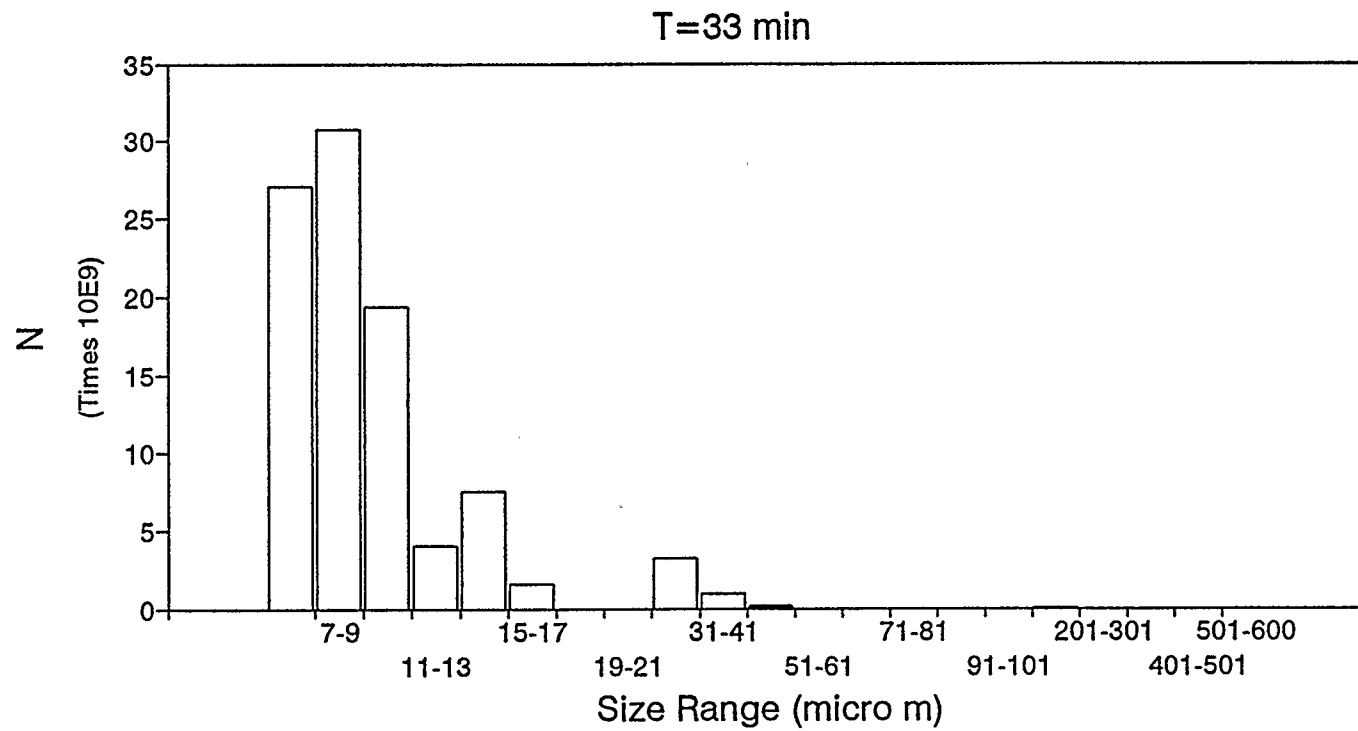


Figure 4.5 Distribution of Particle Number Density, $N(\text{\#}/\text{m}^3)$, with Size (μm).

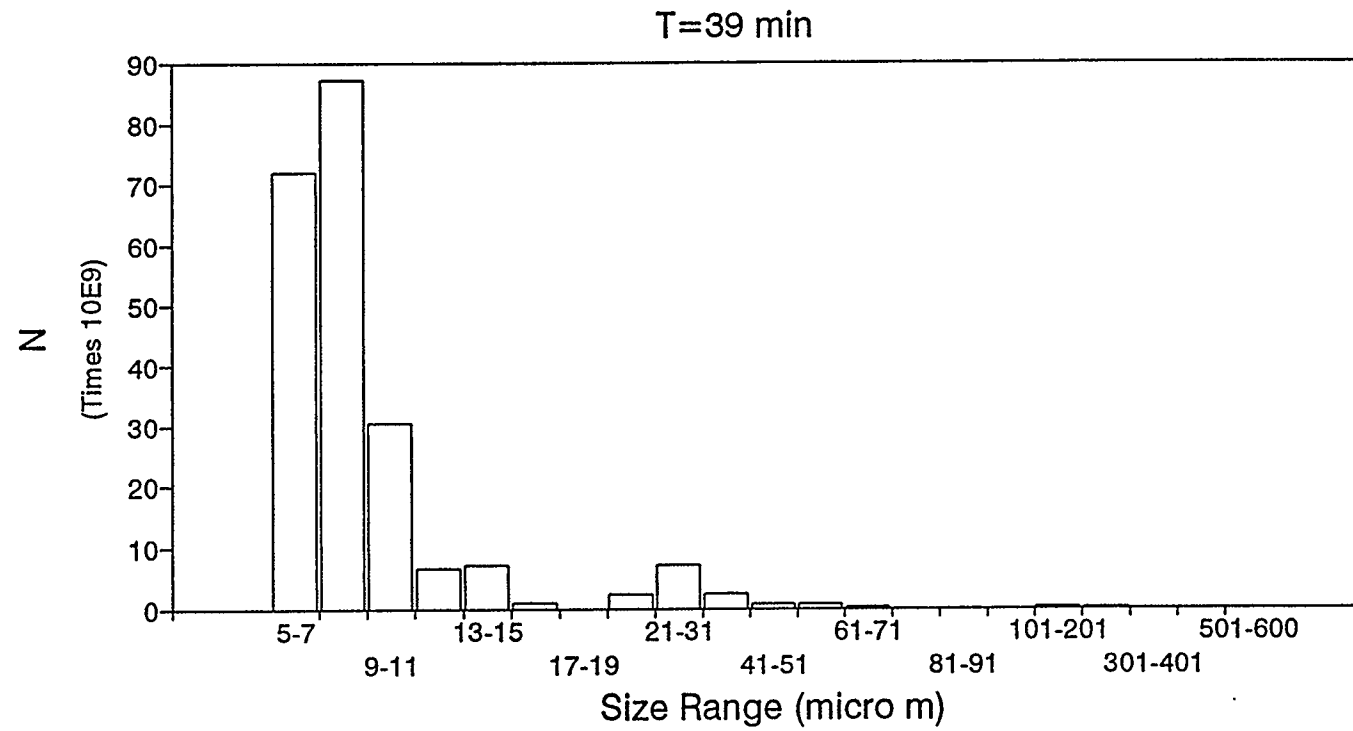


Figure 4.6 Distribution of Particle Number Density, $N(\#/m^3)$, with Size (μm).

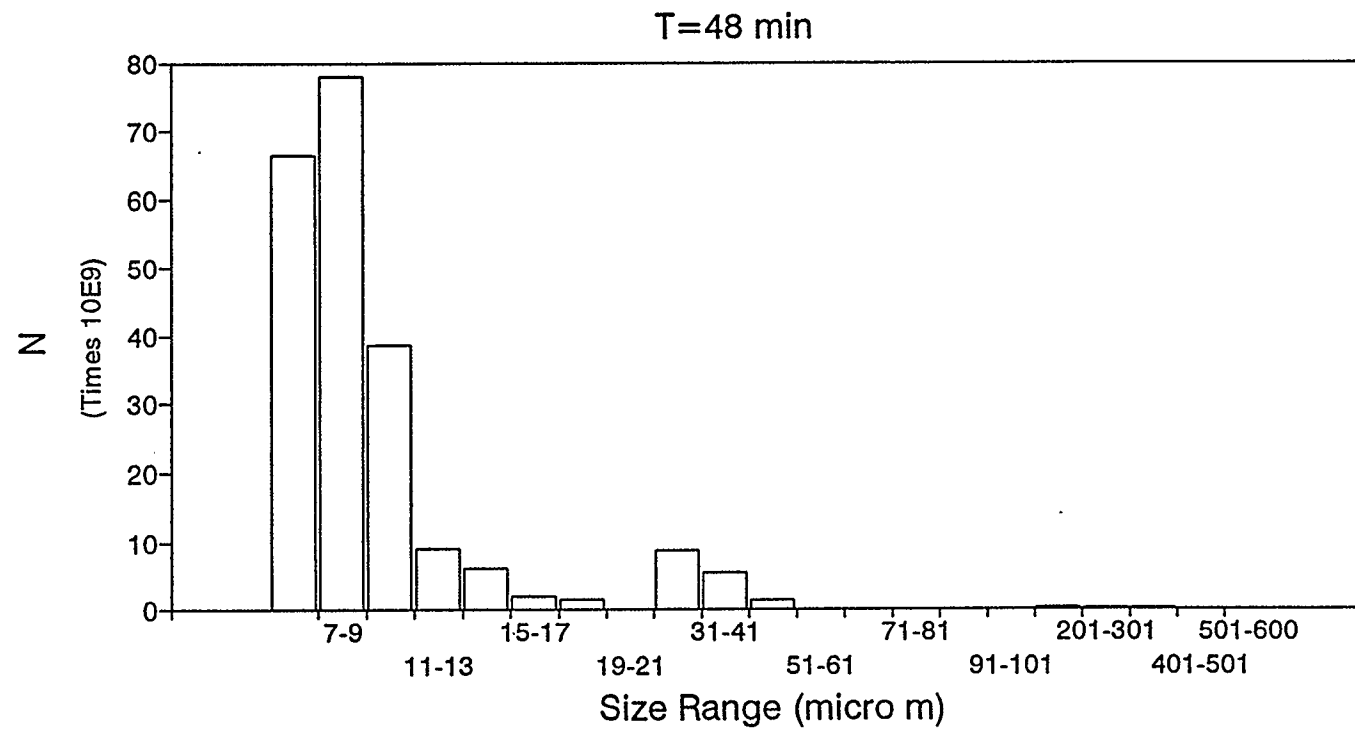


Figure 4.7 Distribution of Particle Number Density, $N(\text{\#}/\text{m}^3)$, with Size (μm).

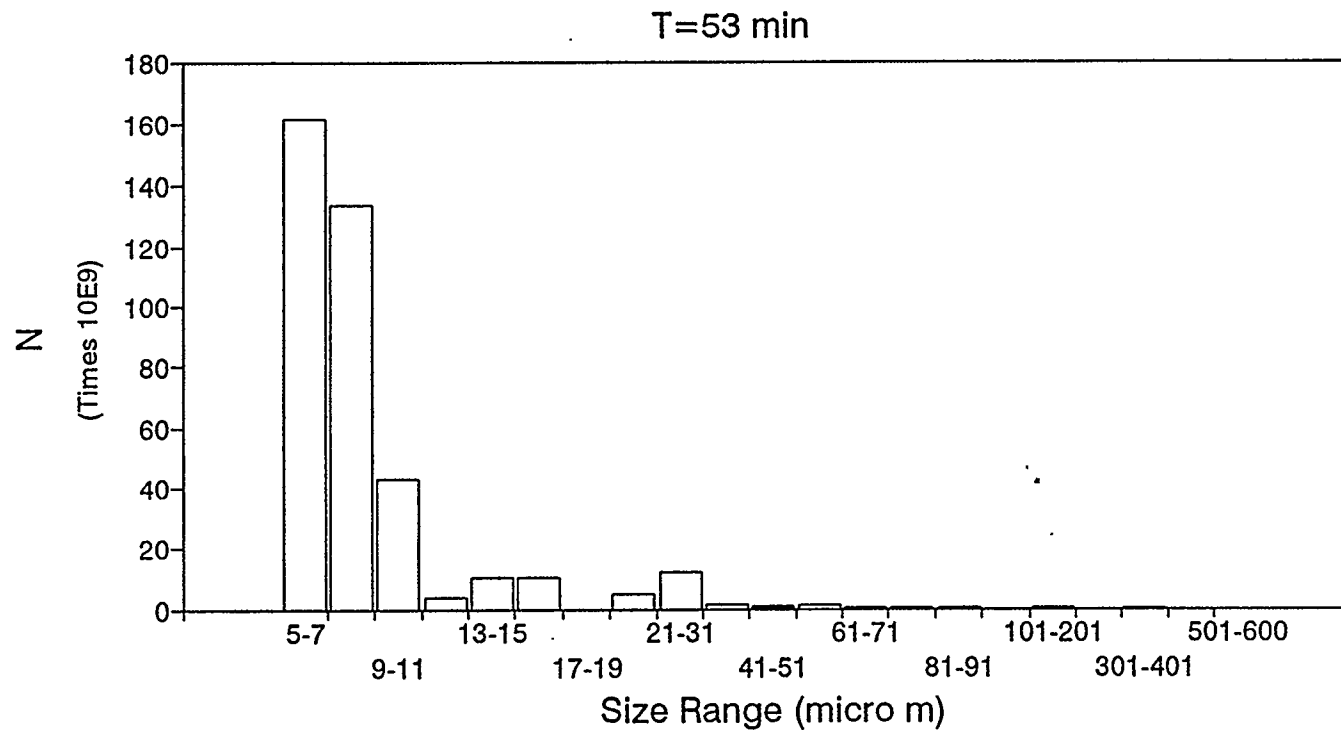


Figure 4.8 Distribution of Particle Number Density, $N(\#/\text{m}^3)$, with Size (μm).

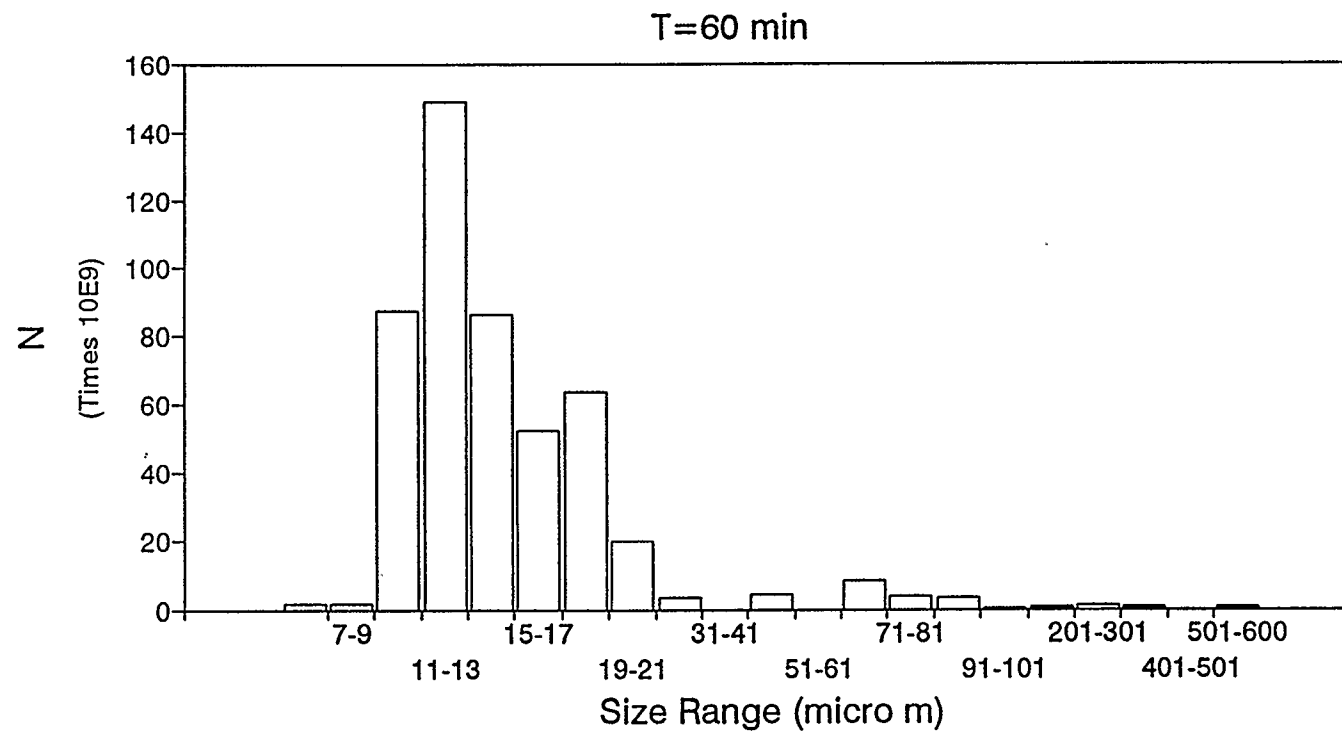


Figure 4.9 Distribution of Particle Number Density, $N(\text{\#}/\text{m}^3)$, with Size (μm).

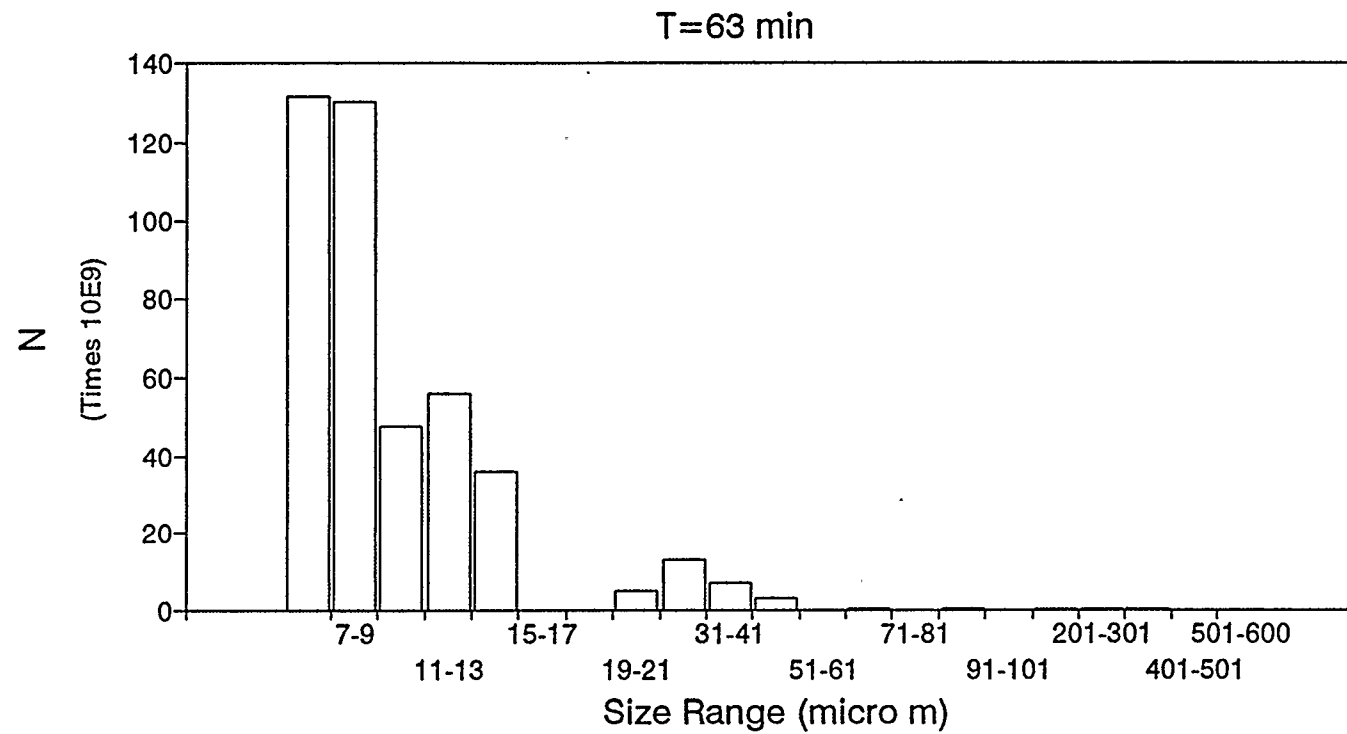


Figure 4.10 Distribution of Particle Number Density, $N(\#/m^3)$, with Size (μm).

that the distribution should continue towards the smaller particle size range below 5 μm . The first three distributions at T=33, 39 and 48 minutes have their peaks in the size range 7-9 μm , both sides of which the distribution descends. The peak of the distribution shifts to the smaller particle size range (5-7 μm) in other plots. In order to ascertain the shape or nature of the distributions of number density, various peak functions such as Log-Normal, Gaussian, Lorentzian, Erfc Peak, Gamma, Weibull, Beta, etc. were fit to the data (least squares), but the log-normal peak function described best, the nature of the data in terms of minimum standard error of fit and maximum coefficient of determination (r^2). Figure 4.11 shows a log-normal fit through the data obtained at time 33 minutes.

4.3.5 Distribution of Area Density

The distribution of area density is a plot of the contribution of each particle size range to the total particle area (surface) density. Figures 4.12 to 4.17 are the distributions of area density for the same data as in section 4.3.4. Clearly the area contribution of the peak size range 7-9 μm and 5-7 μm are not very significant and that larger particle ranges with much fewer particles contribute as much and even more than the smaller size ranges with the largest number of particles.

4.3.6 Distribution of Volume Density

The distribution of volume density is a plot of the contribution of each particle size range to the total particle volume density. Figures 4.18 to 4.23 are the volume density distributions for the same data as in section 4.3.4.

The distributions of particle volume density indicate that most of the volume and therefore the mass of each distribution is in the larger particle size range. This implies that most of the hydrate forming gas is in the larger particles and almost a negligible amount in the smaller size range. Therefore, the absence of the distribution below 5 μm is

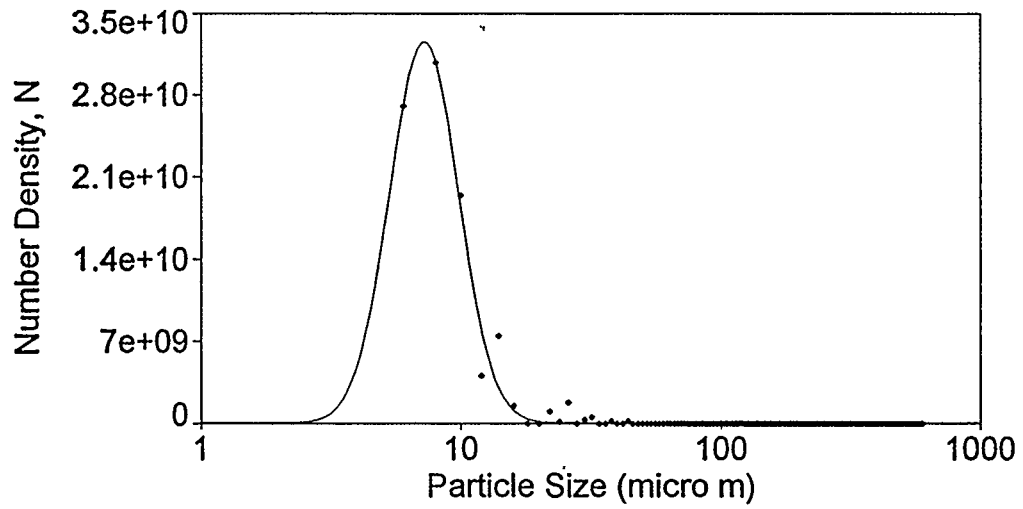


Figure 4.11 Log-Normal Fit through the Distribution of Particle Number Density, N ($\text{\#}/\text{m}^3$), with Size (μm) ("dots" indicate raw data obtained at time=33 min).

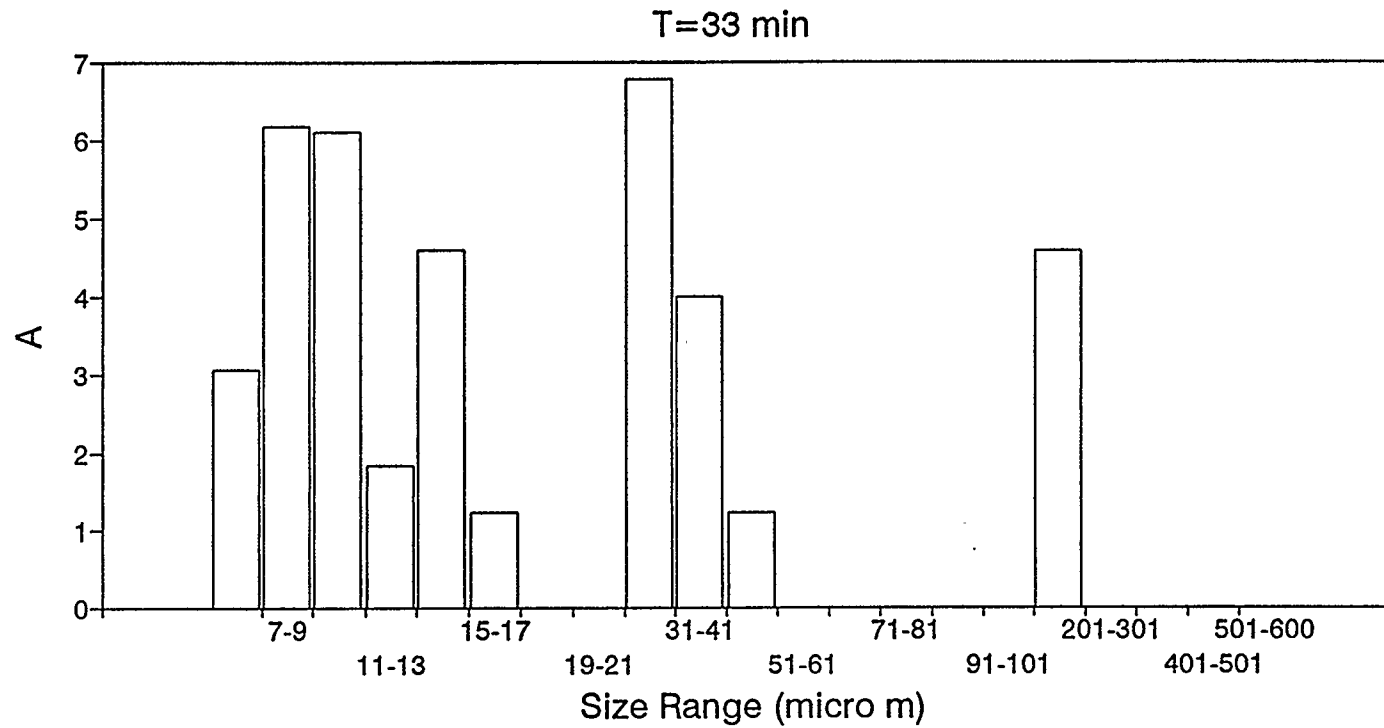


Figure 4.12 Distribution of Particle Area Density, A (m^2/m^3), with Size (μm).

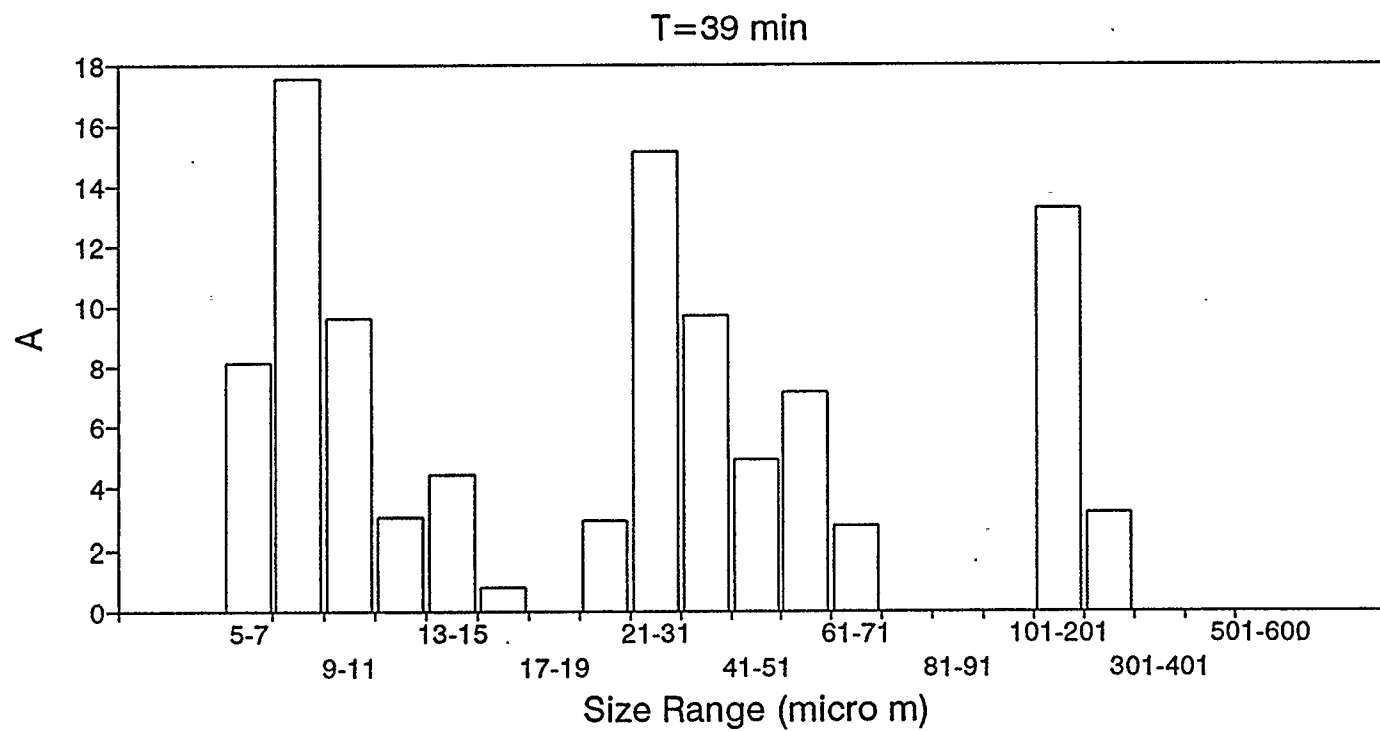


Figure 4.13 Distribution of Particle Area Density, A (m^2/m^3), with Size (μm).

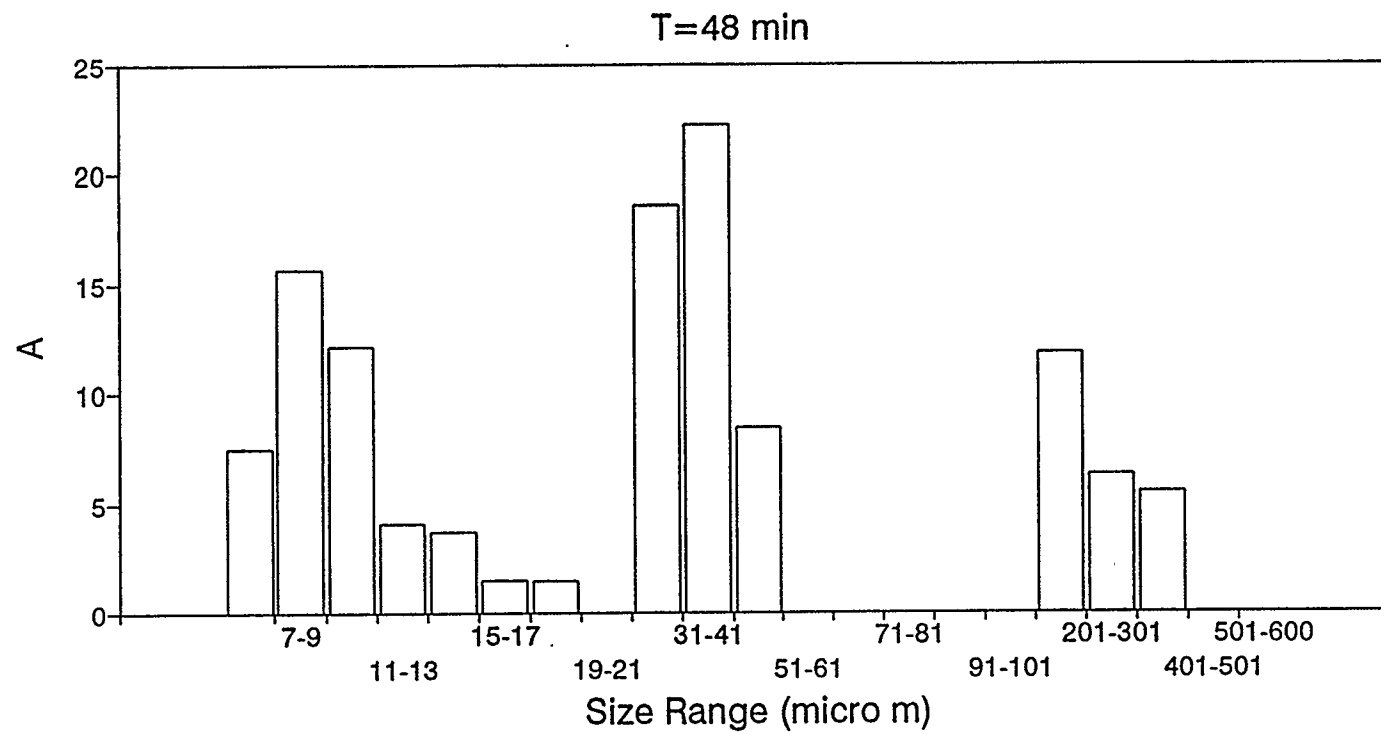


Figure 4.14 Distribution of Particle Area Density, A (m^2/m^3), with Size (μm).

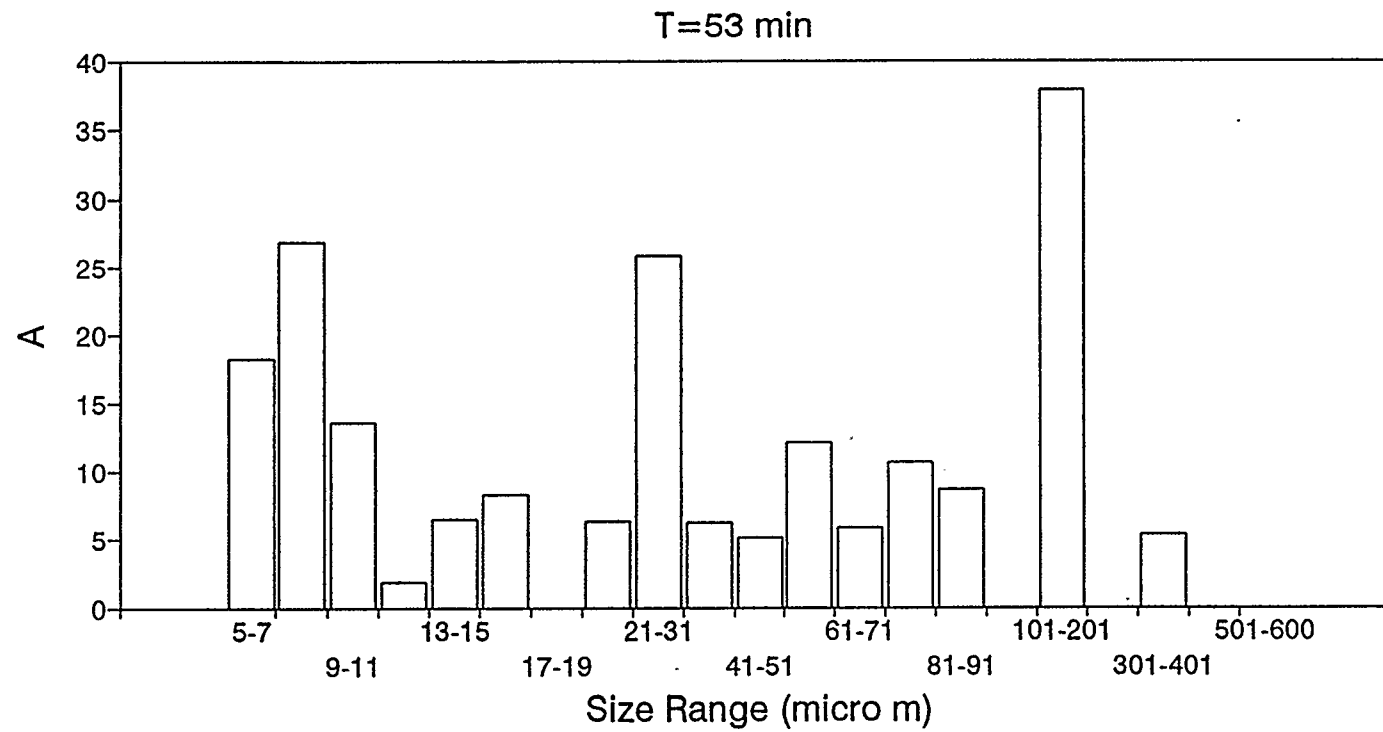


Figure 4.15 Distribution of Particle Area Density, A (m^2/m^3), with Size (μm).

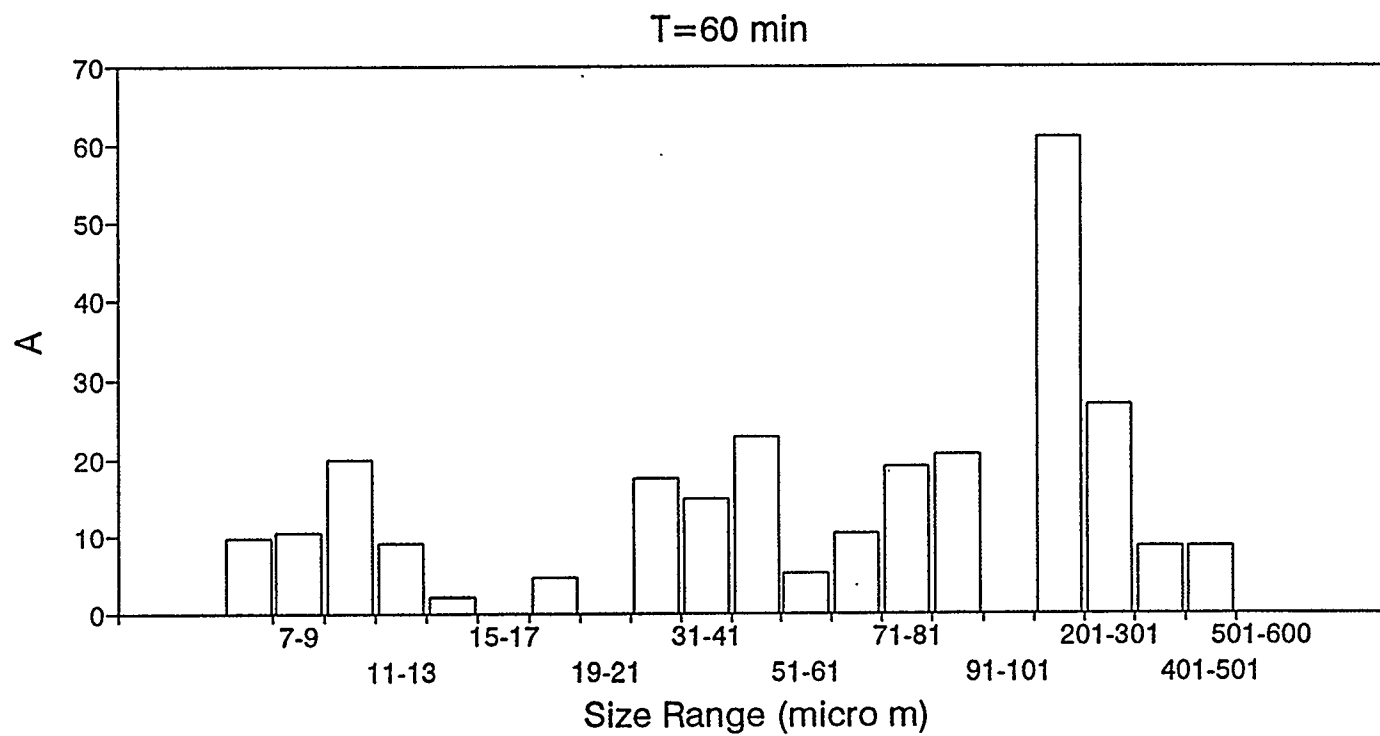


Figure 4.16 Distribution of Particle Area Density, A (m^2/m^3), with Size (μm).

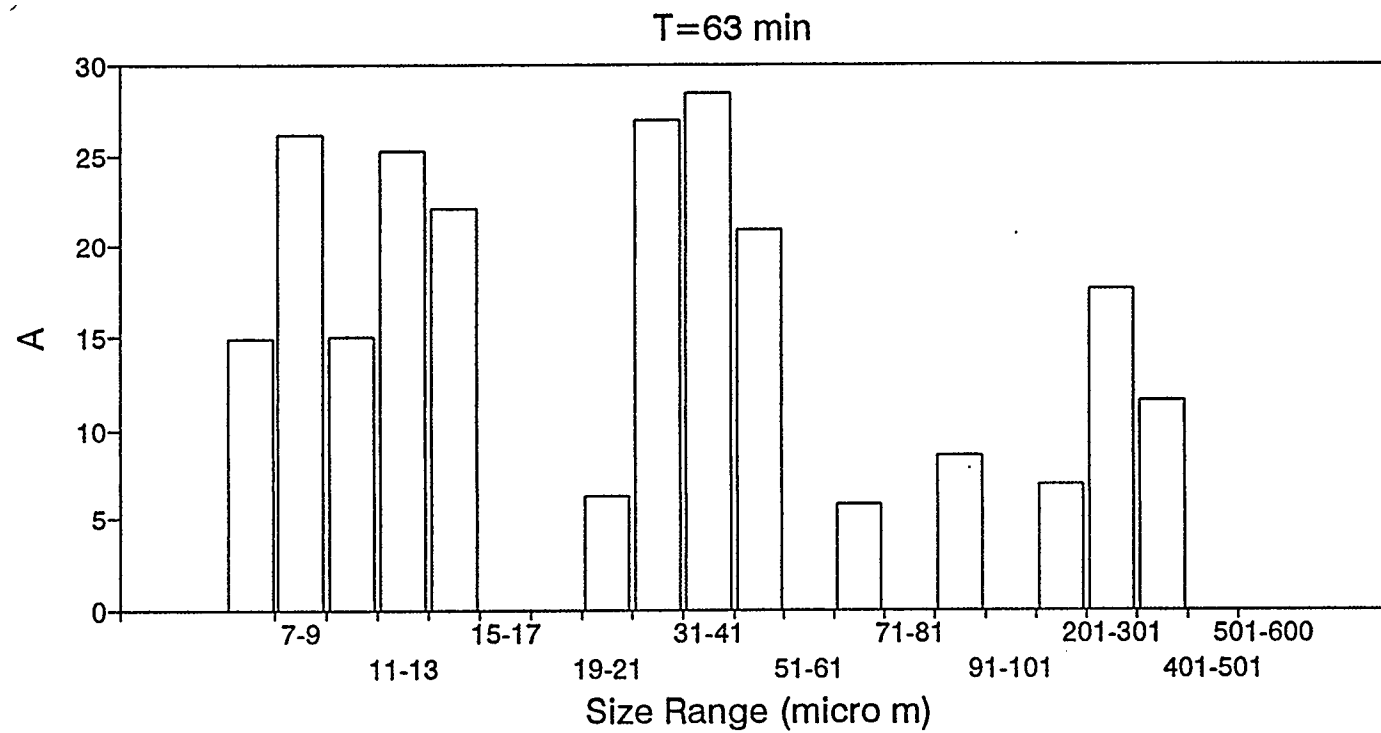


Figure 4.17 Distribution of Particle Area Density, A (m^2/m^3), with Size (μm).

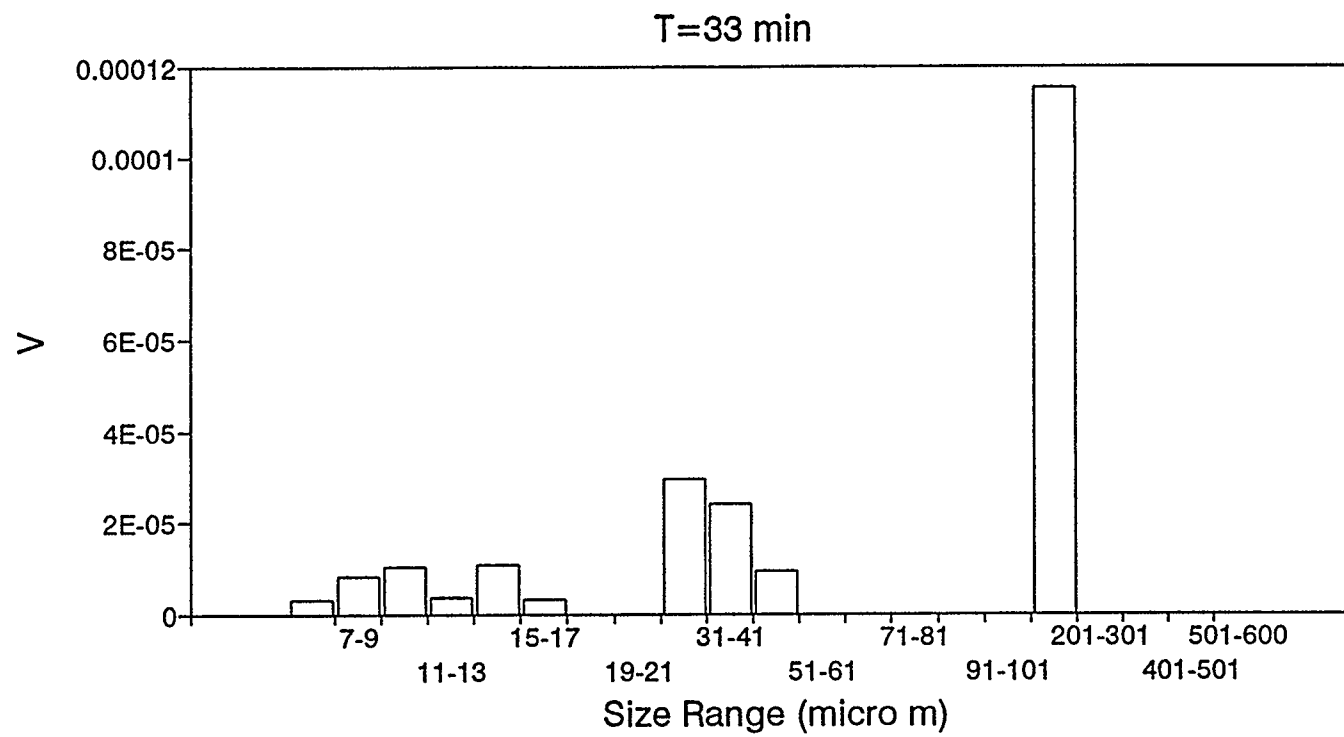


Figure 4.18 Distribution of Particle Volume Density, V (m^3/m^3), with Size (μm).

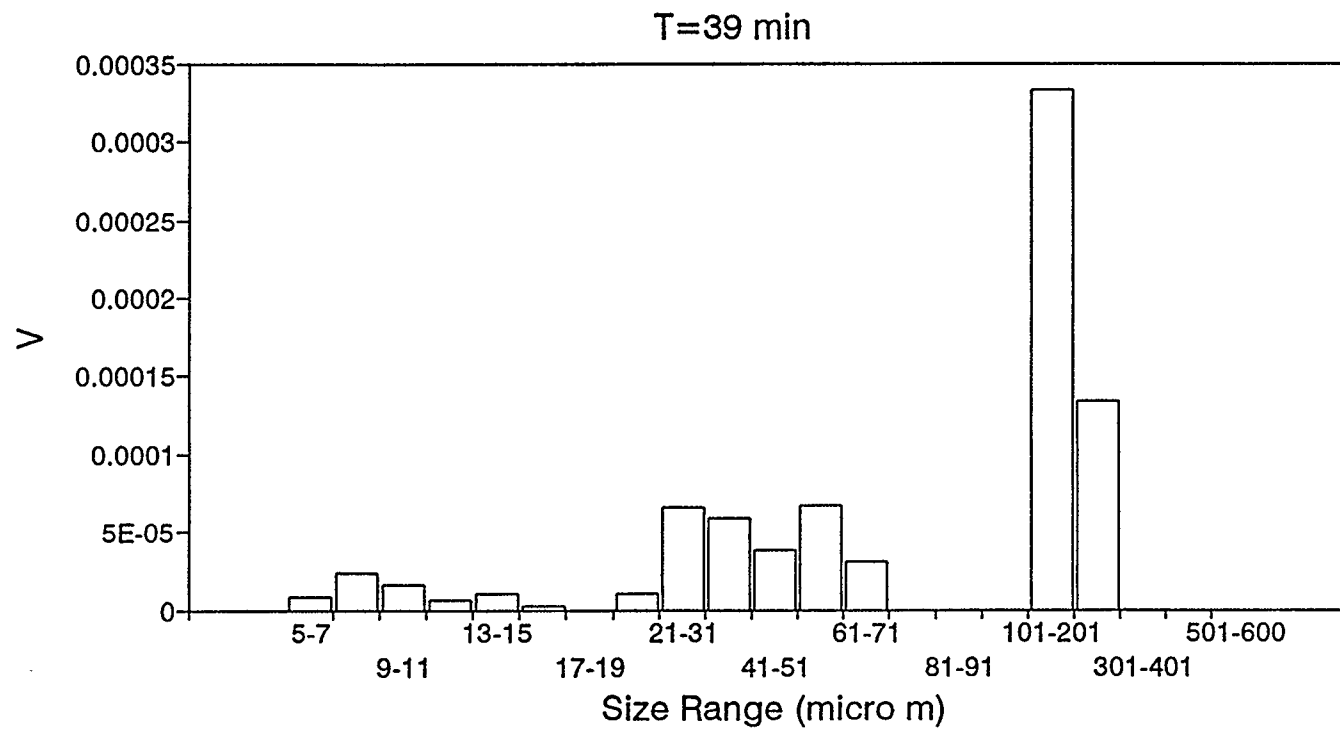


Figure 4.19 Distribution of Particle Volume Density, V (m^3/m^3), with Size (μm).

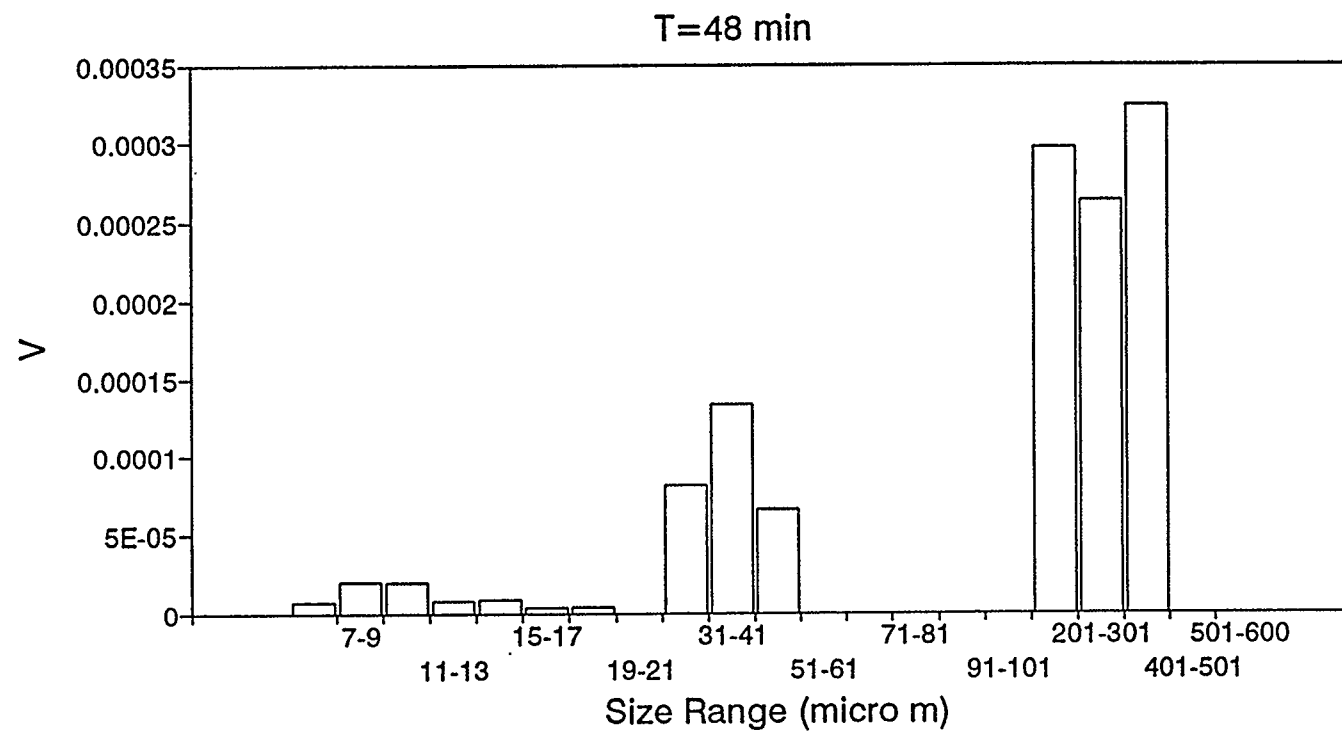


Figure 4.20 Distribution of Particle Volume Density, V (m^3/m^3), with Size (μm).

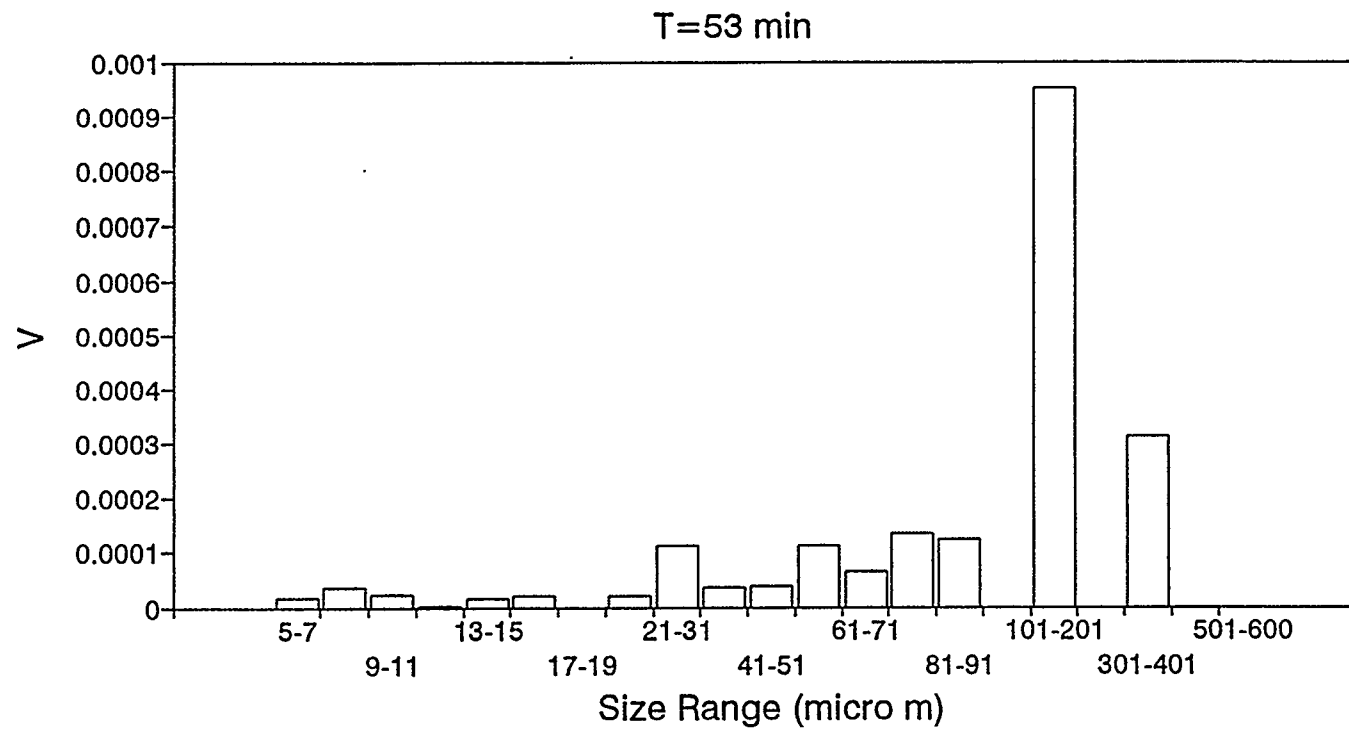


Figure 4.21 Distribution of Particle Volume Density, V (m^3/m^3), with Size (μm).

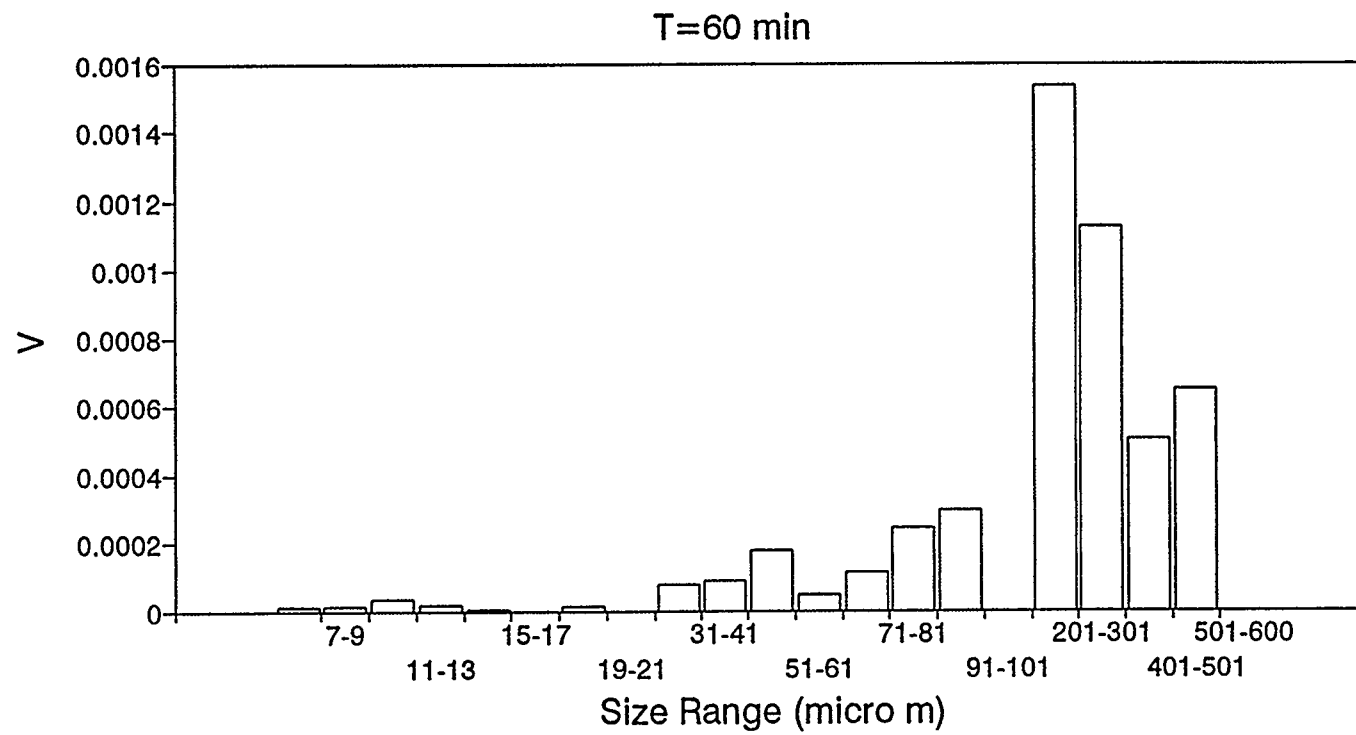


Figure 4.22 Distribution of Particle Volume Density, V (m^3/m^3), with Size (μm).

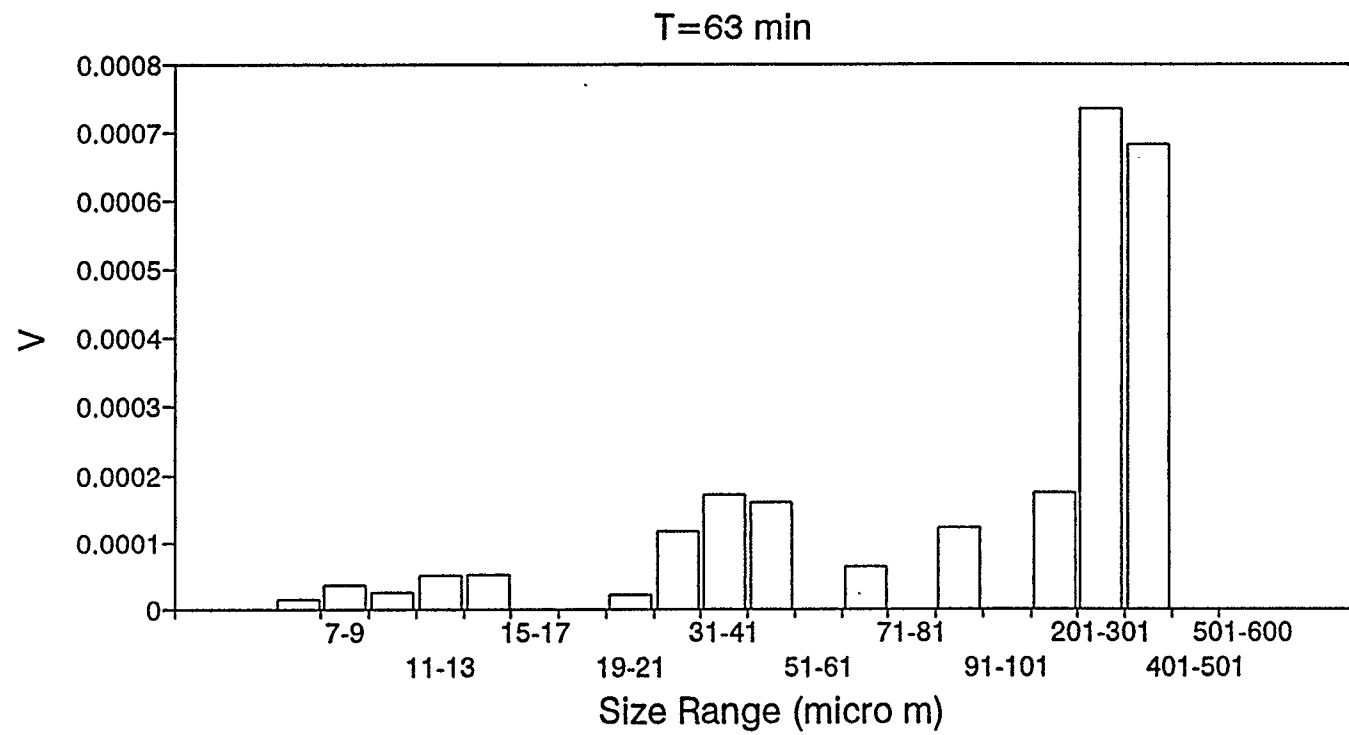


Figure 4.23 Distribution of Particle Volume Density, V (m^3/m^3), with Size (μm).

not expected to cause any significant error in terms of the total gas consumed for hydrate formation.

Therefore, the inability to measure particles above 600 μm would cause errors in terms of the total mass of the hydrates and hence the total moles of gas consumed for hydrate formation. From the obtained analyzer data at each of these points it was observed that the largest particles were well below 600 μm in size. Appendix D shows the raw data from the analyzer at different times. It can then be concluded that in our experimental setup the entire particle population lies in the range $2r_c < \text{particle size} < 600 \mu\text{m}$ where $2r_c$ is the critical particle diameter below which a hydrate particle cannot exist (Refer Appendix A).

4.3.7 Second Moment of Particle Size Distribution

For a particle size distribution (Refer Appendix C), the total area density is given by the expression

$$A = \beta \int_0^{\infty} \phi(x) x^2 dx \quad 4.1$$

where,

- A =Total surface area of particles per unit volume of sample
- β =Surface shape factor of particles
- ϕ (x)=Number distribution function
- x =Particle diameter or size

or,

$$A = \beta \mu_2 \quad 4.2$$

where,

μ_2 =Second Moment of Particle Size Distribution

For spherical particles $\beta=\pi$. Second moment was computed from the data given in Section 4.3.2 and is plotted from the onset of turbidity till the experiment end, in Figure 4.24.

4.3.8 Gas Consumption in Hydrate Formation

The gas moles consumed in hydrate formation can be computed from two sources. First, using the DORIC data acquisition system as discussed in section 4.2 and second, from the particle analyzer data. Of the total gas consumed in a kinetic experiment (Figure 4.1), part of it is dissolved in the bulk water and the remaining gas is consumed for hydrate formation. For details refer to Appendix A.

At any point in time along the gas consumption curve of section 4.2, after the onset of turbidity, the total gas moles in hydrate form can be computed from the particle volume density data, at that point, by simple stoichiometry, assuming thermodynamic occupation of cavities by the gas molecules. Figure 4.25 is a plot of the gas moles consumed in hydrate formation as computed from the analyzer data (particle volume density). Figure 4.26 compares the gas moles consumed in hydrate formation as obtained from the two sources discussed above. Discussion follows in Section 5.3.

4.3.9 Median Particle Size

Figure 4.27 is a plot of the median particle size for each data acquisition from the onset of turbidity till the experiment end. The median particle size is limited to 7 ± 1 μm for the entire experiment. Therefore, while the total number of particles continues to increase the

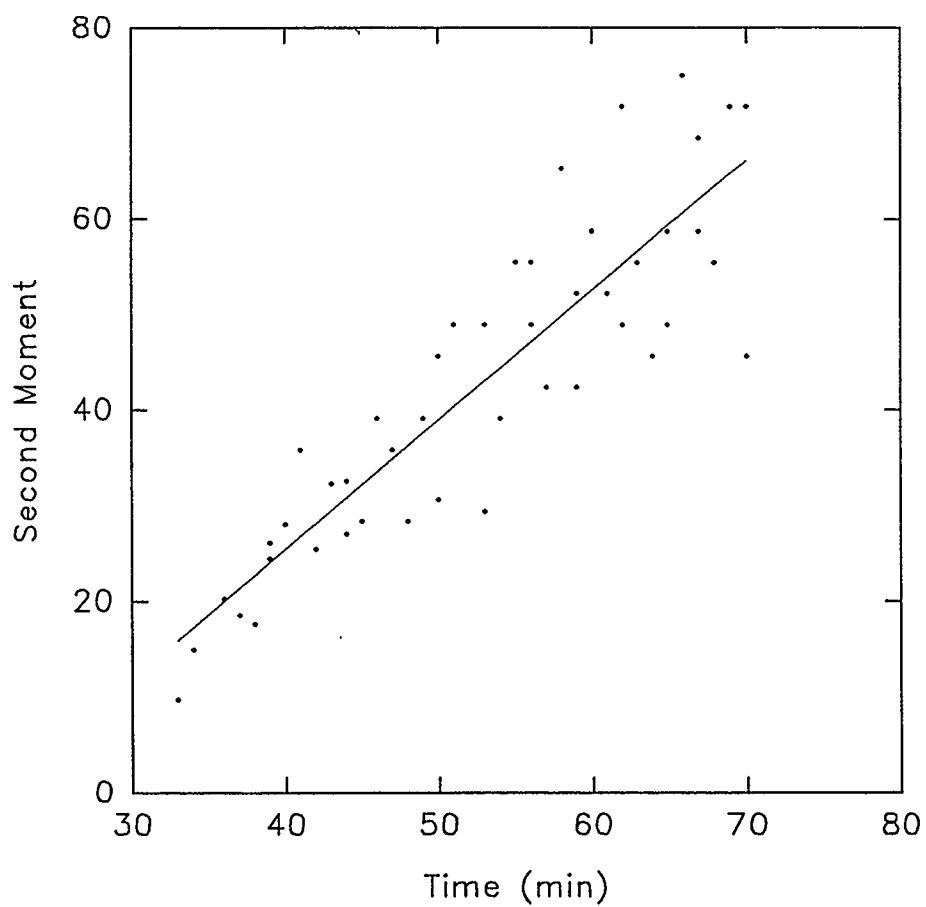


Figure 4.24 Second Moment of Particle Size Distribution, μ_2 (m^2/m^3), vs Time (min).

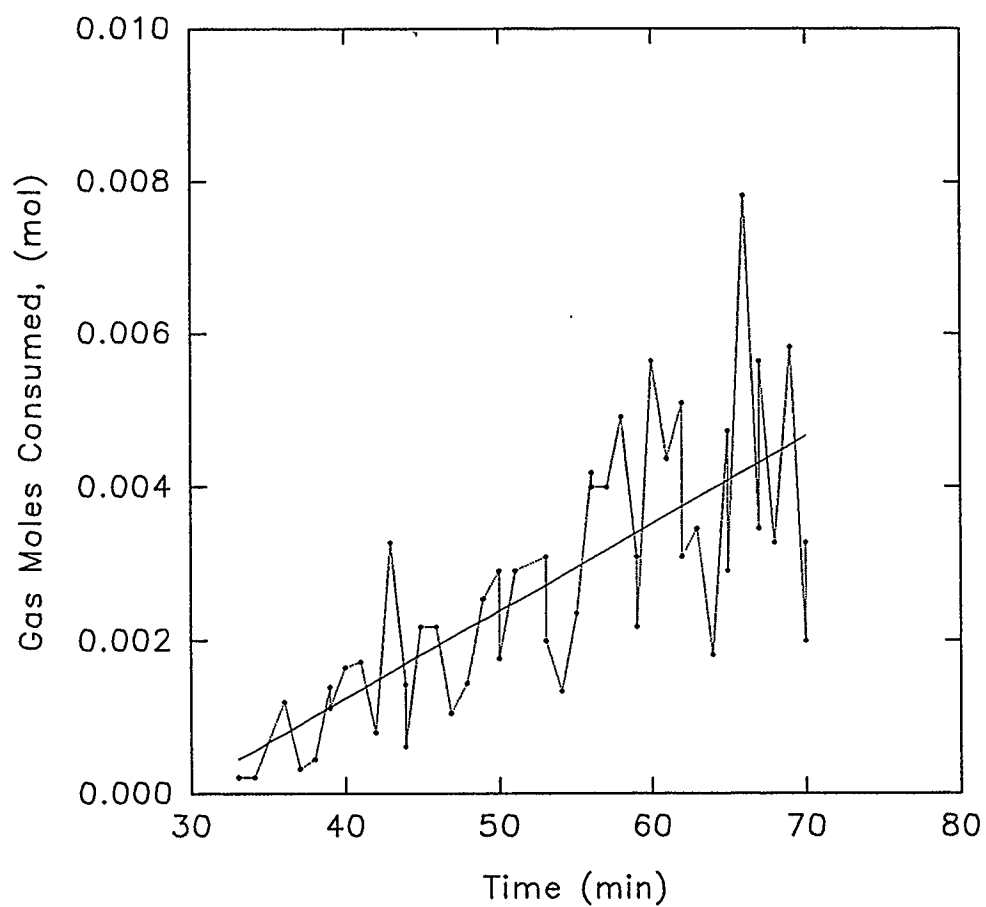


Figure 4.25 Gas Moles Consumed for Hydrate Formation vs Time (min) ("dots" indicate data points. A straight line is regressed through the data).

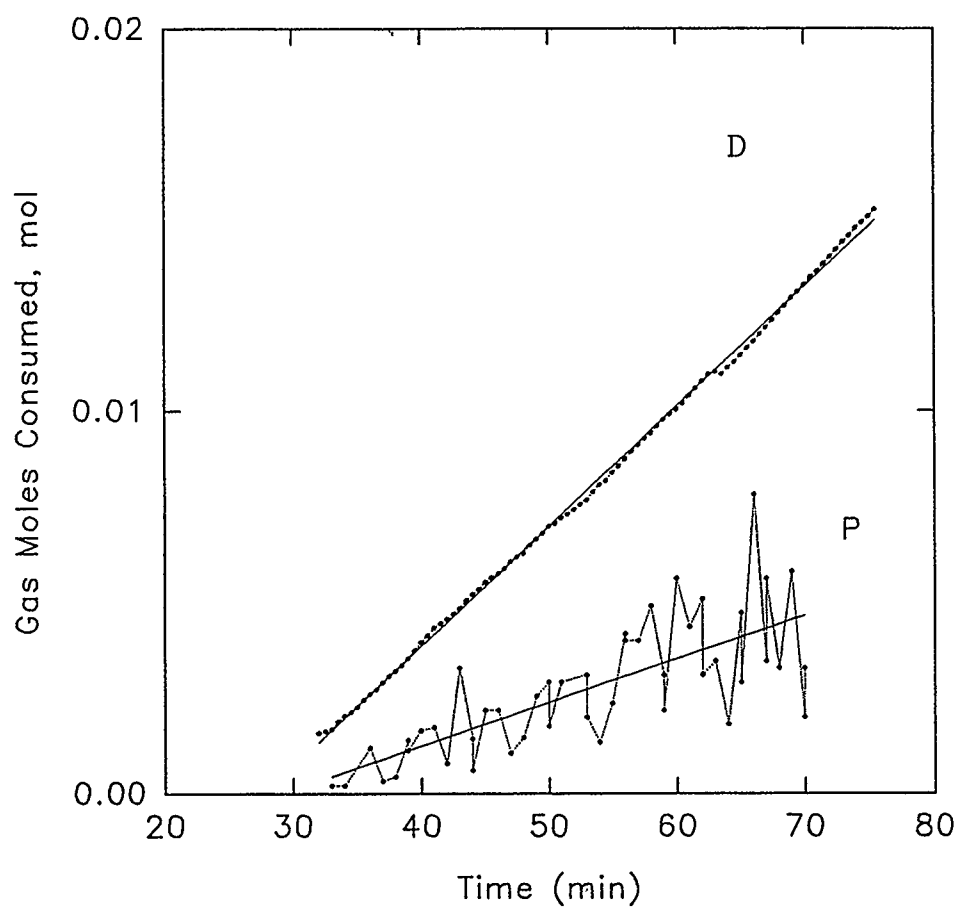


Figure 4.26 Gas Moles Consumed for Hydrate Formation vs Time (min) ("D": DORIC and "P": Analyzer. "Dots" indicate data points).

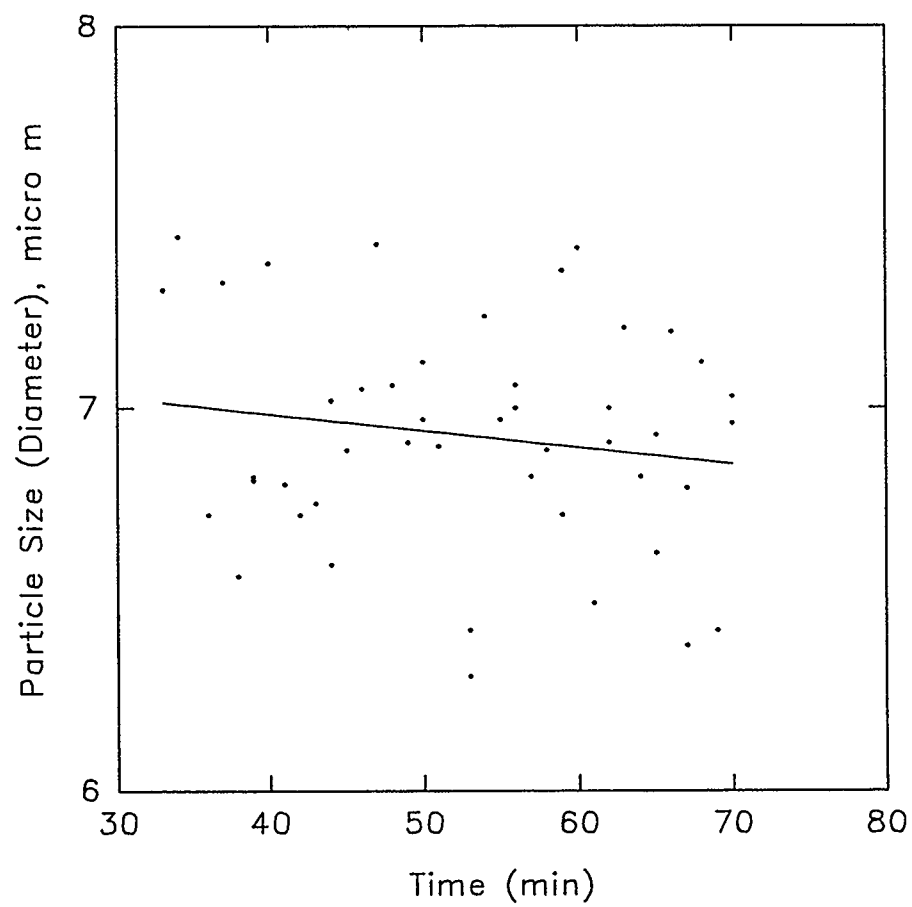


Figure 4.27 Median Particle Size (Diameter, μm) vs Time (min).

median particle size remains almost unchanged. Similar results were obtained for other experiments as well, both for ethane as well as methane.

5.0 DISCUSSION OF RESULTS

To facilitate better understanding, as in chapter 4, only one kinetic experiment, E007 for ethane is discussed in detail here. It is re-emphasized that the discussion is relevant to all other experiments as well due to the similarity in the nature of the data. For the sake of comparison, certain results from other experiments will be presented as well.

5.1 Particle Size and Hydrodynamics

As discussed in section 4.3.9, Figure 4.27, the median particle size for both ethane and methane experiments remain in the size range $7 \pm 1 \mu\text{m}$ throughout the experiment. This is because, as observed from the analyzer data, the distribution of particle number density for the entire experiment remains more or less constant. At the onset of turbidity, the two parameters, the thermodynamic driving force ($f-f_{\text{eq}}$) and the hydrodynamics of the system determine the hydrate growth rate and particle size. Stirring (at 400 rpm) in the reactor has a two-fold influence on hydrate particles.

Firstly, it causes mechanical shear of particles because of particle-stirrer, particle-baffle, particle-particle and particle-wall interactions. The analyzer circuit causes mechanical shear as well. Thus, the mechanical shear controls the particle size range which remains more or less constant (within 0-600 microns) throughout the experiments.

Secondly, the stirring reduces the mass transfer resistance around the particles. For our experimental setup this resistance is virtually eliminated (Englezos et al., 1987).

So, while the particle size range is more or less constant throughout each experiment, maintaining the thermodynamic driving force ($f-f_{\text{eq}}$) constant during experiments causes the hydrate mass to grow. Since, the median size is almost constant, this mass growth occurs in terms of an ever increasing number density. According to Englezos et al. (1987),

there is no further primary nucleation after the turbidity point (this is because the energy barrier to form a new nucleus is greater than that of the enclathration of gas into an existing nucleation centre). Therefore, the new growth centres which cause an increase in the number density must come from secondary nucleation. It can therefore be concluded that the hydrodynamics of the system is responsible for mechanical shear of the particles. It keeps them within a certain size range and causes the formation of new growth centres which then grow as a result of the thermodynamic driving force ($f-f_{eq}$) and break down to form new particles thereby increasing the number density. The growth process thus comprises of simultaneous growth and breakage of particles.

5.2 Extrapolation of Data

The Galai particle size analyzer hardware has been set to measure particles in the range 5-600 μm (chapter 4, section 4.3). It was observed from the experimental data that the distributions of particle number density for both ethane and methane were always well below 600 μm throughout the experiments. Therefore, the distributions were measured completely on the larger particle size range, but not below 5 microns. Extrapolation of the data was performed for evaluation of the distributions below 5 μm .

From chapter 4, section 4.3.4 it was shown that the distributions of number density could be approximated as being log-normal in nature. Based on this assumption, we proceeded to extrapolate the data below size 5 microns. Refer Appendix C for a detailed discussion on particle size analysis.

Between any two particle sizes, x_1 and x_2 , the particle number density, $N(\#/m^3)$, is given by the equation,

$$N = \int_{x_1}^{x_2} \phi(x) dx \quad 5.1$$

where,

$\phi(x)$ = Number Distribution Function

x = Particle Size or Diameter

The particle area density, A (m^2/m^3), is given by the equation,

$$A = \beta \int_{x_1}^{x_2} \phi(x) x^2 dx \quad 5.2$$

where,

β = Surface Shape Factor

β = π for Spherical Particles

and the particle volume density, V (m^3/m^3), is given by the equation

$$V = \alpha \int_{x_1}^{x_2} \phi(x) x^3 dx \quad 5.3$$

where,

α = Volume Shape Factor

α = $\pi/6$ for Spherical Particles

The number distribution function, $\phi(x)$, is obtained from the Cumulative Oversize Number Distribution Function. Equation 5.4 is a cumulative (log-normal) number distribution function that was fitted to our data using Jandel Scientific regression software package.

$$y = a + 0.5b \operatorname{Erfc}(-\ln(c/x)/(2^{0.5}d)) \quad 5.4$$

where a,b,c and d are adjustable constants.

Therefore, the number distribution function $\phi(x)$ is given by

$$\phi(x) = \frac{dy}{dx} \quad 5.5$$

$$\phi(x) = \left(-\frac{b}{d\sqrt{2\pi}}\right)\left(\frac{1}{x}\right)\text{Exp}\left(-0.5\left(\frac{\ln(c/x)}{d}\right)^2\right) \quad 5.6$$

By substituting Equation 5.6 into Equations 5.1,5.2 and 5.3, the number, area and volume distributions below $5\mu\text{m}$ can be evaluated.

Figures 5.1 and 5.2 show cumulative number oversize distributions for the ethane experiment E007 at times 33, 48, 60, 63 minutes from the start of the experiment, corresponding to times 33, 48, 60 and 63 minutes on the gas consumption curve of chapter 4, section 4.2, Figure 4.1. The number distribution function, $\phi(x)$, was obtained and the particle number, area and volume distributions evaluated for particles below 5 microns, using equations 5.1, 5.2 and 5.3. Integrations were performed using a numeric computation software (MATLAB), using Simpson's rule.

Since, from the analysis, the number of particles below 5 microns are now available, we know the total number of particles in the range $2r_c < \text{size} < 600$ microns and can therefore plot the number distributions as a percentage of particles corresponding to a particular size range. Figures 5.3 to 5.6 show the completed distributions of particle number density between the particle size range $2r_c < \text{size} < 600 \mu\text{m}$, where $2r_c$ is the critical particle size or diameter, below which a hydrate particle is thermodynamically unstable and cannot exist (Refer Appendix A for details on the estimation of r_{cr}).

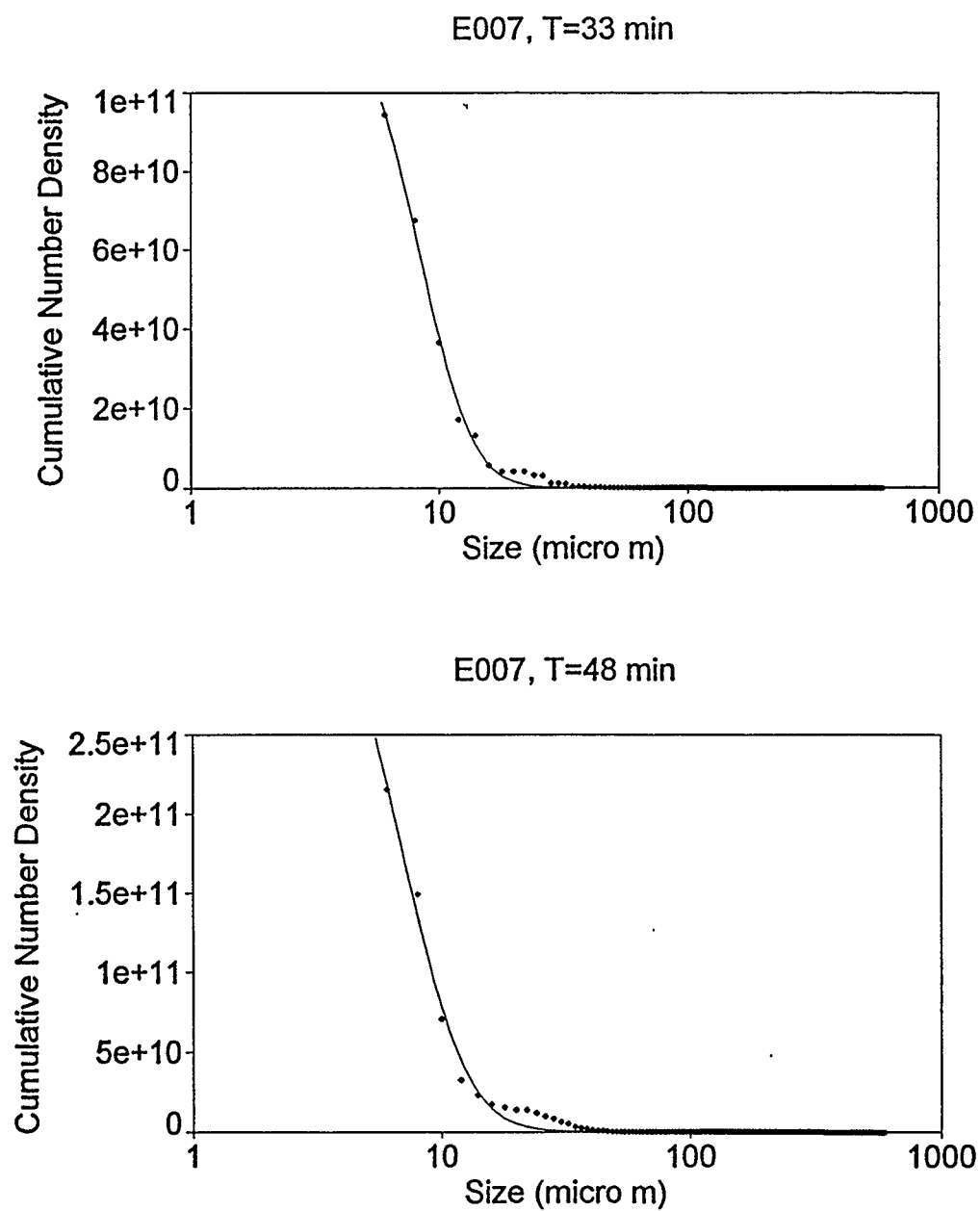


Figure 5.1 Cumulative Number Density Oversize ($\#/m^3$) vs Size (μm).

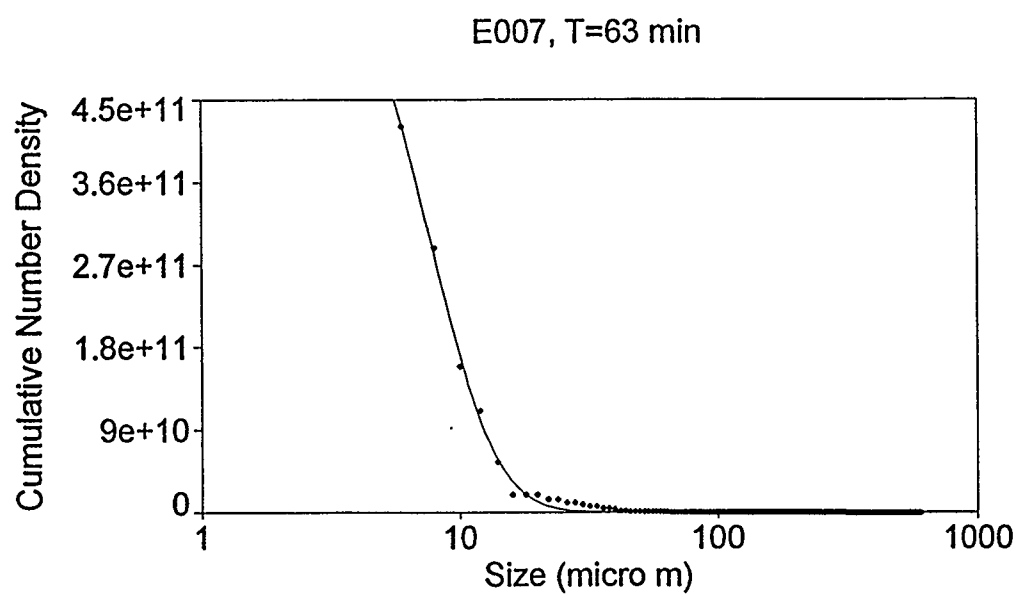
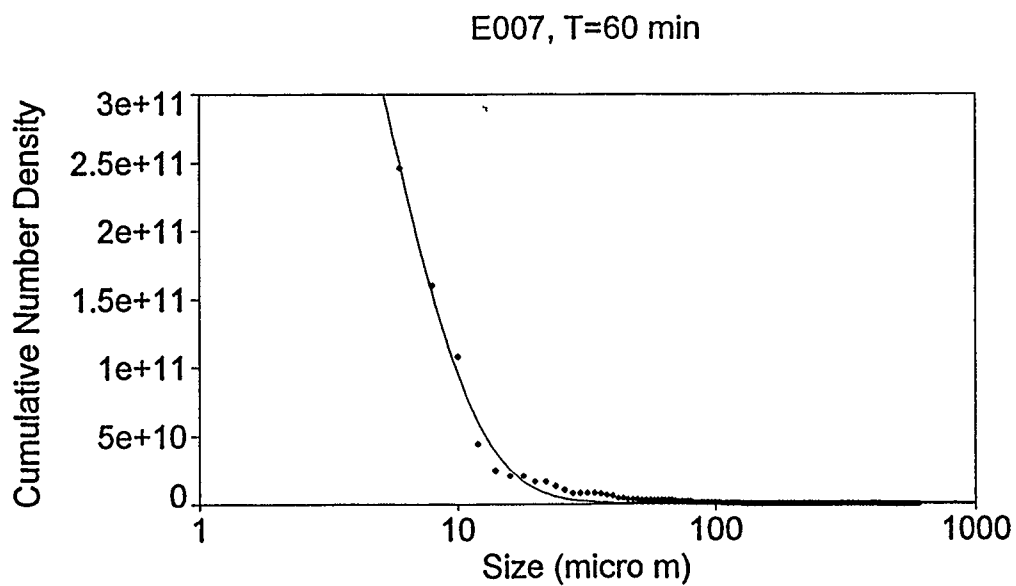


Figure 5.2 Cumulative Number Density Oversize ($\#/m^3$) vs Size (μm).

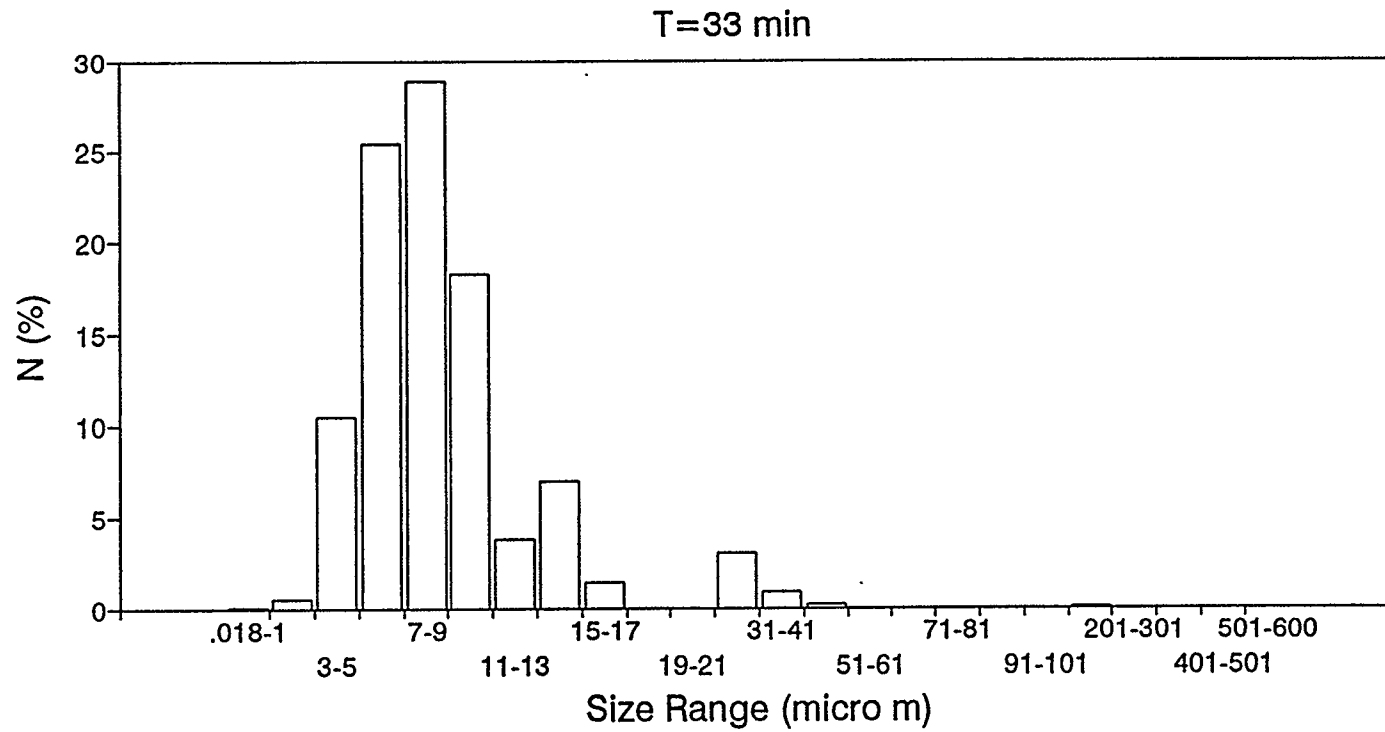


Figure 5.3 Distribution of Particle Number Density, N (%), with Size (μm).

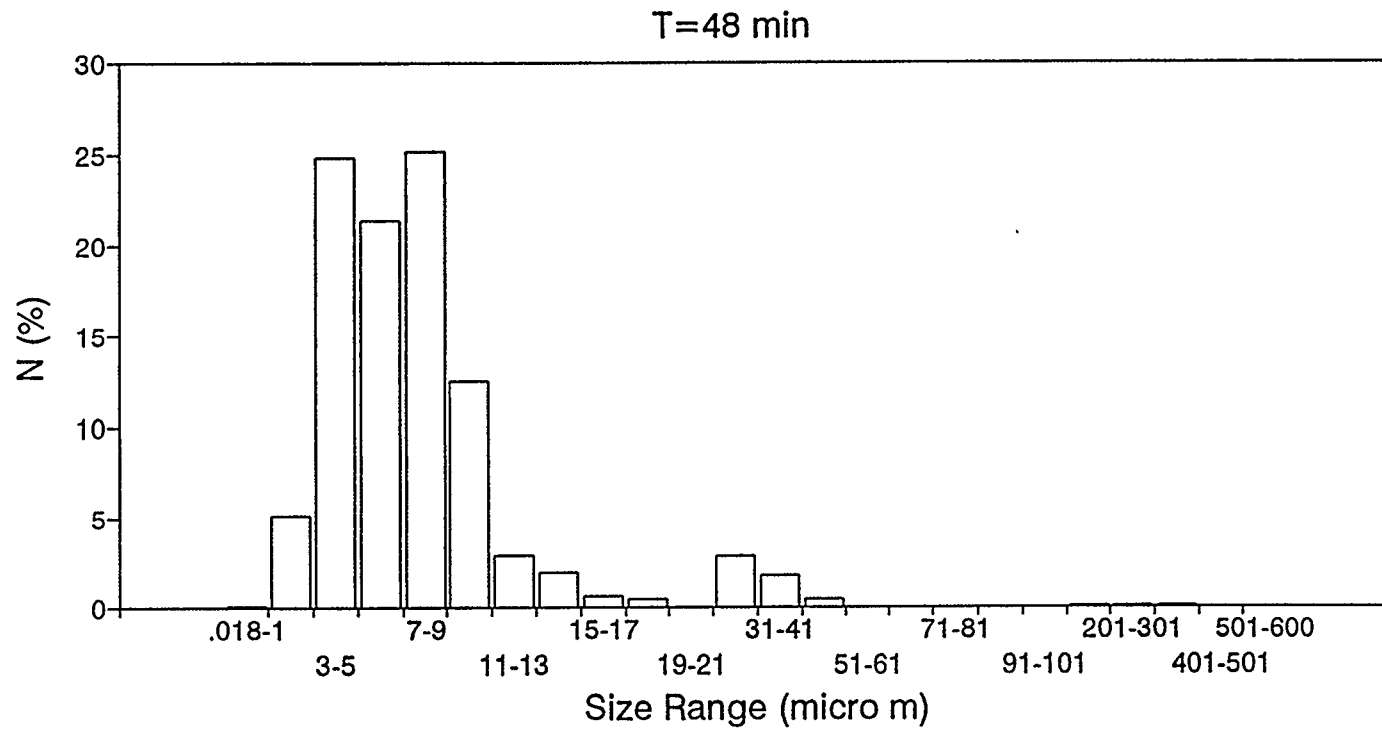


Figure 5.4 Distribution of Particle Number Density, N (%), with Size (μm).

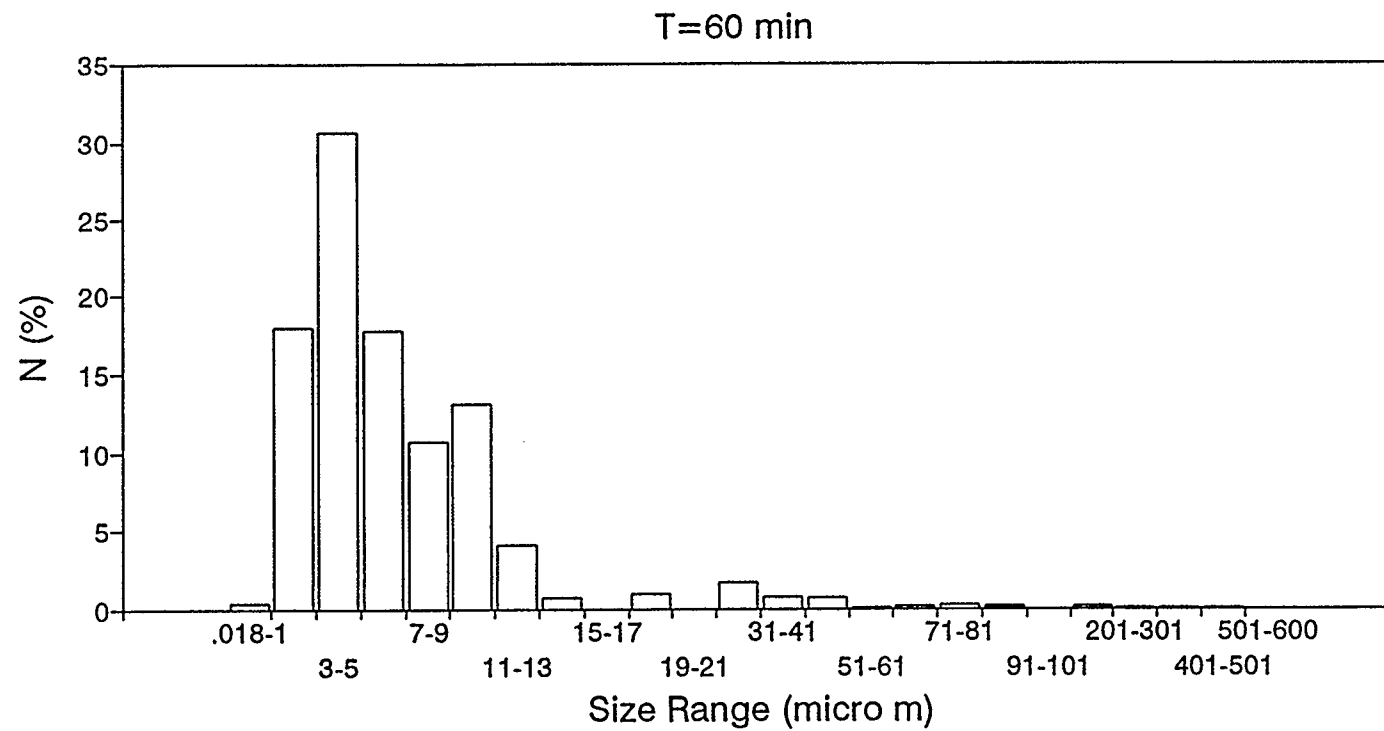


Figure 5.5 Distribution of Particle Number Density, N (%), with Size (μm).

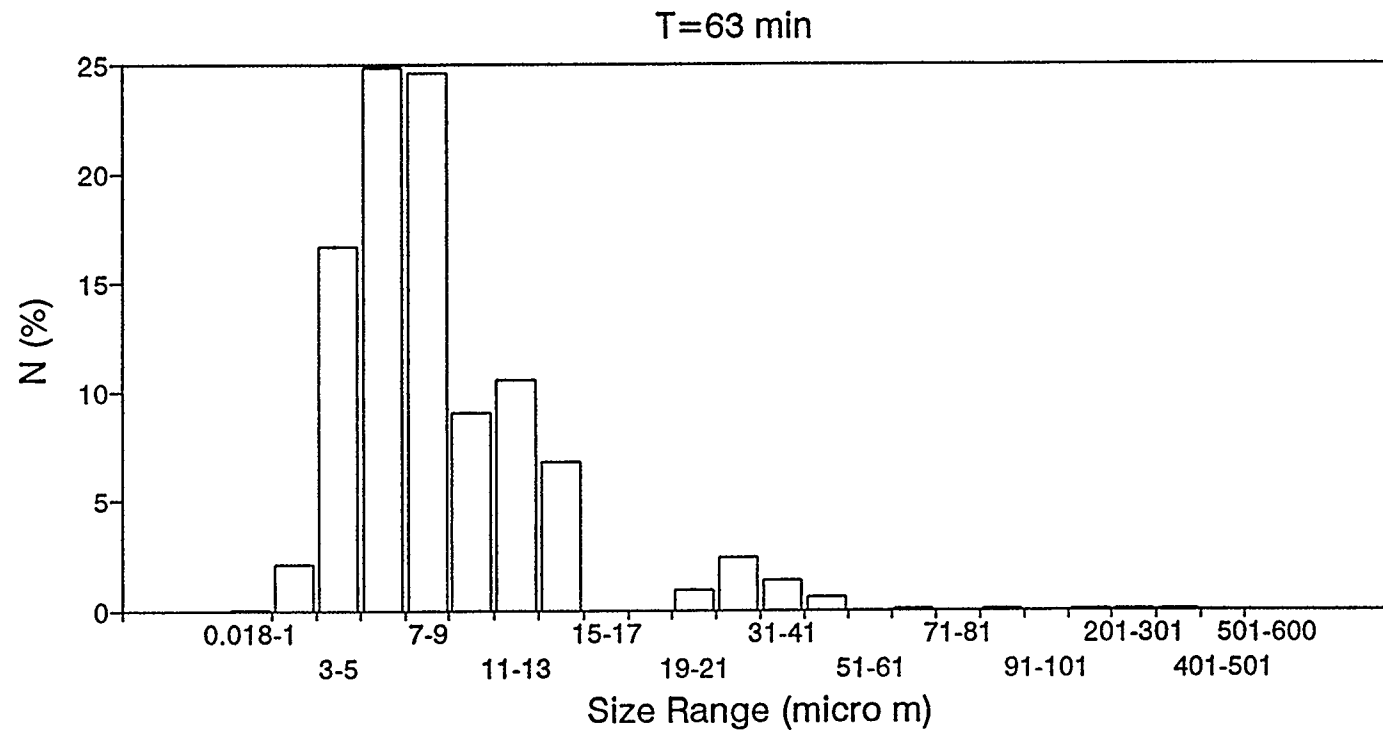


Figure 5.6 Distribution of Particle Number Density, N (%), with Size (μm).

Figures 5.7 to 5.10 are the complete distributions of area density for the same time points and Figures 5.11 to 5.14 are the complete distributions of volume density for the same time points.

It can clearly be observed from the analysis that the contribution of particles below 5 μm is *significant* in number distributions, *very small* in area distributions and *insignificant* in volume distributions.

Similar calculations were performed on other ethane and methane experiments and the results in terms of the percentage contribution of the particles below 5 μm to the number, area and volume distributions are listed in Tables 5.1, 5.2, 5.3 and 5.4 for experiments E007, E009, M014 & M015. While the contribution of particles below 5 μm to the number distributions is significant, the area contributions are always below 5% and the volume contributions below 1%.

Volume contribution and therefore the mass contribution of these hydrate particles is negligible. The moles of gas in these small particles is less than 1% of the total moles in hydrate form. Thus, the error contribution of these particles, not being measured by the laser analyzer, to the total gas moles consumed for hydrate formation is negligible. Hence, there is no loss in the moles of gas in hydrate form by not measuring these small particles. Similarly, the area contribution of these particles is always less than 5%. It can safely be concluded that neglecting these particles in terms of the particle volume densities and area densities results in negligible error.

5.3 Mole Balance and Shape Factor

As discussed in Chapter 4, Section 4.3.8, the gas moles in the hydrate are computed from two sources, DORIC, the overall data acquisition system and the Galai Particle Size

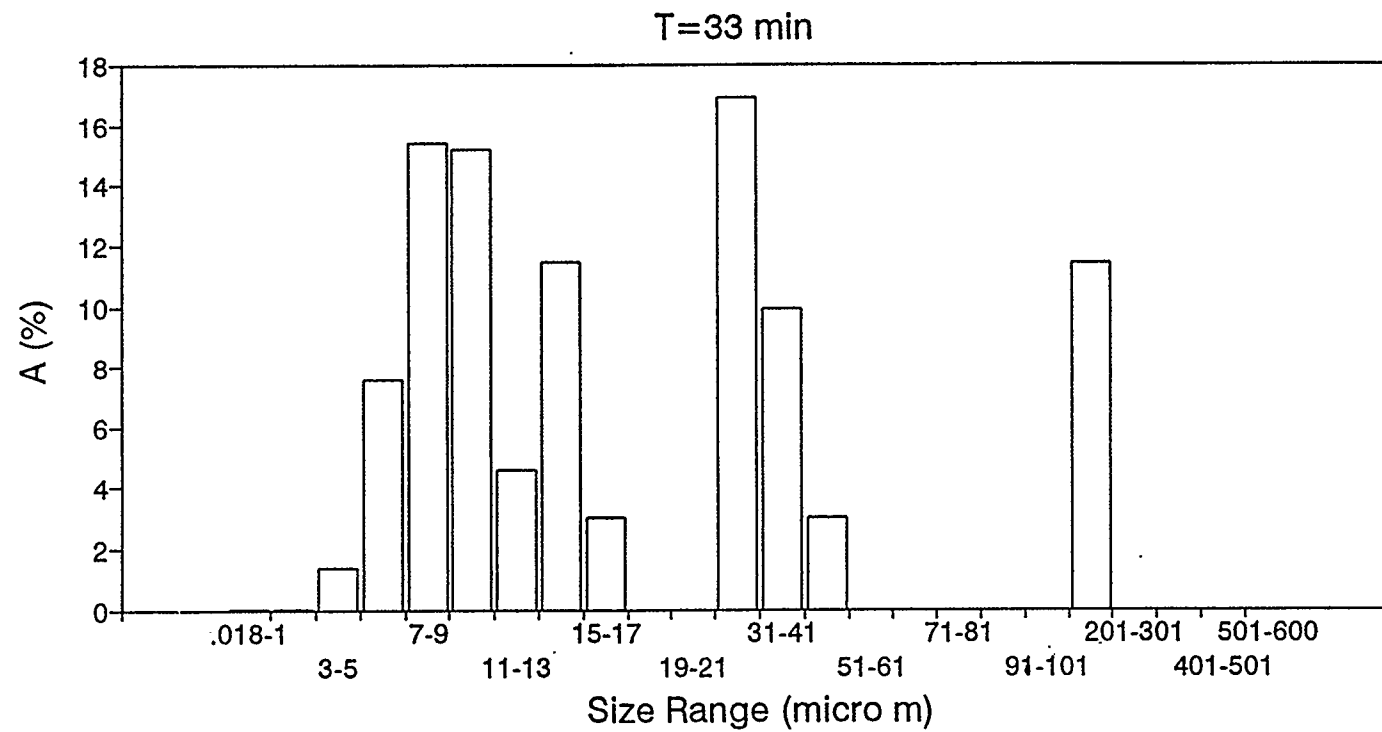


Figure 5.7 Distribution of Particle Area Density, A (%), with Size (μm).

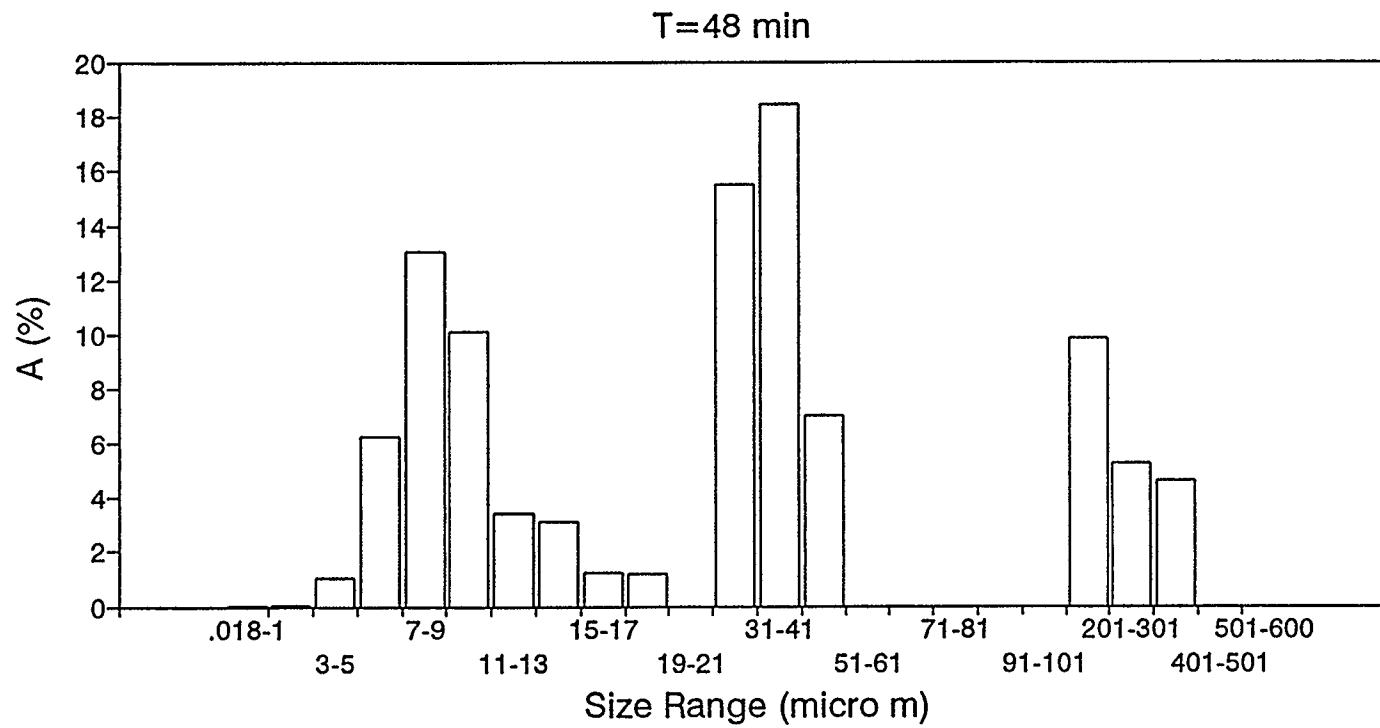


Figure 5.8 Distribution of Particle Area Density, A (%), with Size (μm).

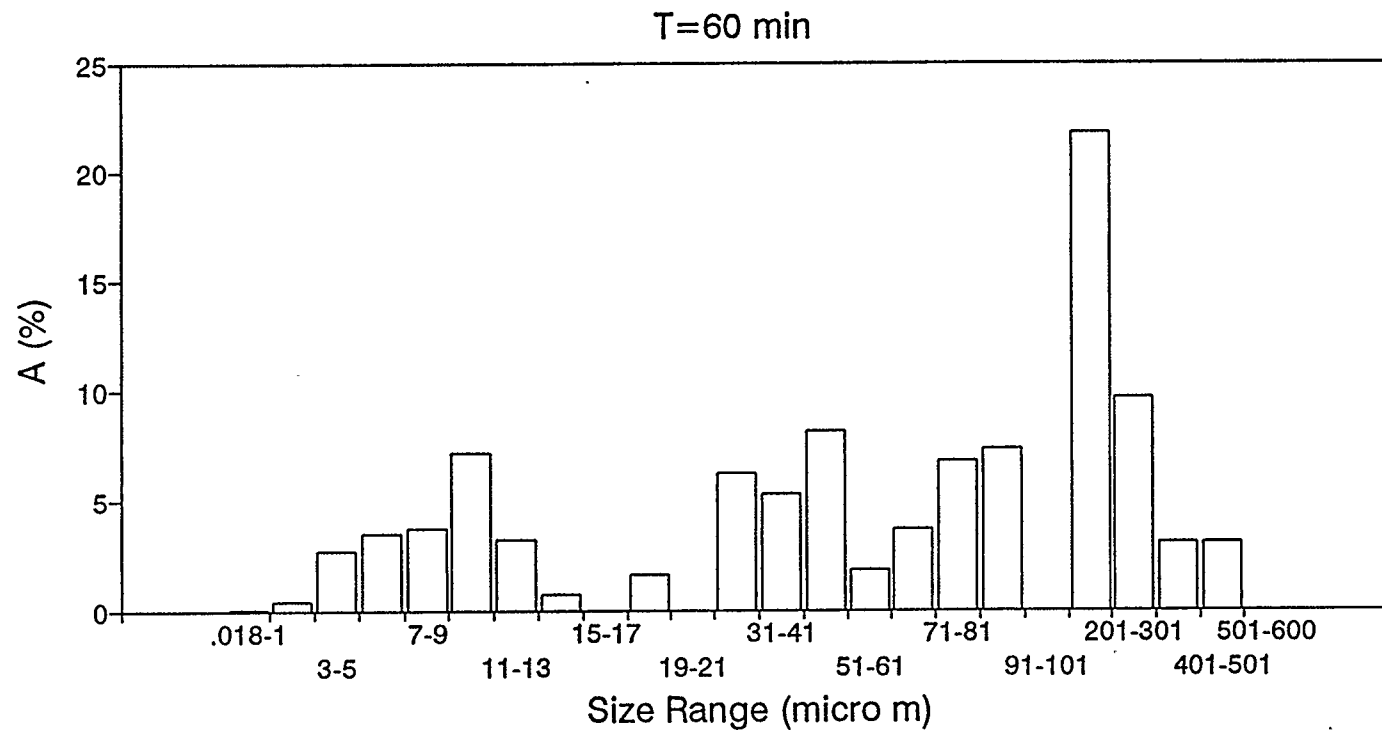


Figure 5.9 Distribution of Particle Area Density, A (%), with Size (μm).

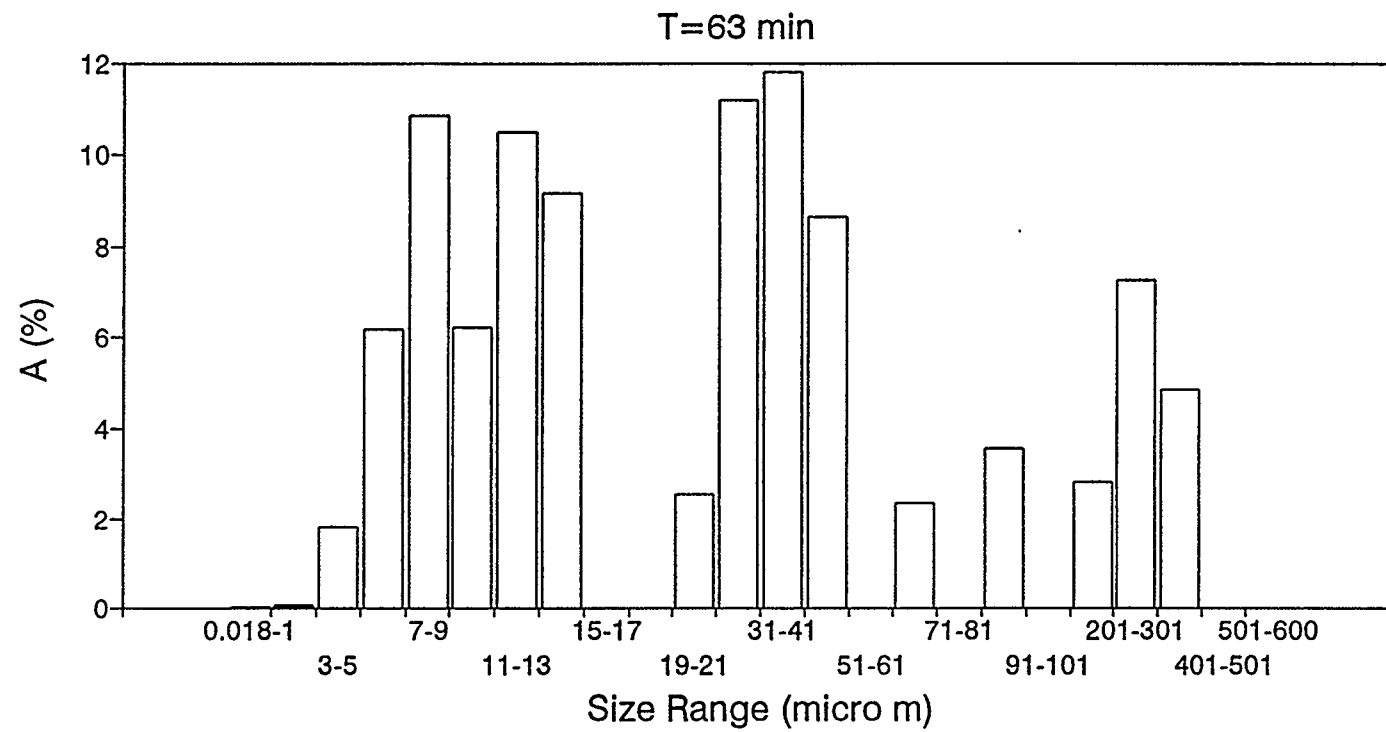


Figure 5.10 Distribution of Particle Area Density, A (%), with Size (μm).

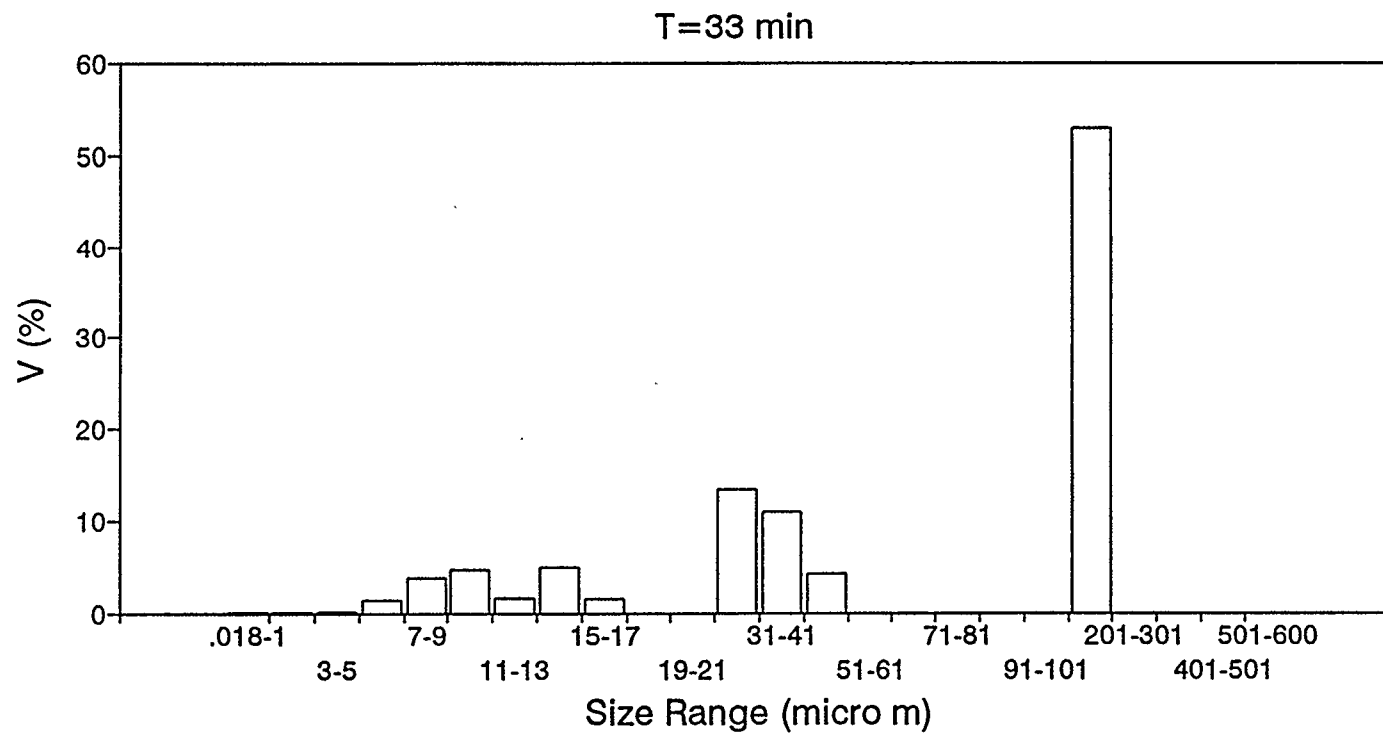


Figure 5.11 Distribution of Particle Volume Density, V (%), with Size (μm).

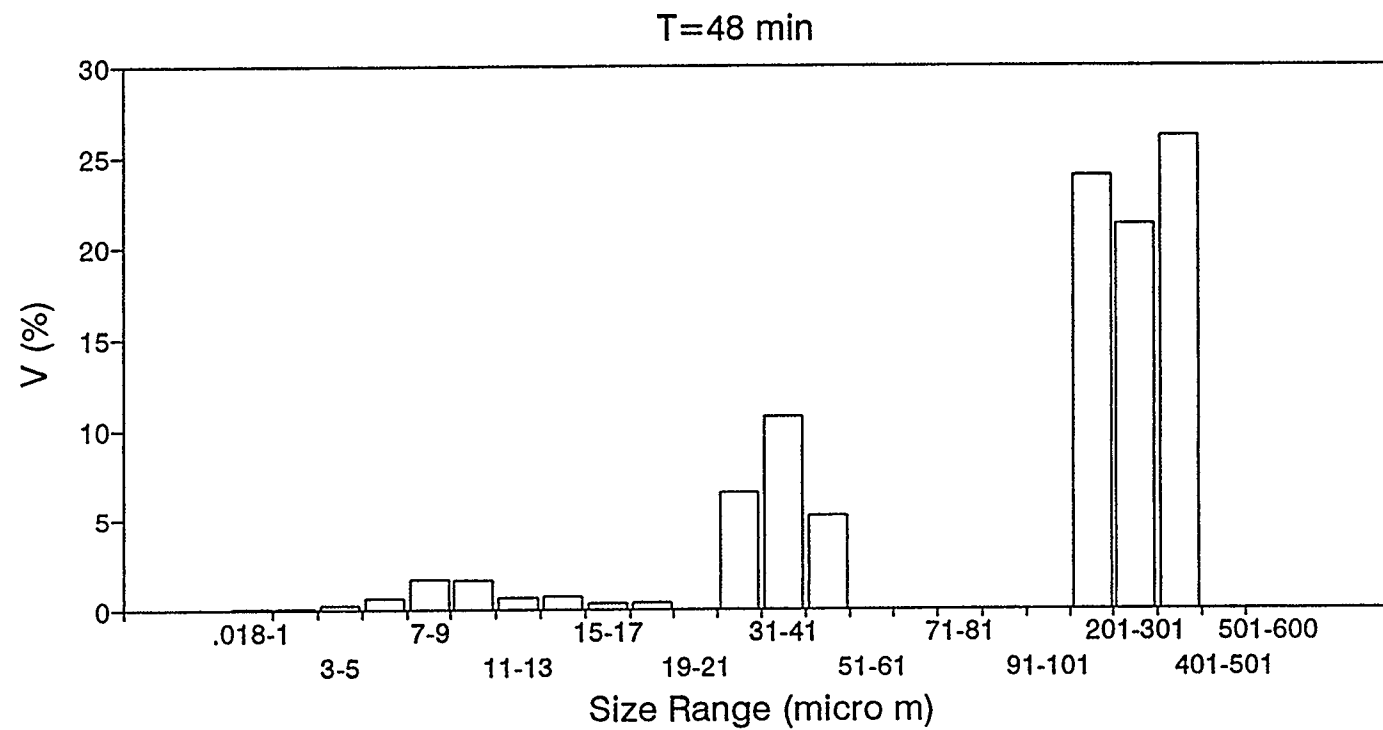


Figure 5.12 Distribution of Particle Volume Density, V (%), with Size (μm).

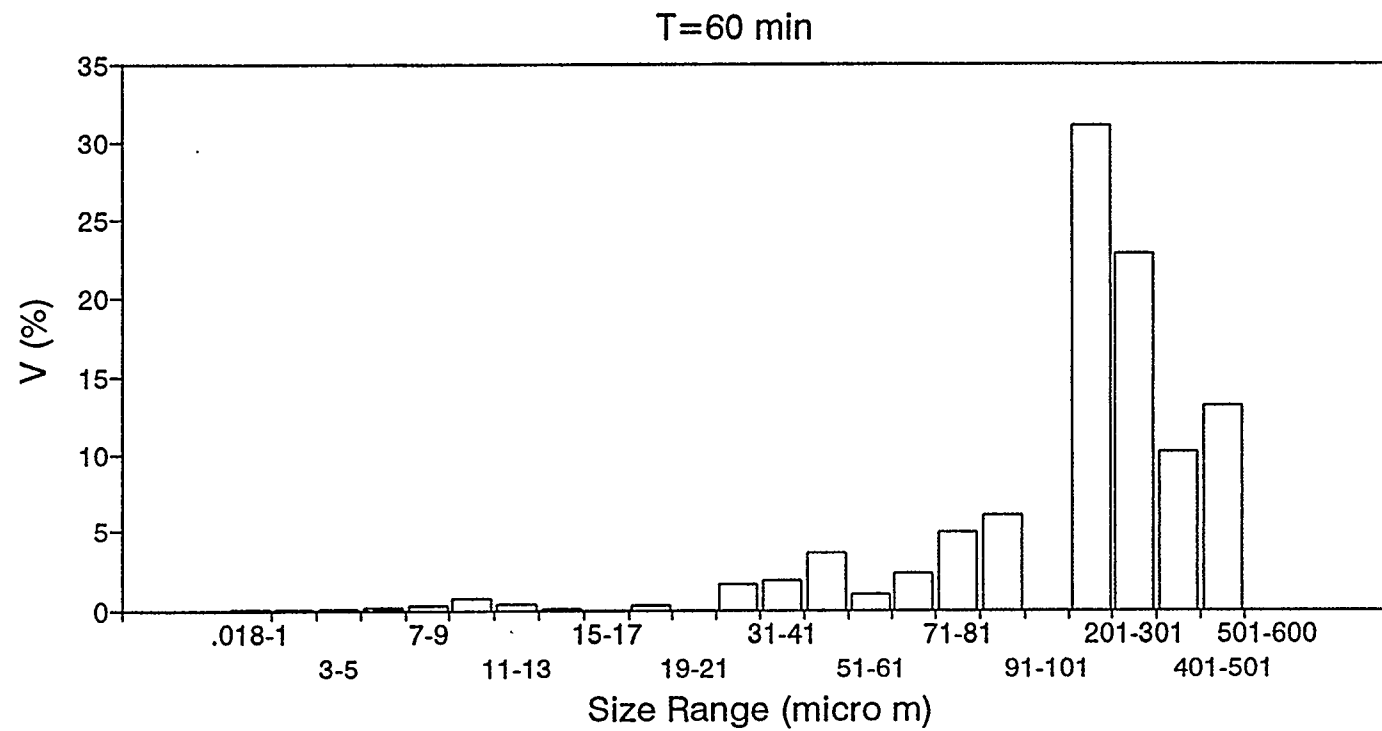


Figure 5.13 Distribution of Particle Volume Density, V (%), with Size (μm).

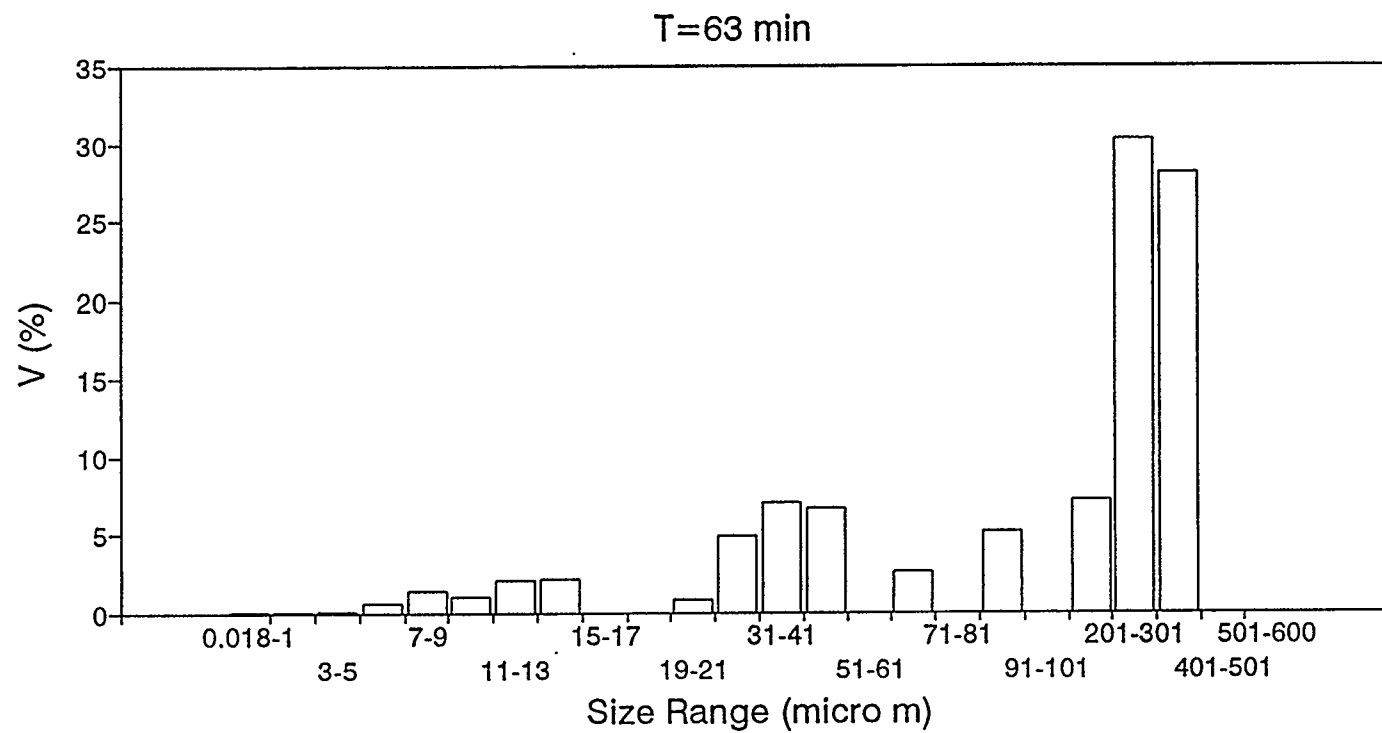


Figure 5.14 Distribution of Particle Volume Density, V (%), with Size (μm).

Particle Number Density (%)

Time (min)	3-5 μm	1-3 μm	.018-1 μm
33	10.47	0.54	3.96E-6
48	24.98	5.19	4.08E-3
60	30.81	17.99	0.34
63	16.95	2.11	3.70E-3

Particle Area Density (%)

Time (min)	3-5 μm	1-3 μm	.018-1 μm
33	1.53	0.02	9.00E-9
48	3.69	0.19	9.50E-6
60	3.50	0.51	5.90E-4
63	2.15	0.07	7.34E-9

Particle Volume Density (%)

Time (min)	3-5 μm	1-3 μm	.018-1 μm
33	0.26	1.65E-3	1.9E-10
48	0.30	7.86E-3	9.67E-8
60	0.15	0.01	3.26E-6
63	0.15	2.29E-3	6.23E-12

Table 5.1 Experiment E007.

Particle Number Density (%)

Time (min)	3-5 μ m	1-3 μ m	.018-1 μ m
66	1.56	6.88E-3	5.65E-12
73	3.55	0.04	6.3E-10
88	30.20	15.75	0.22
97	31.65	13.13	0.08

Particle Area Density (%)

Time (min)	3-5 μ m	1-3 μ m	.018-1 μ m
66	0.21	2.22E-4	1.14E-14
73	0.54	1.37E-3	1.5E-12
88	3.91	0.70	6.2E-4
97	4.10	0.51	1.94E-4

Particle Volume Density (%)

Time (min)	3-5 μ m	1-3 μ m	.018-1 μ m
66	0.03	1.78E-5	2.30E-16
73	0.11	1.44E-4	3.95E-14
88	0.51	0.03	7.31E-6
97	0.21	0.01	1.04E-6

Table 5.2 Experiment E009.

Particle Number Density (%)

Time (min)	3-5 μ m	1-3 μ m	.018-1 μ m
48	6.15	0.12	2.3E-8
84	14.94	1.00	1.58E-5
100	12.73	0.70	5.33E-6
112	17.07	1.61	8.88E-5

Particle Area Density (%)

Time (min)	3-5 μ m	1-3 μ m	.018-1 μ m
48	1.02	5.02E-3	5.97E-11
84	1.76	0.03	2.90E-8
100	1.32	0.02	8.65E-9
112	1.60	0.04	1.30E-7

Particle Volume Density (%)

Time (min)	3-5 μ m	1-3 μ m	.018-1 μ m
48	2.39E-11	5.87E-14	1.75E-22
84	0.12	9.75E-4	2.40E-10
100	0.07	4.76E-4	5.65E-11
112	0.08	9.41E-4	8.12E-10

Table 5.3 Experiment M014.

Particle Number Density (%)

Time (min)	3-5 μm	1-3 μm	.018-1 μm
61	1.78	4.18E-3	1.90E-13
88	6.99	0.11	7.25E-9
116	9.45	0.35	6.73E-7
124	12.00	0.79	1.17E-5

Particle Area Density (%)

Time (min)	3-5 μm	1-3 μm	.018-1 μm
61	0.22	1.31E-4	3.72E-18
88	0.87	3.52E-3	1.41E-13
116	0.89	8.27E-3	9.96E-12
124	1.14	0.02	1.74E-10

Particle Volume Density (%)

Time (min)	3-5 μm	1-3 μm	.018-1 μm
61	2.67E-12	7.85E-16	5.56E-31
88	0.05	1.01E-4	1.01E-16
116	0.04	2.07E-4	6.24E-15
124	0.06	4.90E-4	1.15E-13

Table 5.4 Experiment M015.

Analyzer data acquisition system. The gas moles in the hydrate as computed from the analyzer were found to be always less than those from DORIC system.

As discussed in chapter 2, section 2.2, the Galai analyzer assumes the particles to be spherical. Makogan (1981) and Nerheim (1993) have reported that ethane and methane hydrates form needle or thread like particles under static conditions. A dynamic system would cause mechanical shear on these particles causing the dimensions of the needle or thread to be reduced. Mullin (1972) states that particles that are elongated or needle shaped can be approximated as cylinders for shape factor determination.

Calculations were performed to estimate the error in volume by assuming the particle to be spherical rather than cylindrical. Cylinders of various dimensions were considered and different scenarios of laser-particle interactions assumed. The loss in particle volume in assuming it to be a sphere was found as high as 500% and greater depending on the dimensions of the cylinder.

Gas moles in hydrate form as computed from the DORIC data acquisition system are about three times those computed from the analyzer, with the analyzer moles being lesser because of hydrate particles being approximated as spheres. A cylinder of three times the volume of a sphere of equivalent diameter was considered to evaluate the volume and surface shape factors. The volume shape factor was evaluated as $\alpha=\pi/2$ and the surface shape factor as $\beta=5\pi/2$. The shape factors for both ethane and methane are assumed to be the same since their median particle sizes are the same. Figures 5.15 and 5.16 are plots of the moles in hydrate form computed from DORIC (bold) and those from the analyzer (dotted), using the new volume shape factor. It can be seen that the moles of gas from the two sources now match more closely by correcting for the shape factor.

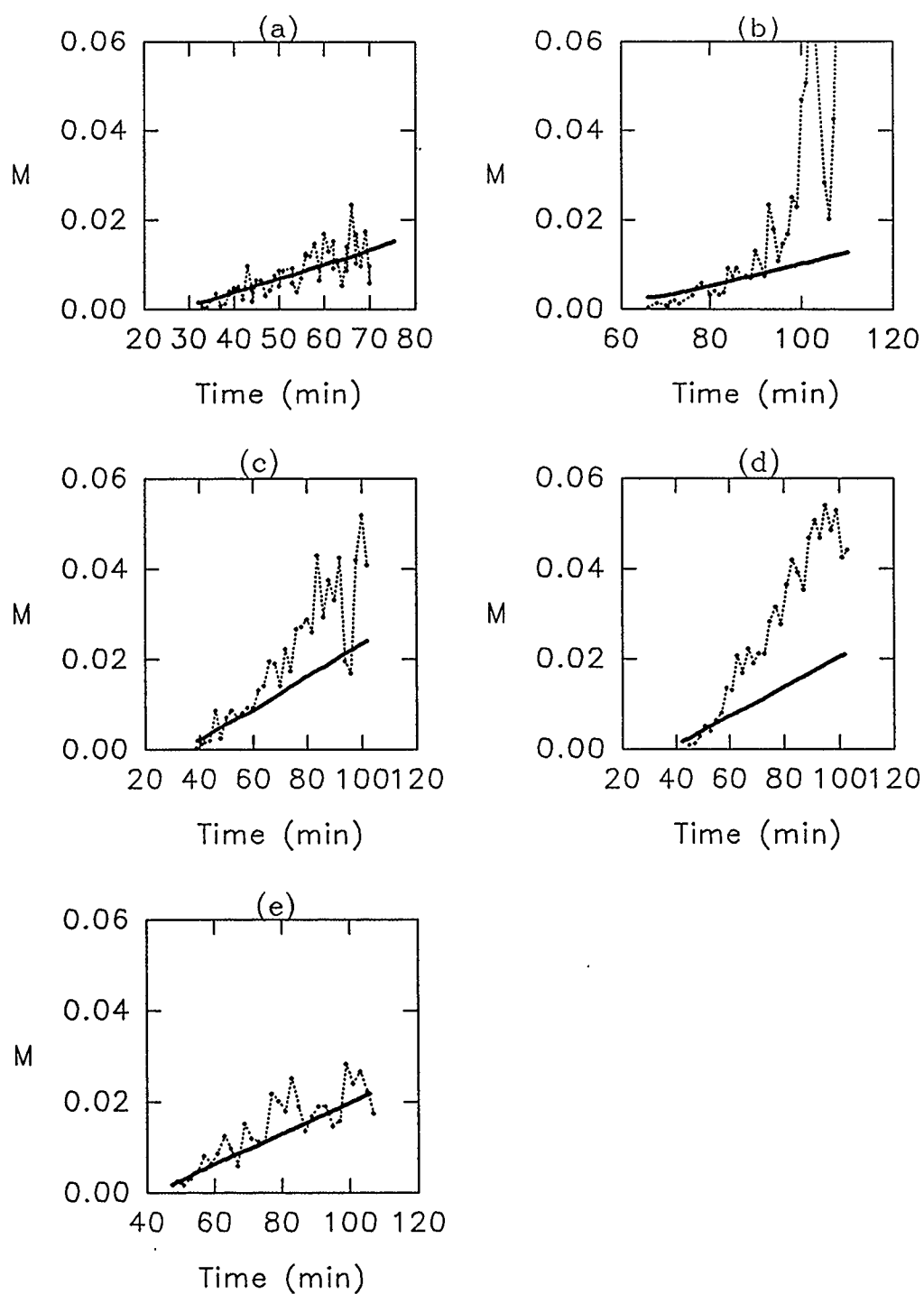


Figure 5.15 Gas Moles Consumed for Hydrate Formation, M (mol), vs Time (min) ("bold": DORIC; "dots": Analyzer) (Expt. E007-a, E009-b, E011-c, E016-d, E019-e).

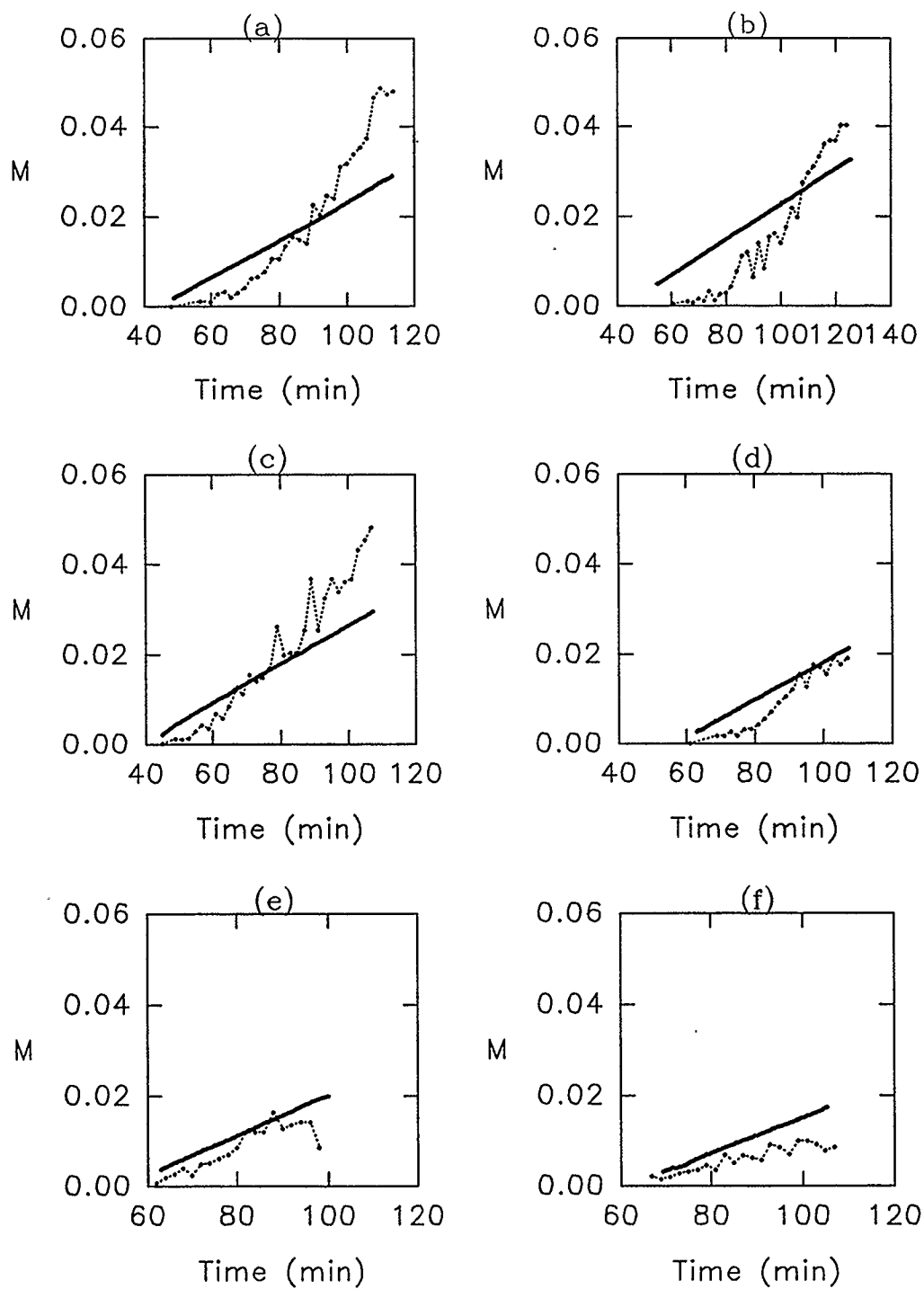


Figure 5.16 Gas Moles Consumed for Hydrate Formation, M (mol), vs Time (min) ("bold": DORIC; "dots": Analyzer) (Expt. M014-a, M015-b, M011-c, M012-d, M004-e, M005-f).

5.4 Least Squares Estimation of K^*

A total of five experiments for ethane and six for methane at three different isotherms were used for estimation of K^* . Englezos et al. (1987) reported that for each isotherm the pressure dependence of the kinetic parameter, K^* , was statistically insignificant. Therefore, it was decided to limit the number of experiments to those performed. The two differential equations 3.19 and 3.20 with their initial conditions constitute the governing equations which describe the dynamic behaviour of the physical system. Second moment (μ_2) of particle size distribution obtained from the Galai analyzer was supplied as a second order function of time. The function for each experiment is tabulated in Appendix B.

The gas moles consumed versus time experimental data obtained using DORIC were used to determine the only unknown parameter in the model which is the combined rate constant, K^* , by minimizing the sum of the squares of the difference between the model predictions and the measurements of the moles of gas consumed during hydrate formation.

The resulting nonlinear least squares problem was solved iteratively using the Gauss-Newton method (Englezos, 1986). The equations were integrated using IMSL's DGEAR differential equation solver.

For both gases three optimum parameters, one at each isotherm were computed.

Figures 5.17 shows the experimental data (bold) for ethane along with the estimated consumption curves (dotted) by the model. Figure 5.18 shows the experimental and estimated curves for methane. In these figures, the data are shown only after the onset of turbidity which is defined as the zero time in the plots.

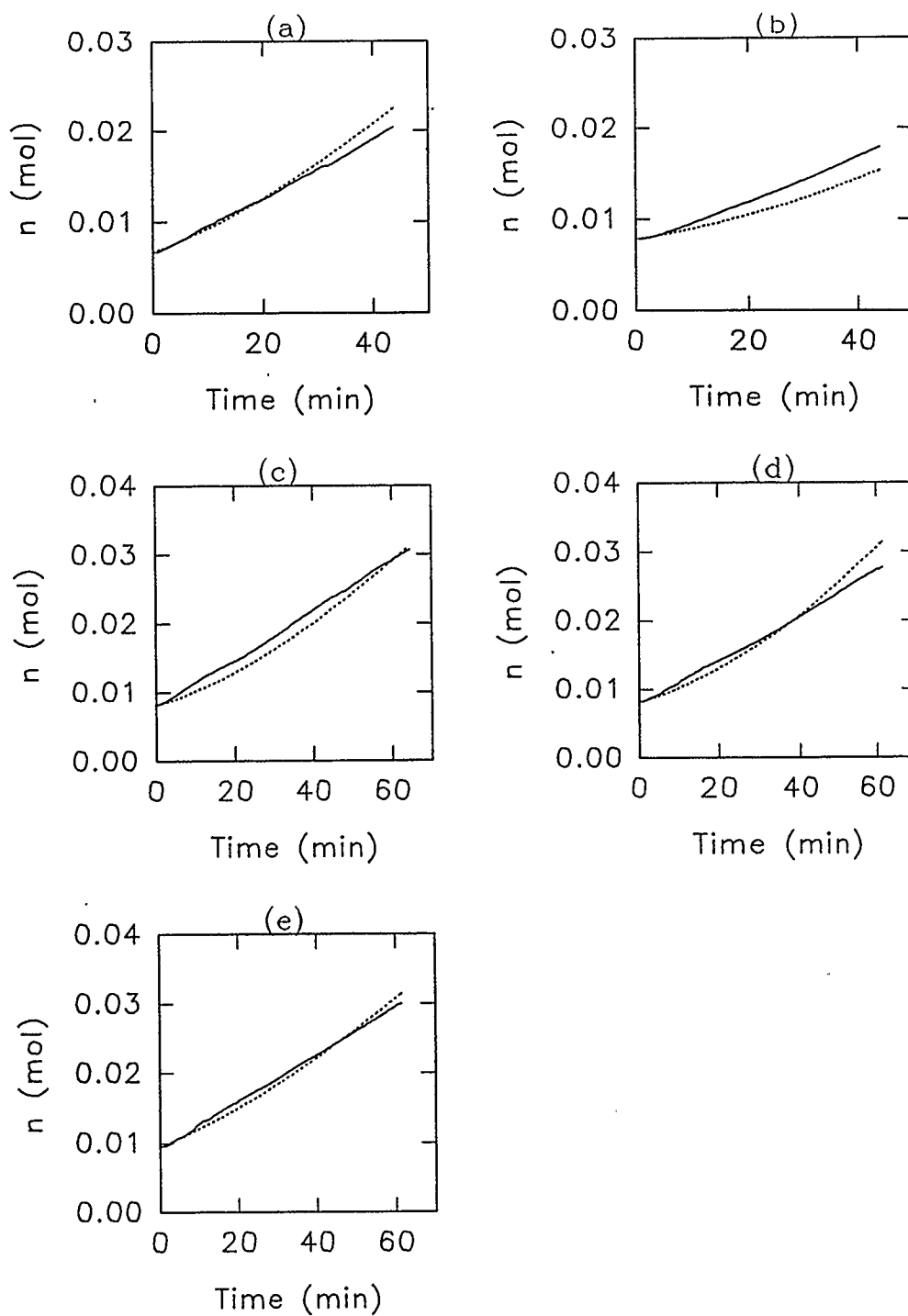


Figure 5.17 Gas Moles Consumed for Hydrate Formation, n (mol), vs Time (min) ("bold": Experimental; "dots": Predicted) (Expt. E007-a, E009-b, E011-c, E016-d, E019-e).

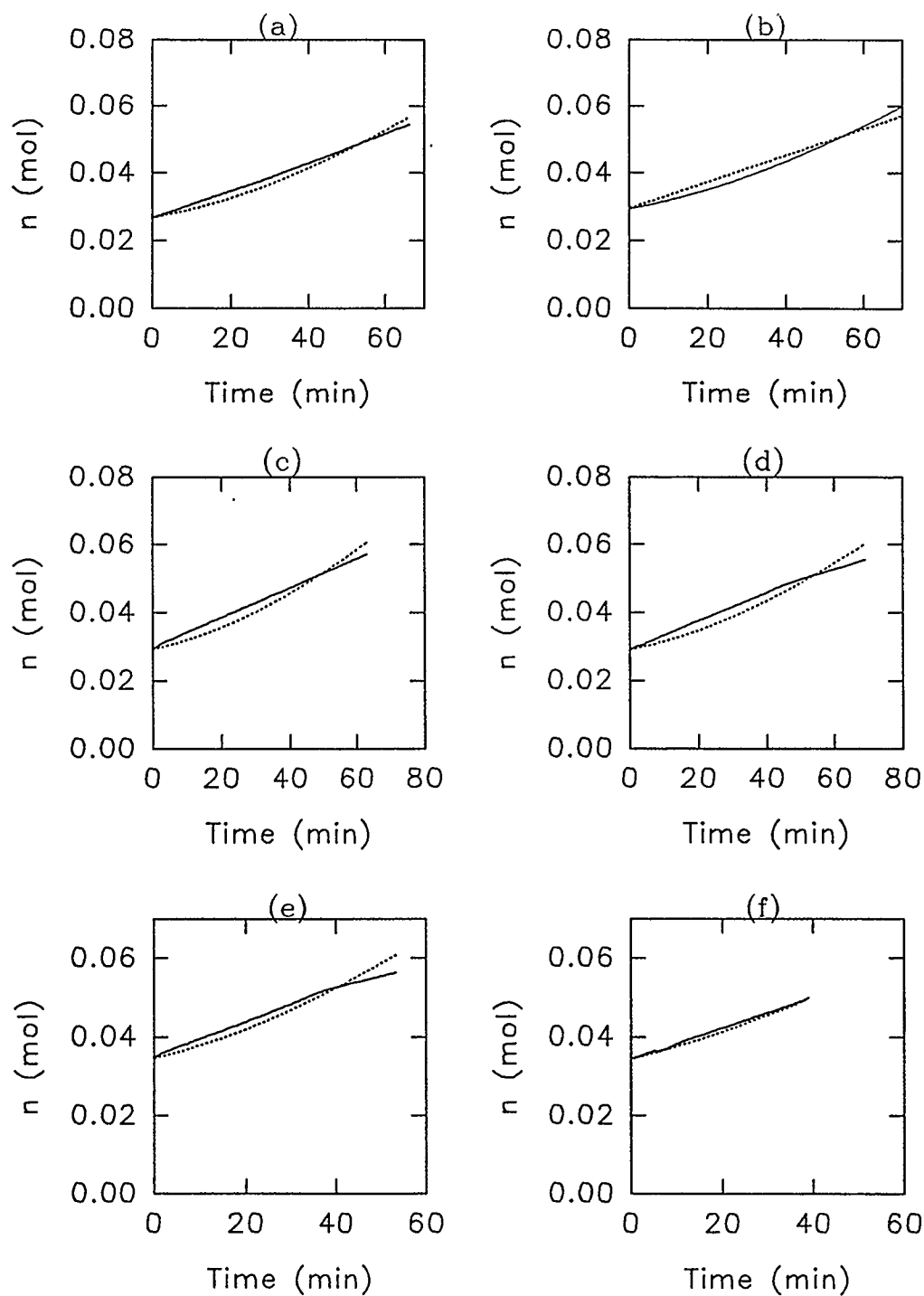


Figure 5.18 Gas Moles Consumed for Hydrate Formation, n (mol), vs Time (min) ("bold": Experimental; "dots": Predicted) (Expt. M014-a, M015-b, M011-c, M012-d, M004-e, M005-f).

In general, the nature of the experimental and the predicted curves is similar for all the isotherms. The estimated gas consumption with time is in good agreement with the experimental data.

The estimated parameter values at each isotherm are given in Tables 5.5 and 5.6 for ethane and methane, respectively. Sensitivity analysis of K^* was performed by taking the extremities of the function μ_2 as 95 % confidence interval, $\mu_2 \pm 2\sigma$. Sigma, “ σ ”, is the standard error of fit of the function to the experimental μ_2 versus time data. Tables 5.5 and 5.6 tabulate the values of K^* computed without and with the 95 % confidence interval in μ_2 , at the three isotherms, for ethane and methane, and the values are plotted in Figure 5.19. Percentage deviation in K^* computed at 95 % confidence interval in μ_2 is also tabulated; it can be as high as 95.8 % and as low as 10.0 %. For ethane, the average value of K^* for the three isotherms, is 0.2 mol/m².s.MPa. It is seen that it lies within the range of K^* computed at 95 % confidence interval in μ_2 , for all the three isotherms. Similarly, for methane, the average value of K^* is 0.1 mol/m².s.MPa, which lies within the range of K^* computed at 95 % confidence interval in μ_2 , for all the three isotherms.

Error analysis was also performed on K^* to estimate the error in K^* due to the error in approximating the experimental data of μ_2 , as a function of time (Refer Appendix E) by assuming that errors in all the other measured quantities are negligible. Tables 5.7 and 5.8 list the estimated K^* values with their 95 % confidence intervals. It should be noted that the 95 % confidence interval in K^* would increase if errors in other measured quantities were also considered. Further, the value of μ_2 taken in estimating the error in K^* is approximately midway in an experiment. If a smaller value of μ_2 is taken, closer to the start of the experiment, the 95 % confidence interval in K^* would increase, the relation being inversely proportional. Again, it can be seen that the average values of K^* for the

T (K)	K^*	K^* at " $\mu-2\sigma$ "	K^* at " $\mu+2\sigma$ "	% Dev. of K^* at " $\mu-2\sigma$ "	% Dev. of K^* at " $\mu+2\sigma$ "
274	0.21	0.36	0.15	71.4	28.6
276	0.17	0.21	0.15	23.5	11.8
278	0.24	0.47	0.17	95.8	29.2

Table 5.5 Kinetic Parameter K^* (mol/m².s.MPa) for Ethane Hydrate Formation and Sensitivity Analysis.

T (K)	K^*	K^* at " $\mu-2\sigma$ "	K^* at " $\mu+2\sigma$ "	% Dev. of K^* at " $\mu-2\sigma$ "	% Dev. of K^* at " $\mu+2\sigma$ "
274	0.06	0.11	0.04	83.3	33.3
276	0.10	0.11	0.09	10.0	10.0
278	0.18	0.29	0.09	61.1	50.0

Table 5.6 Kinetic Parameter K^* (mol/m².s.MPa) for Methane Hydrate Formation and Sensitivity Analysis.

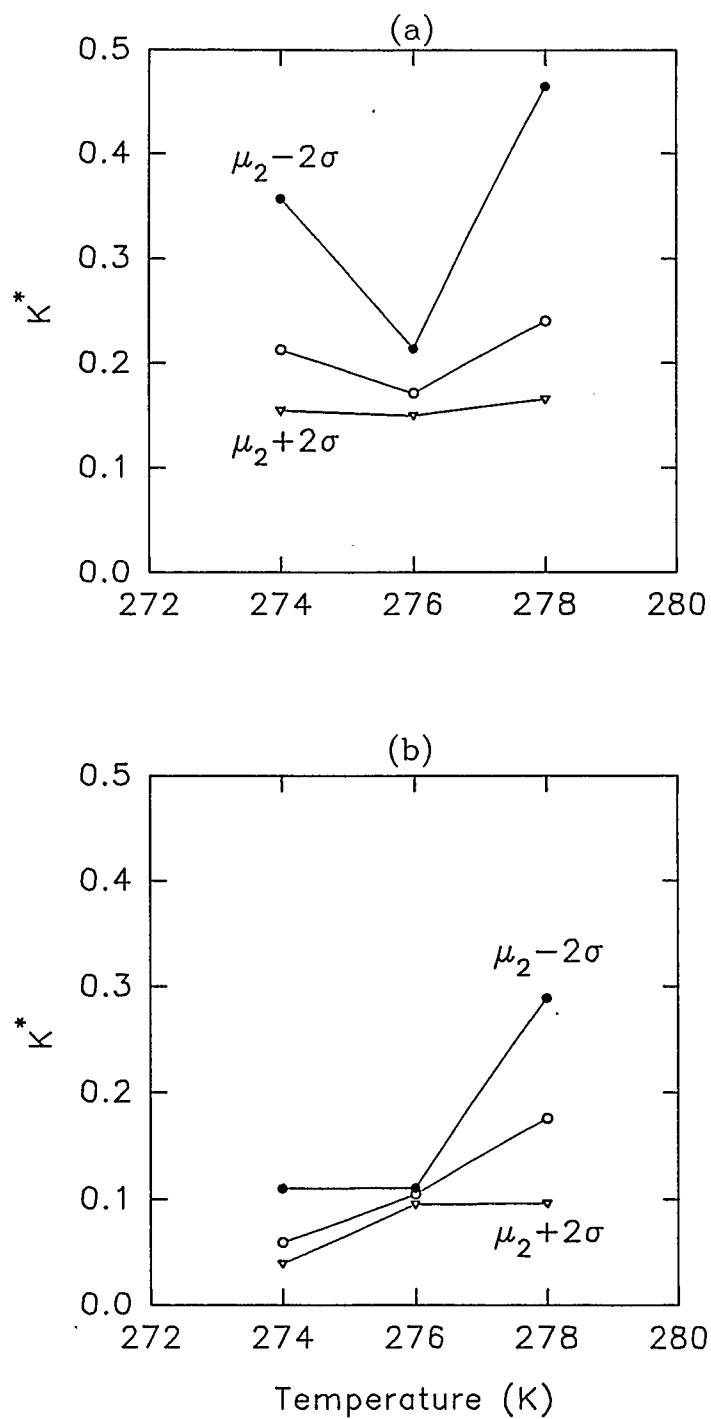


Figure 5.19 Plot of K^* ($\text{mol/m}^2\cdot\text{s}\cdot\text{MPa}$) and K^* Computed at 95 % Confidence Interval in μ_2 (Ethane-(a), Methane-(b)).

T (K)	K^*	95% Conf. Int. (2σ) in K^*	Range of K^*	% Dev. of K^*
274	0.21	0.08	0.13 to 0.29	38.1
276	0.17	0.04	0.13 to 0.21	23.5
278	0.24	0.08	0.16 to 0.32	33.3

Table 5.7 Kinetic Parameter K^* (mol/m².s.MPa) for Ethane Hydrate Formation and Error Analysis.

T (K)	K^*	95% Conf. Int. (2σ) in K^*	Range of K^*	% Dev. of K^*
274	0.06	0.04	0.02 to 0.10	66.6
276	0.10	0.02	0.08 to 0.12	20.0
278	0.18	0.1	0.08 to 0.28	52.9

Table 5.8 Kinetic Parameter K^* (mol/m².s.MPa) for Methane Hydrate Formation and Error Analysis.

three isotherms, for ethane is 0.2 and for methane is 0.1 mol/m².s.MPa, lie within their 95 % confidence interval at each isotherm.

Based on the above discussion, it is proposed to take K^* as independent of temperature for both the gases. It may be approximated as a single value for each gas as reported in Table 5.9.

Tables 5.10 and 5.11 present the estimated parameter as reported by Englezos et al. (1987). It can be seen that our K^* is approximately 10^4 times of that reported by Englezos et al. In the Englezos et al. (1987) model, the product " $K^*\mu_2$ " is nearly a constant. A decrease in the magnitude of μ_2 causes an increase in K^* and vice versa. The μ_2 estimated by Englezos et al. was based on the Kane et al. model (1974) for the kinetics of secondary nucleation in batch crystallizers and was approximately 10^4 times that of our measured μ_2 . Thus, this difference in the magnitude of the computed and measured values of μ_2 caused the difference in the values of K^* . It should be emphasized here that Englezos et al. were of the strong opinion that particle size measurement was a must in order to obtain improved estimate of μ_2 and therefore K^* .

Gas	K^* (mol/m ² .s.MPa)
Ethane	0.2
Methane	0.1

Table 5.9 Average Kinetic Parameter K^* for Ethane and Methane Hydrate Formation

Temperature (K)	K^* (mol/m ² .s.MPa)	95% Conf. Int. (% of K^*)
274	$0.12 \cdot 10^{-4}$	2.8
276	$0.11 \cdot 10^{-4}$	3.1
279	$0.13 \cdot 10^{-4}$	0.9

Table 5.10 Kinetic Parameter K^* Reported by Englezos et al. for Ethane Hydrate Formation.

Temperature (K)	K^* (mol/m ² .s.MPa)	95% Conf. Int. (% of K^*)
274	$0.65 \cdot 10^{-5}$	2.2
276	$0.55 \cdot 10^{-5}$	2.0
279	$0.57 \cdot 10^{-5}$	3.4

Table 5.11 Kinetic Parameter K^* Reported by Englezos et al. for Methane Hydrate Formation.

6.0 CONCLUSIONS AND RECOMMENDATIONS

6.1 Conclusions

Kinetic experiments were performed to study ethane and methane gas hydrate formation. The data were used to evaluate K^* , the overall rate constant (Englezos et al., 1987) for hydrate growth.

A high pressure micro-flow cell was employed to enable the measurement of ethane and methane hydrate particles using a He-Ne laser particle analyzer with a measuring range 5-600 μm . Particle size data were obtained using a laser analyzer for all the experiments by circulation of the hydrate-water slurry through the micro-flow cell using a high pressure Gilson 303 reciprocating pump.

The distributions of particle number density were found to be log-normal in nature.

The median hydrate particle size from the beginning to the end of each experiment was in the range 7 ± 1 microns. Hydrodynamics of the system may have controlled the particle size range.

The growth of the hydrate mass was therefore not in terms of particle size but in terms of the particle number density ($\#/\text{m}^3$).

Analysis of the data showed that all the particle size distributions were well below 600 microns. Since the analyzer could measure particles only in the range 5-600 microns, data was extrapolated to complete the distribution below 5 microns.

The volume distribution of particles below 5 microns was always found to be lower than 1% of the total volume of the distribution while the surface contribution of the same was lower

than 5%.

Gas moles in the hydrate form obtained from the DORIC and analyzer data acquisition systems did not match. This suggested that the shape of hydrate particles under dynamic conditions was not spherical. Assuming the particles to be cylindrical, new surface and volume shape factors were calculated to match the moles obtained from the two sources.

Experimentally obtained second moment of particle size distribution, μ_2 , was used to estimate K^* .

6.2 Recommendations

Effect of hydrodynamics on the particle size distribution should be studied and mathematically modelled to generate the size distribution.

Shape analysis of the hydrates should be performed to improve the surface and volume shape factors. For this the high pressure micro-flow cell has to be re-designed to accommodate the analyzer camera assembly.

Agglomeration of the hydrate particles can be studied by using a larger size piping and modifying the microflow cell accordingly.

Effect of methanol, electrolytes and other inhibitors on the particle size distribution should be studied.

Change in particle size distribution for the hydrate decomposition kinetics should be studied as well.

BIBLIOGRAPHY

Anderson, F.E. & Prausnitz, J.M., "Inhibition of Gas Hydrates by Methanol", AIChE J., **32**(8), 1321(1986).

Bishnoi, P.R., Gupta, A.K., Englezos, P., Kalogerakis, N., "Multi Phase Equilibrium Flash Calculations for Systems Containing Gas Hydrates" Fluid Phase Equilibria, **53**, 97 (1989).

Christiansen, R.L. & Sloan, E.D.Jr., "Mechanism and Kinetics of Hydrate Formation", The International Conference on Gas Hydrates, New York (1993).

Dholabhai, P.D. & Bishnoi, P.R., "Hydrate Equilibrium Conditions in Aqueous Electrolyte Solutions: Mixtures of Methane and Carbondioxide", J. Chemical and Engineering Data, **39**, 191 (1994).

Dholabhai, P.D., Englezos, P., Kalogerakis, N. & Bishnoi, P.R., "Equilibrium Conditions for Methane Hydrate Formation in Aqueous Mixed Electrolyte Solutions", Canadian J. of Chemical Engineering, **69**, 800 (1991).

Dholabhai, P.D., Kalogerakis, N. & Bishnoi, P.R., "Kinetics of Methane Hydrate Formation in Aqueous Electrolyte Solutions", Canadian J. of Chemical Engineering, **71**, 68 (1993).

Englezos, P., "C1-C2 Gas Hydrate Formation Kinetics", M.Sc. Thesis, Department of Chemical & Petroleum Engineering, University of Calgary, Calgary, Canada (1986).

Englezos, P. & Bishnoi, P.R., "Prediction of Gas Hydrate Formation from Aqueous Electrolyte Solutions", AIChE J., **34**(10), 1718(1988).

Englezos, P., Huang, Z. & Bishnoi, P.R., "Prediction of Natural Gas Hydrate Formation

Condition in the Presence of Methanol Using Trebble-Bishnoi Equation of State", *Journal of Canadian Petroleum Technology*, **30**, 148(1991).

Englezos, P. Kalogerakis, N., Dholabhai, P.D. & Bishnoi, P.R., "Kinetics of Formation of Methane and Ethane Gas Hydrates", *Chemical Engineering Science*, **42**, 2647 (1987).

Holder, G.D., Corbin, G. & Papadopoulos, K.D., "Thermodynamic and Molecular Properties of Gas Hydrates from Mixtures Containing Methane, Argon and Krypton", *Ind. and Engg. Chem.*, **19**, 282 (1980).

Holder, G.D., Zetts, S.P. & Pradhan, N., "Phase Behaviour in Systems Containing Clathrate Hydrates, A Review", *Reviews in Chemical Engineering*, **5**(1-4), 1(1988).

Hutz^a, U. & Englezos, P., "Measurement of Structure H Hydrate Phase Equilibrium and the Effect of Electrolytes", *Fluid Phase Equilibria*, **117**, 178(1996).

Jandel Scientific, "TableCurve 2D".

John, V.T. & Holder, G.D., "Langmuir Constants for Spherical and Linear Molecules in Clathrate Hydrates. Validity of the Cell Theory", *J. of Physical Chemistry*, **89**, 3279(1985).

Kane, S.G., Evans, T.W., Brian, P.L.T. & Sarofim, A.F., "Determination of the Kinetics of Secondary Nucleation in Batch Crystallizers", *AIChE J.*, **20**(5), 855(1974).

Karasikov, N., Bornstein, F., Barazani, G. & Krauss, M., "Resolution of Complex Mixtures of Latex Particles Using time of Transition Analysis", Presented at the Fine Particle Society Meeting, Boston, Mass., (August 1987).

Karpinski, P.H., "Crystallization as a Mass Transfer Phenomenon", *Chem. Eng Sci.*, **35**,

2321 (1980).

Lekvam, K. & Bishnoi, P.R., "Dissolution of Methane in Water at Low Temperatures and Intermediate Pressures", Manuscript Submitted to Fluid Phase Equilibria, (September 9, 1995).

Lekvam, K. & Ruoff, P., "A Reaction Kinetic Mechanism for Methane Hydrate Formation in Liquid Water", J. of the American Chemical Society, (1993).

Makogan, Y.F., "Hydrates of Natural Gas", Translated from Russian by W.J. Cieslesicz, PennWell Books, Tulsa, Oklahoma (1981).

"MATLAB", The MathWorks Inc., Cochituate Place, 24 Prime Park Way, Natick, Mass. 01760, USA.

"MEGHA", Megha Technologies Inc., Calgary, Canada.

Monford, J.P. & Nzihou, A. "Light Scattering Kinetics Study of Cyclopropane Hydrate Growth", J. of Crystal Growth, **128**, 1182(1993).

Muller-Bongartz, B., Wildeman, T.R. & Sloan, E.D.Jr., "A Hypothesis for Hydrate Nucleation Phenomenon", The International Society of Offshore and Polar Engineering, San Francisco (1992).

Mullin, J.W., "Crystallization", Butterworth & Co. Publishers, 14, Curity Avenue, Toronto, Canada (1972).

Natarajan, V. and Bishnoi, P.R., "Formation and Decomposition of Gas Hydrates", Fluid Phase Equilibria, **117**, 168 (1996).

Nerheim, A.R., "Investigation of Gas Hydrate Formation Kinetics by Laser Light Scattering", Ph.D. Thesis, Department of Physics, The Norwegian Institute of Technology, The University of Trondheim (1993).

Ng, H.J. & Robinson, D.B., "The Measurement and Prediction of Hydrate Formation in Liquid Hydrocarbon-Water Systems", *Industrial & Engineering Chemistry Fundamentals*, **15**(4), 293(1976).

Nielsen, B.B., "Effects of Temperature & Pressure on Asphaltene Particle Size Distribution in Bitumen-Diluent Mixtures", M.Sc. Thesis, Department of Chemical & Petroleum Engineering, University of Calgary, Calgary, Canada (1993).

Parent, J.S. and Bishnoi, P.R., "Investigation into the Nucleation Behaviour of Methane Gas Hydrates", *Chem. Engg. Comm.*, **144**, 51 (1996)

Parrish, W.R. & Prausnitz, J.M., "Dissociation Pressures of Gas Hydrates Formed by Gas Mixtures", *Industrial Engineering Chemical Process Design Development*, **11**(1), 26(1972).

Ripmeester, J.A. & Ratcliffe, C.I., "¹²⁹Xe NMR Studies of Clathrate Hydrates: New Guests for Structure II and Structure H", *J. of Physical Chemistry*, **94**, 8773(1990).

Ripmeester, J.A., Tse, J.S., Ratcliffe, C.I. & Powell, B.M. "A New Clathrate Hydrate Structure", *Nature*, **325**, 135(1987).

Sloan, E.D.Jr., "Hydrate Nucleation from Ice", Presented at the 69th Annual GPA Convention, Phoenix, Arizona (1990).

Sloan, E.D.Jr., "Clathrate Hydrates of Natural Gases", Marcel Dekker Inc., New York, 1, (1991a).

Sloan, E.D.Jr., "Natural Gas Hydrates", J. of Petroleum Technology, December (1991b).

Sloan, E.D.Jr. & Fleyfel, F., "A Molecular Mechanism for Gas Hydrate Nucleation from Ice", AIChE J., **37**, 1281(1991).

Tse, C.W. & Bishnoi, P.R., "Prediction of Carbondioxide Gas Hydrate Formation Conditions in Aqueous Electrolyte Solutions", Canadian J. of Chemical Engineering, **72**, 119(1994).

van der Waals, J.H. & Platteeuw, J.C., "Clathrate Solutions", Advances in Chemical Physics, **2**(1), 1(1959).

von Stackelberg, M., Naturwiss, **36**, 327 (1949).

von Stackelberg, M. & Muller, H.R., Naturwiss, **38**, 456 (1951a).

von Stackelberg, M. & Muller, H.R., J. Chemical Physics, **19**, 1319 (1951b).

Vysniauskas, A. & Bishnoi, P.R., "A Kinetic Study of Methane Hydrate Formation", Chemical Engineering Science, **38**, 1061(1983).

APPENDIX-A

Solubility and Kinetic Experiments

Solubility Experiments

Two solubility runs for each isotherm (274, 276 and 278 K) were carried out for both the gases (ethane and methane), at a pressure slightly below the three phase equilibrium pressure corresponding to that temperature, following the procedure described in Chapter 2, Section 2.5. By measuring the rate at which the gas is being dissolved into the liquid water, we can estimate the liquid mass transfer coefficient ($k_L a$) and the Henry's constant (H) of the dissolved gas in equilibrium with the partial pressure of the gas at the gas-liquid interface.

The gas moles experimental data were used to determine the unknown parameters by minimizing the difference between the predicted and the measured moles of the gas consumed during the solubility experiment. The resulting non-linear least squares problem was solved iteratively using the Gauss-Levenberg method (Englezos, 1986). The governing equations are given below.

$$\frac{dn}{dt} = k_L a (n^* - n) \quad \text{A-1}$$

$$f = H x_m^* \quad \text{A-2}$$

$$x_m^* = \frac{n^*}{n_{mw} + n^*} \quad \text{A-3}$$

where,

dn/dt =Rate of Gas Consumption

n^* =Solubility of Gas in Water

n =Moles of Gas Consumed

n_{mw} =Moles of Water

x_m^* = Mole Fraction of Gas in Liquid Phase
 f = Gas Phase Fugacity of Dissolving Gas

Figures A-1 and A-2 are plots of the gas consumption curves for the solubility runs for gases ethane and methane, respectively.

Kinetic Gas Consumption Curves

Figures A-3 and A-4 are plots of the gas consumption curves for the kinetic experiments of gases ethane and methane, respectively. " n_{tb} " is the turbidity point while " n_{eq} " is the gas moles dissolved at the three phase equilibrium pressure and same isotherm.

Critical Radius (r_{cr})

Englezos et al. (1987) calculated the critical size or diameter, $2r_{cr}$, of the nucleus assuming primary homogeneous nucleation. When a new phase is formed, a change in the free energy of the system is due to the appearance of this phase and the formation of a boundary between the phases, i.e.,

$$\Delta G = \Delta G_s + \Delta G_v = A_p \sigma + \Delta g V_p \quad A-4$$

where, ΔG_s is the change in free energy due to the formation of a boundary between the phases (it is always positive) and ΔG_v is the change in free energy due to the appearance of a certain amount of a new phase (always negative). Δg is free energy of change per unit volume of the product formed. A_p and V_p are the surface area and volume of particle and σ the surface energy for the system hydrate-water. The sign of ΔG depends on the relative magnitudes of ΔG_s and ΔG_v which in turn depend on the dimensions of the nuclei of the new phase. The function $\Delta G = \Delta G(r)$ passes through a maximum at a certain

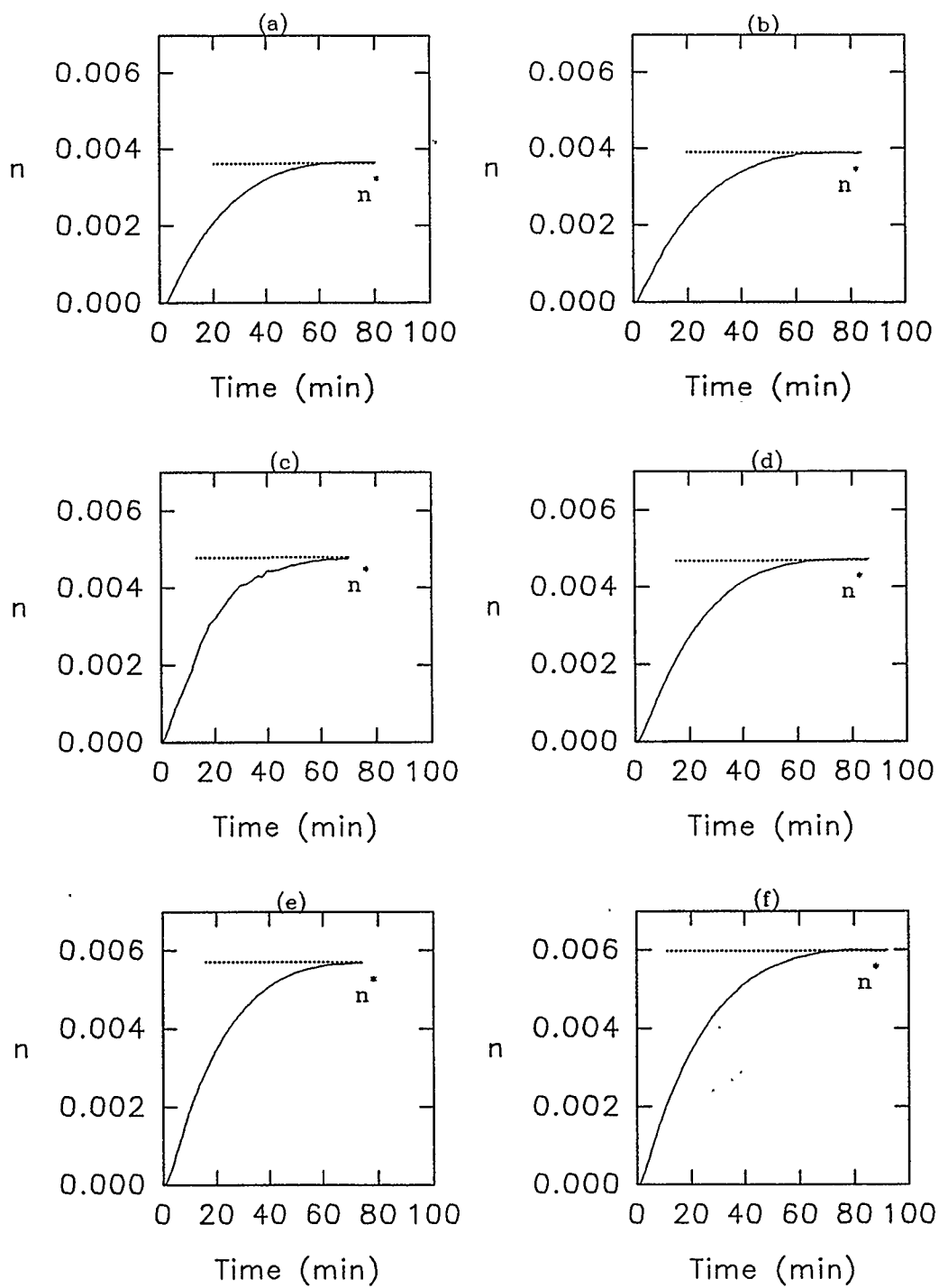


Figure A-1 Gas Moles Consumed, n (mol), vs Time (min)
(Expt. E006-a, E008-b, E014-c, E018-d, E020-e,
E021-f).

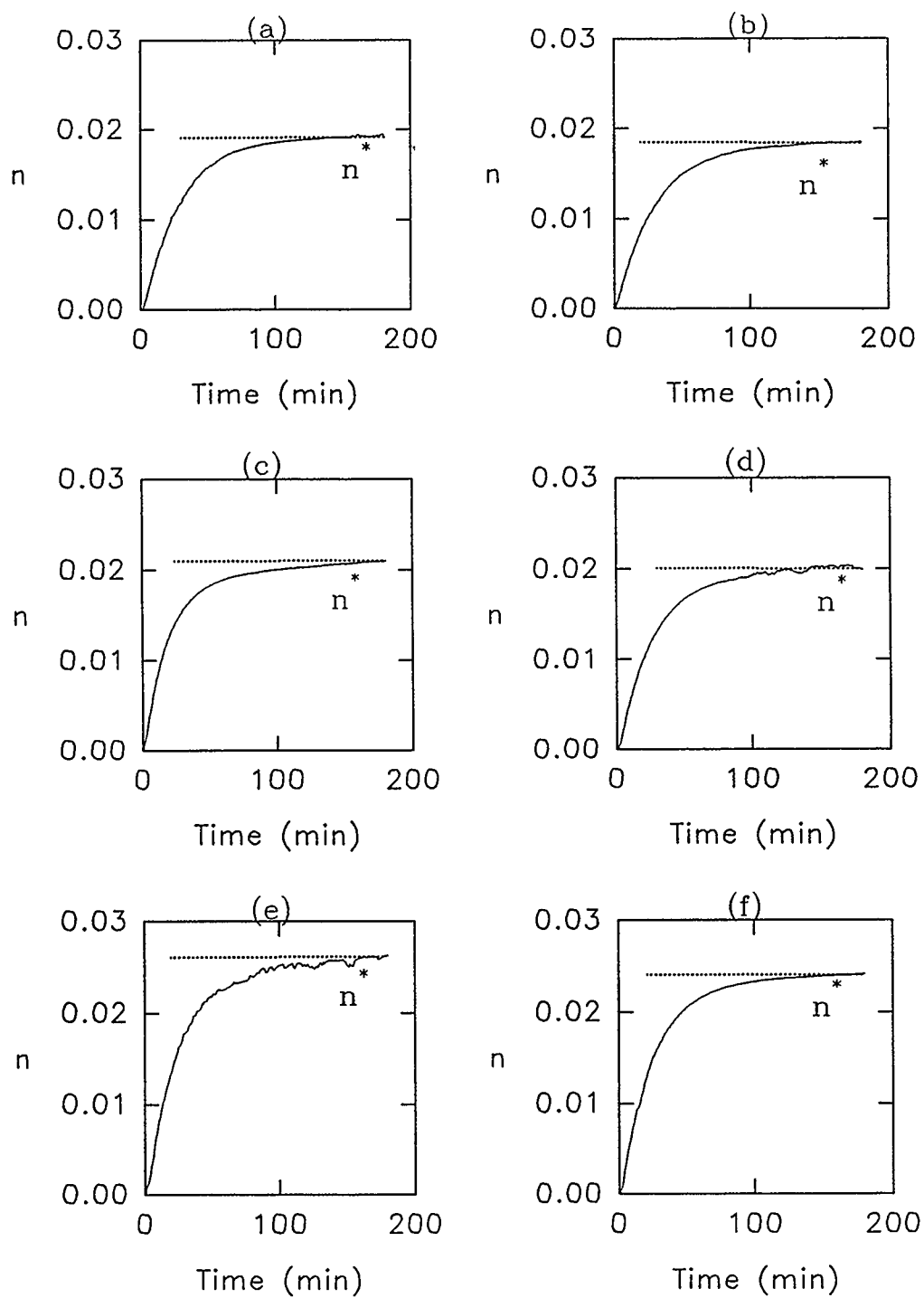


Figure A-2 Gas Moles Consumed, n (mol), vs Time (min)
 (Expt. M016-a, M017-b, M010-c, M013-d, M007-e,
 M008-f).

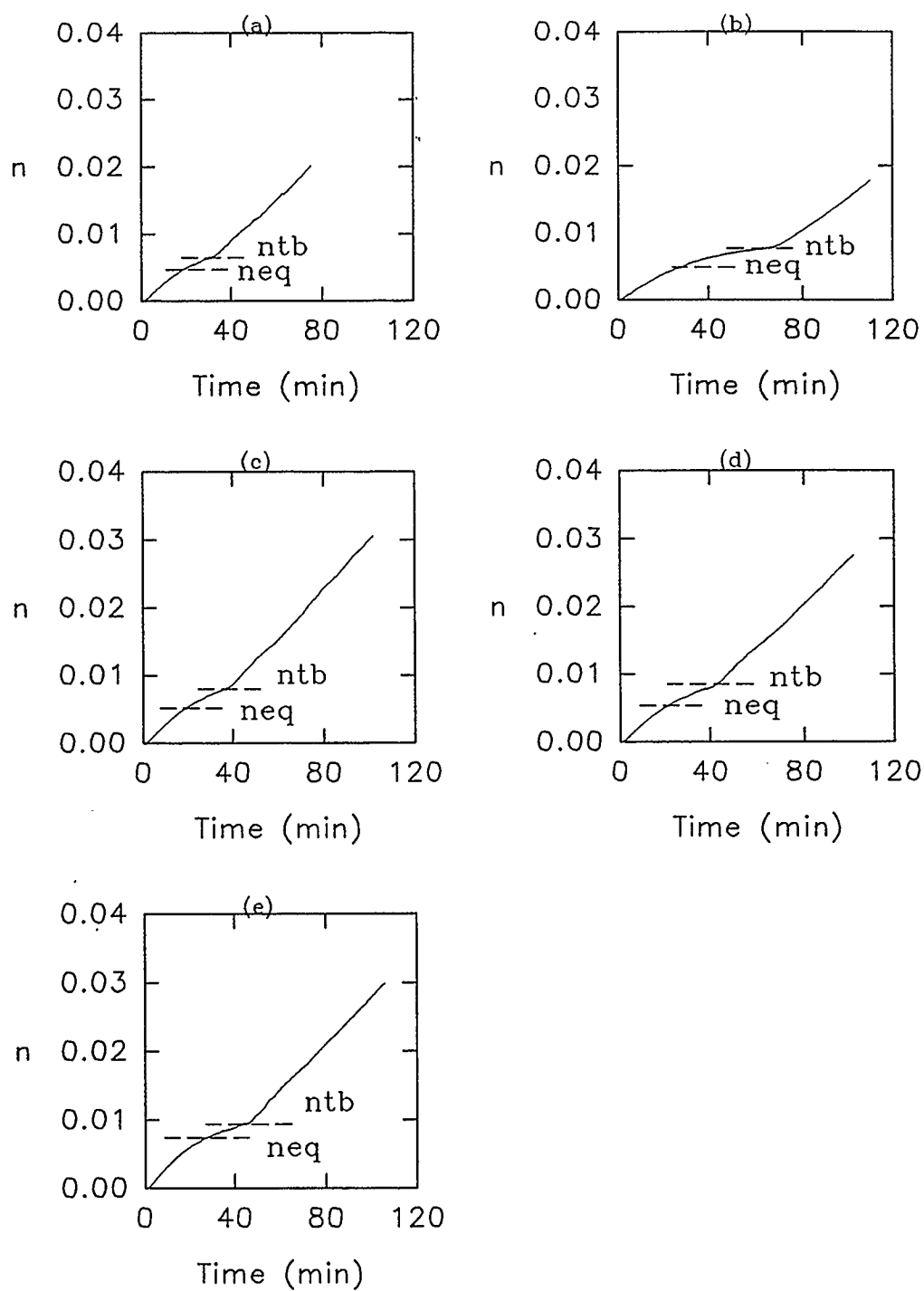


Figure A-3 Gas Moles Consumed, n (mol), vs Time (min)
(Expt. E007-a, E009-b, E011-c, E016-d, E019-e).

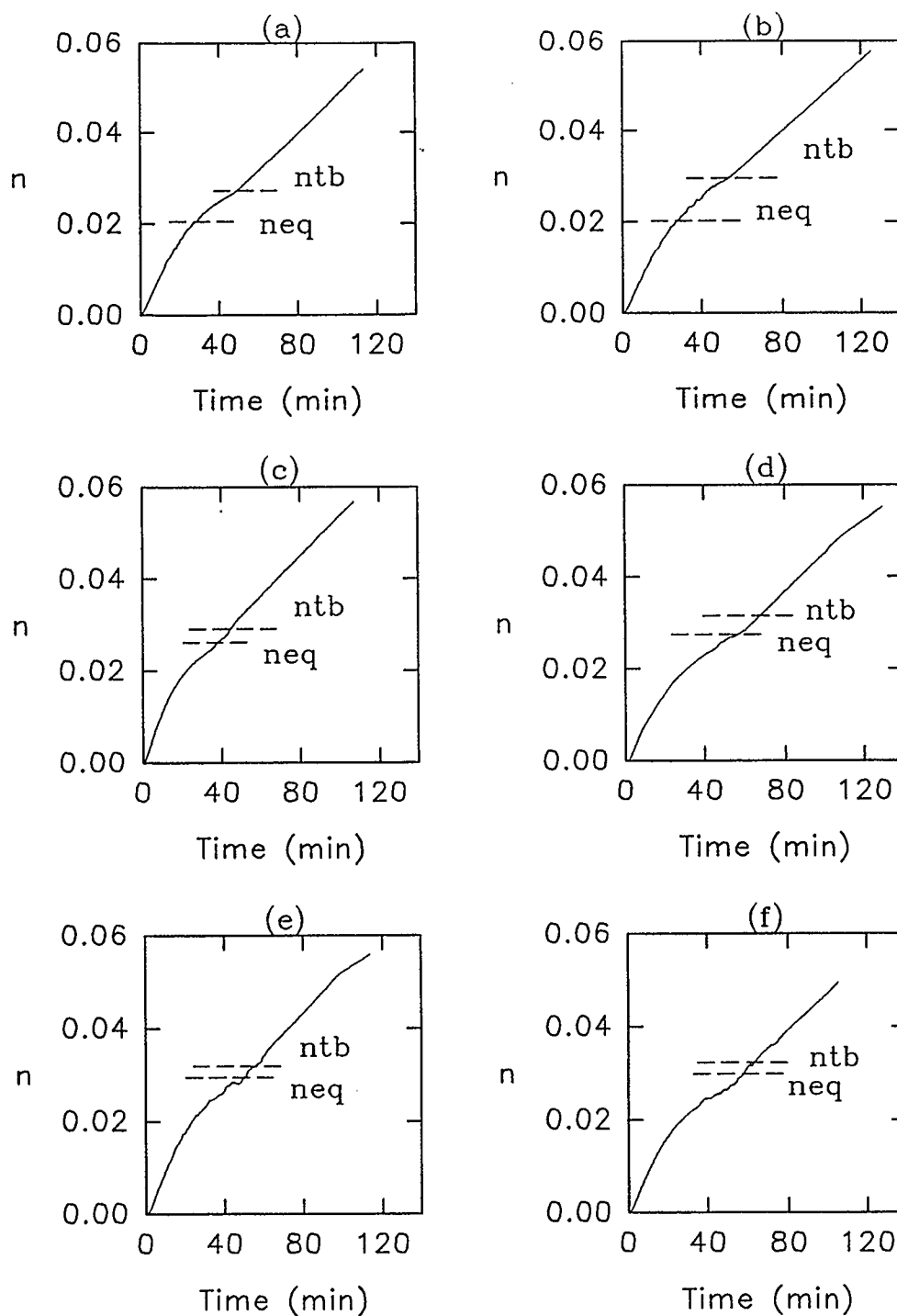


Figure A-4 Gas Moles Consumed, n (mol), vs Time (min)
(Expt. M014-a, M015-b, M011-c, M012-d, M004-e,
M005-f).

critical particle radius, r_{cr} . The particles of the new phase whose radius is $r < r_{cr}$ are dissolved while particles whose radius is $r > r_{cr}$ continue to grow. Hence, using Equation A-4 and setting $d\Delta G/dr=0$ they obtained the expression,

$$r_{cr} = -\frac{2\sigma}{\Delta g} \quad A-5$$

$$(-\Delta g) = \left(\frac{RT_{exp}}{v_m}\right) \left(\ln \frac{f_b}{f_{eq}} + \frac{n_w v_w (P_{exp} - P_{eq})}{RT_{exp}}\right) \quad A-6$$

Gas Consumption in Hydrate Formation

The gas moles consumed in hydrate formation can be computed from the data obtained from DORIC data acquisition system. Of the total gas consumed in a kinetic experiment, part of it is dissolved in the bulk water and the remaining is consumed for hydrate formation.

Mole fraction of gas in liquid phase is given by

$$x_m = \frac{f_b}{H} \quad A-7$$

where,

f_b = Fugacity of Gas in Liquid Bulk Phase

H = Henry's Constant

Mole fraction of gas in terms of moles is given by

$$x_m = \frac{n_b}{n_{mw} + n_b} \quad A-8$$

where,

n_b = Moles of Gas Dissolved in Liquid Bulk

n_{mw} = Total Moles of Water

From A-8 we obtain the expression

$$n_b = n_{mw} \left(\frac{x_m}{1 - x_m} \right) \quad \text{A-9}$$

The fugacity of gas in the bulk liquid phase, f_b , was computed from Eqn. 3.18 of the Englezos et al. model and found to be almost equal to the three phase equilibrium fugacity. Therefore, n_b was taken equal to n_{eq} .

Hence moles of gas in hydrate form at any time is simply the difference between the total gas moles consumed till that time and the moles of gas consumed at the three phase equilibrium conditions, i.e., $n - n_{eq}$.

APPENDIX-B

Particle Analyzer Results of Ethane and Methane Kinetic Experiments

Figures B1 to B10 are analyzer results for kinetic experiments of gases ethane and methane. In each Figure,

Plot (a): Particle Number Density, $N(\#/m^3)$, vs Time (min)

Plot (b): Particle Area Density, $A(m^2/m^3)$, vs Time (min)

Plot (c): Particle Volume Density, $V(m^3/m^3)$ vs Time (min)

Plot (d): Second Moment, $SM(m^2/m^3)$, vs Time (min)

Plot (e): Gas Moles Consumed for Hydrate Formation, $M(mol)$, vs Time (min) (“P”: Analyzer, “D”, DORIC)

Plot (f): Gas Moles Consumed for Hydrate Formation, $M(mol)$, vs Time (min) (“P”: Analyzer, “D”: DORIC)

Figures B11 to B14 are complete distributions of particle number density, $N(\#/m^3)$, with size (micro m) for experiment M014. Figures B15 to B18 are complete distributions of the area density, $A(m^2/m^3)$ and Figures B19 to B22 are complete distributions of the volume density, $V(m^3/m^3)$ for the same experiment.

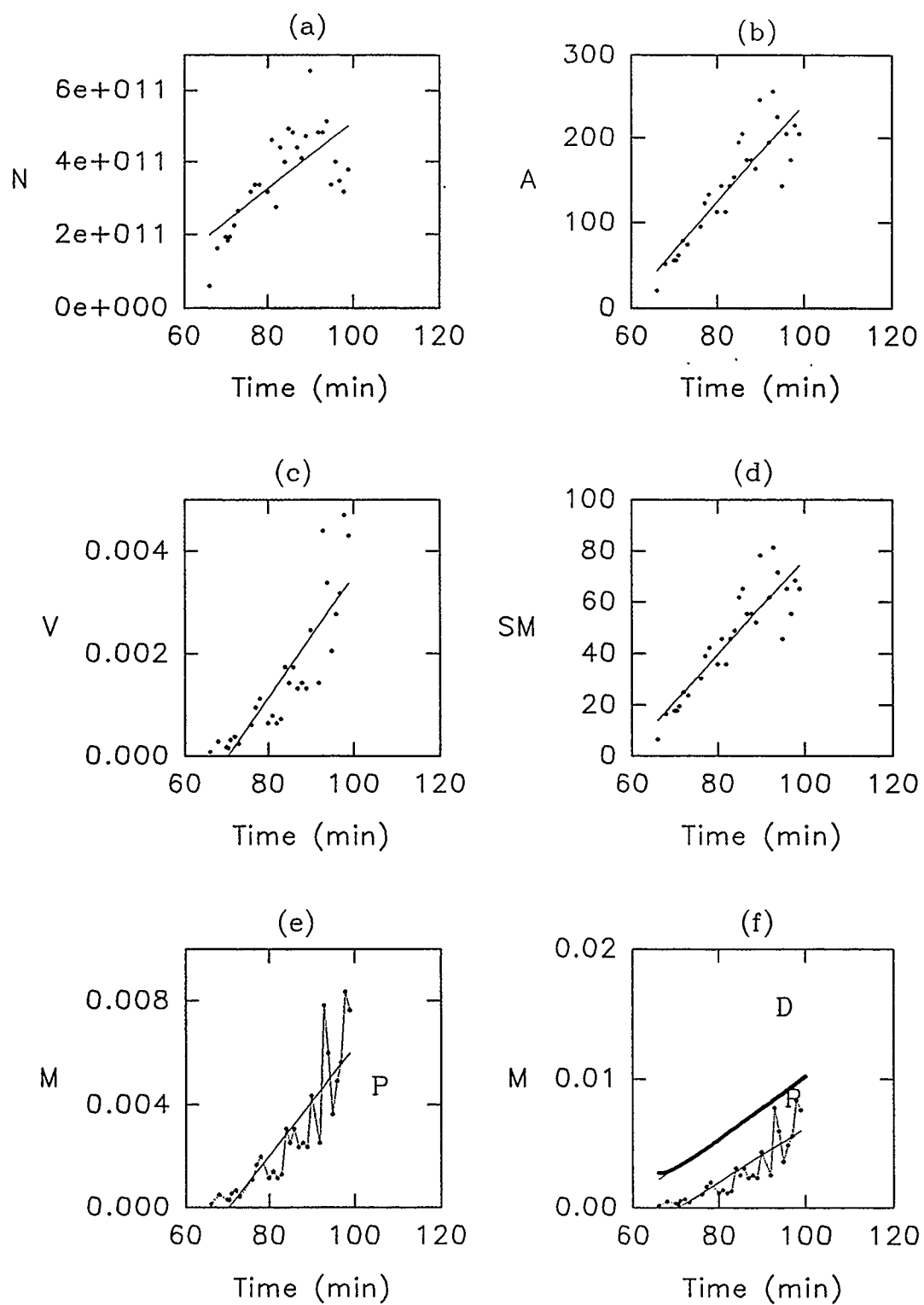


Figure B1 Experiment E009.

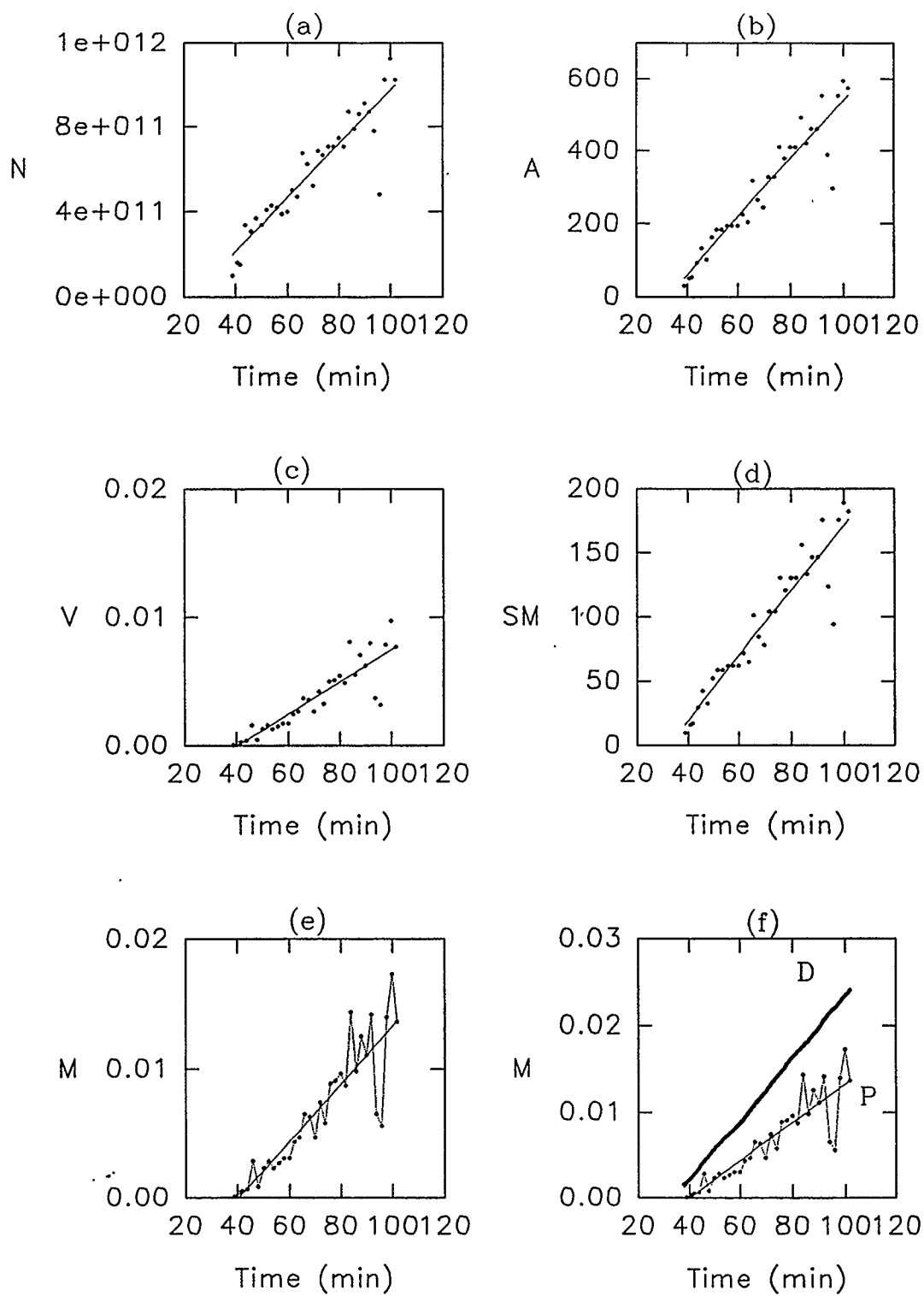


Figure B2 Experiment E011.

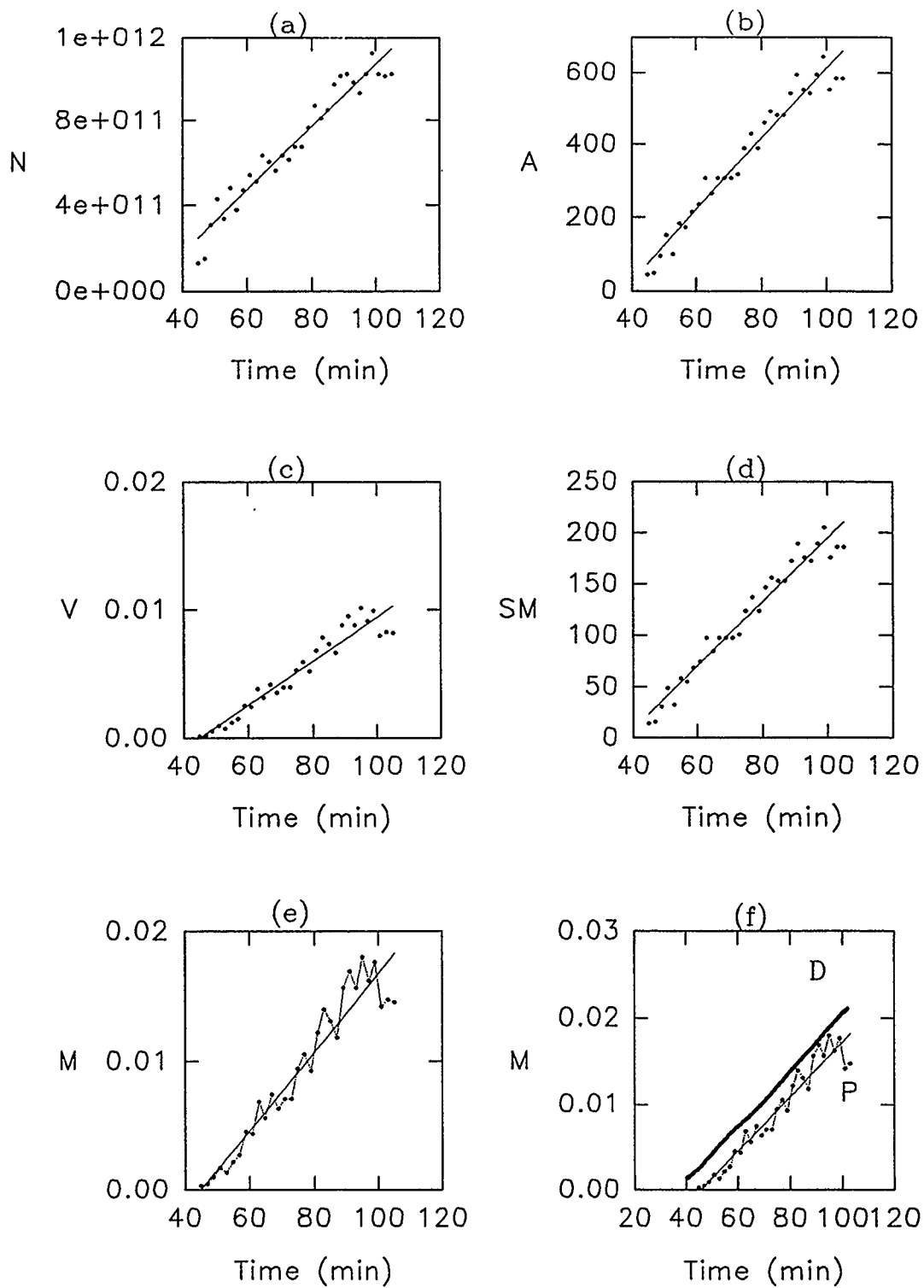


Figure B3 Experiment E016.

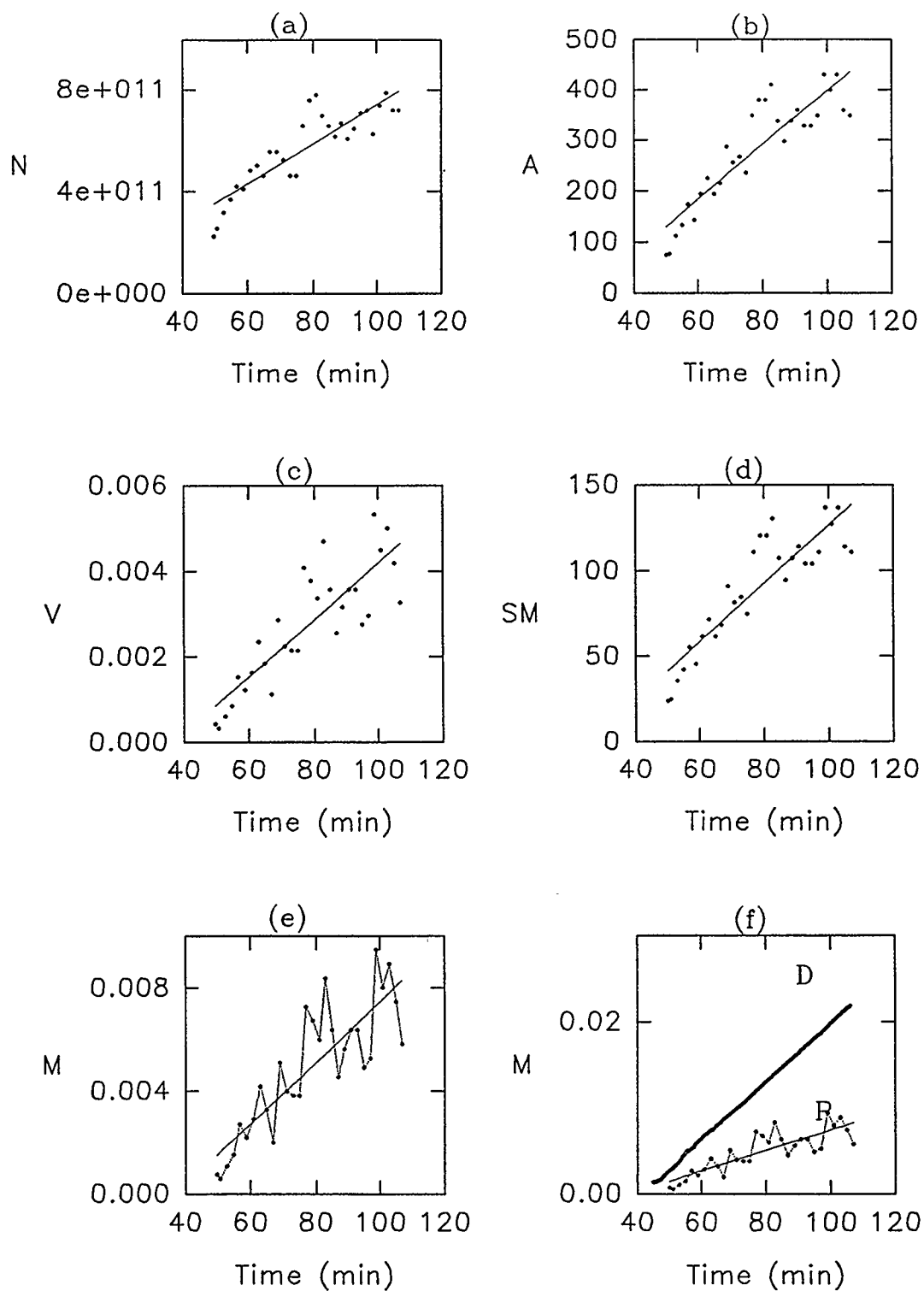


Figure B4 Experiment E019.

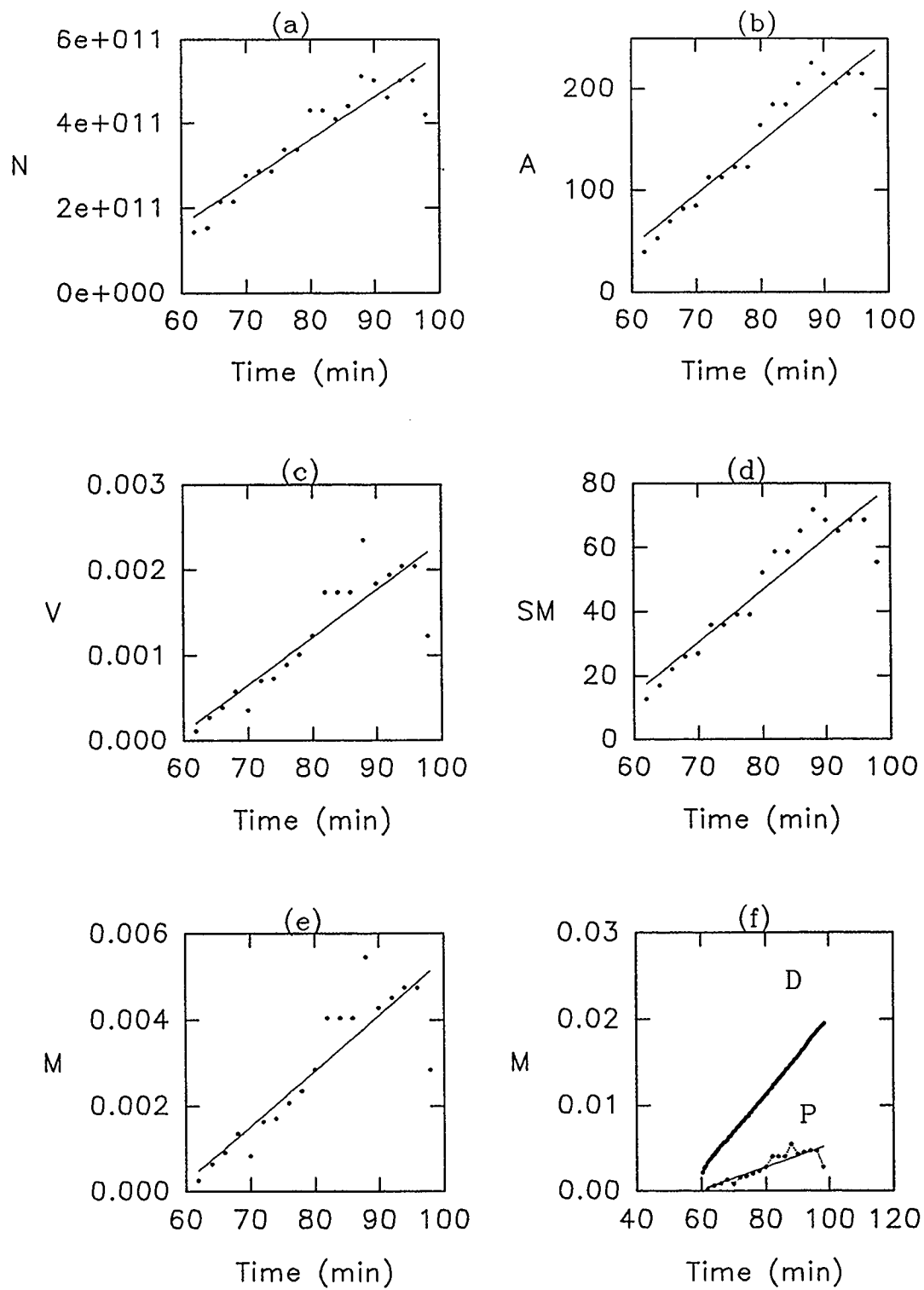


Figure B5 Experiment M004.

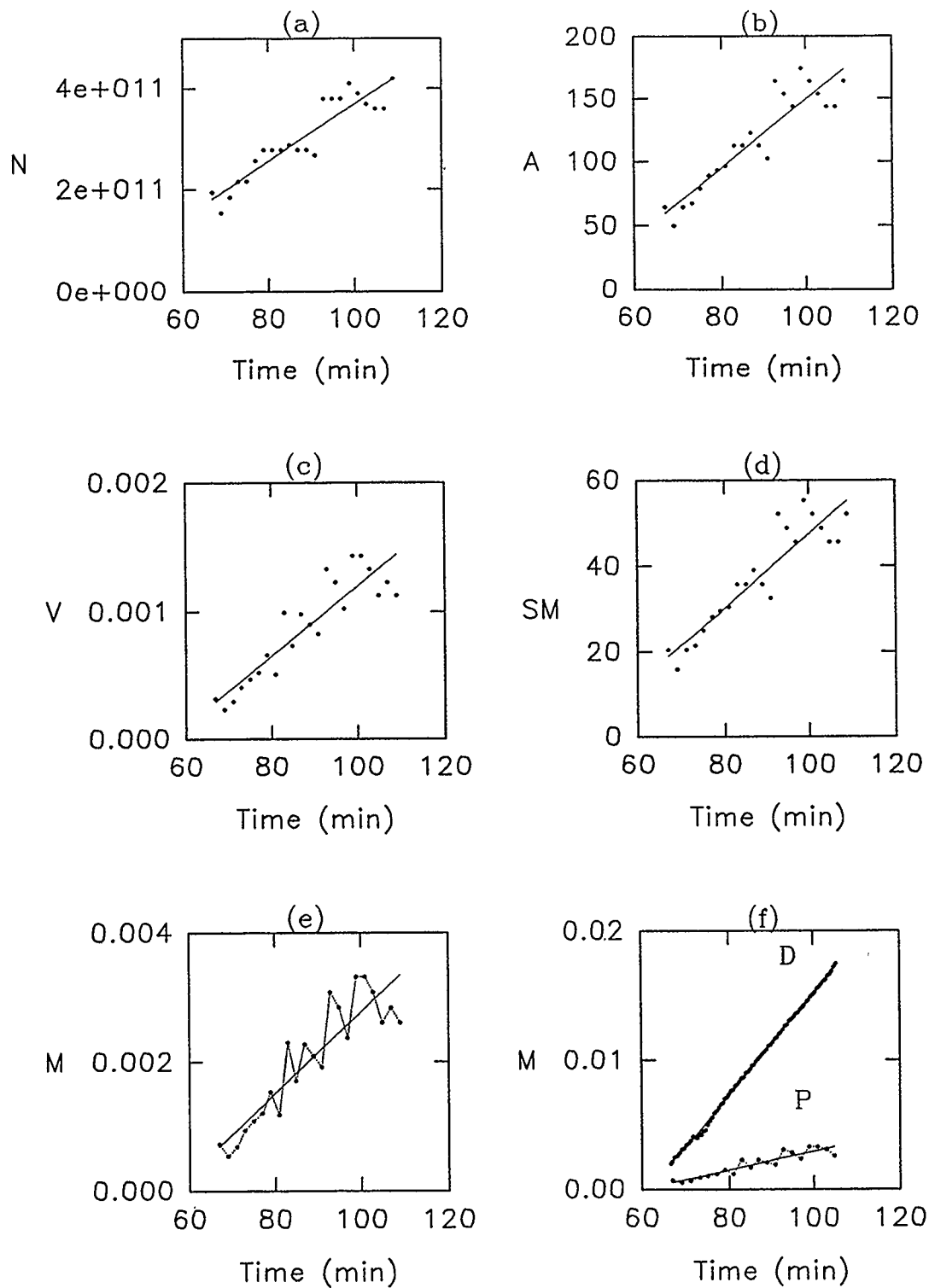


Figure B6 Experiment M005.

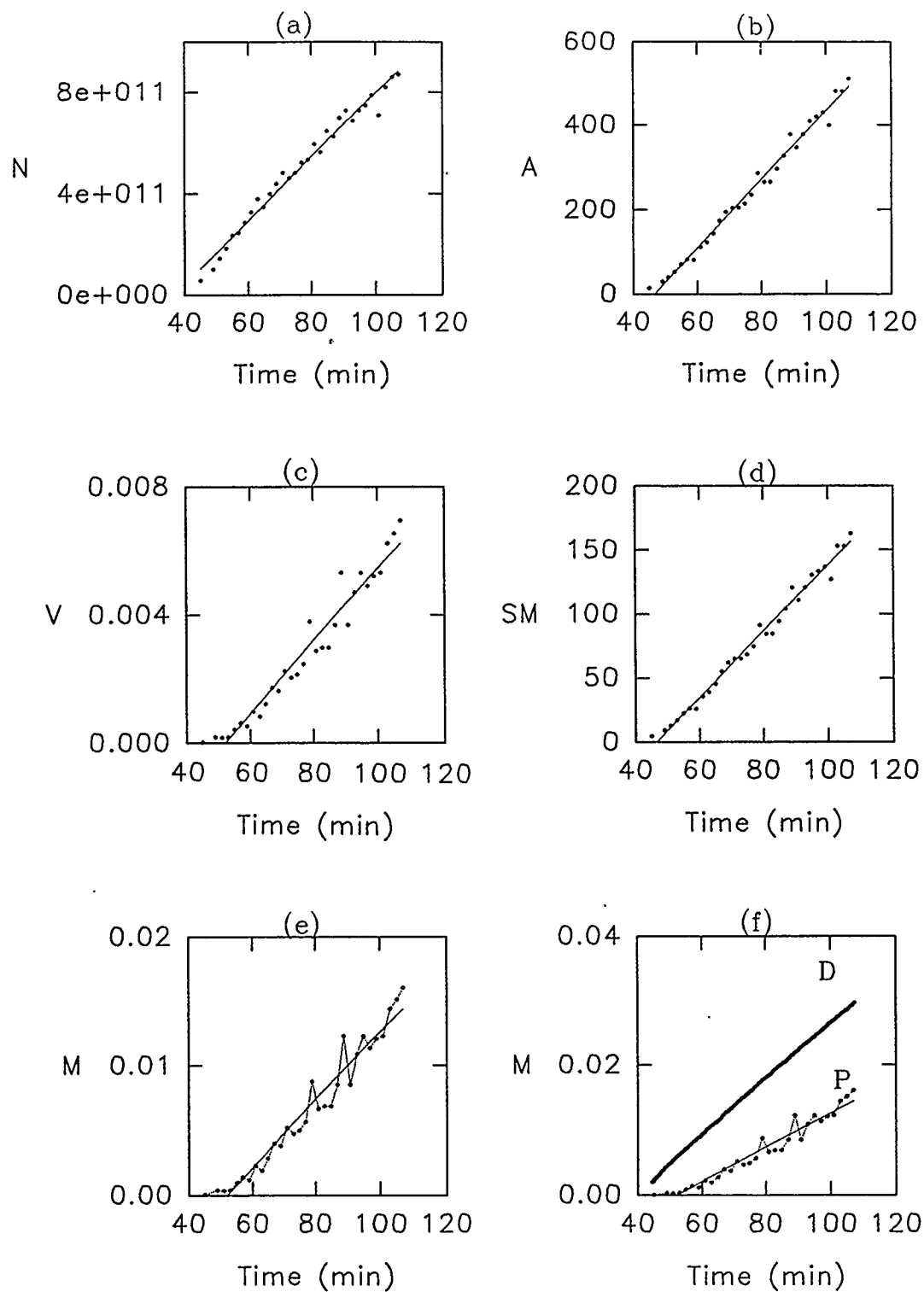


Figure B7 Experiment M011.

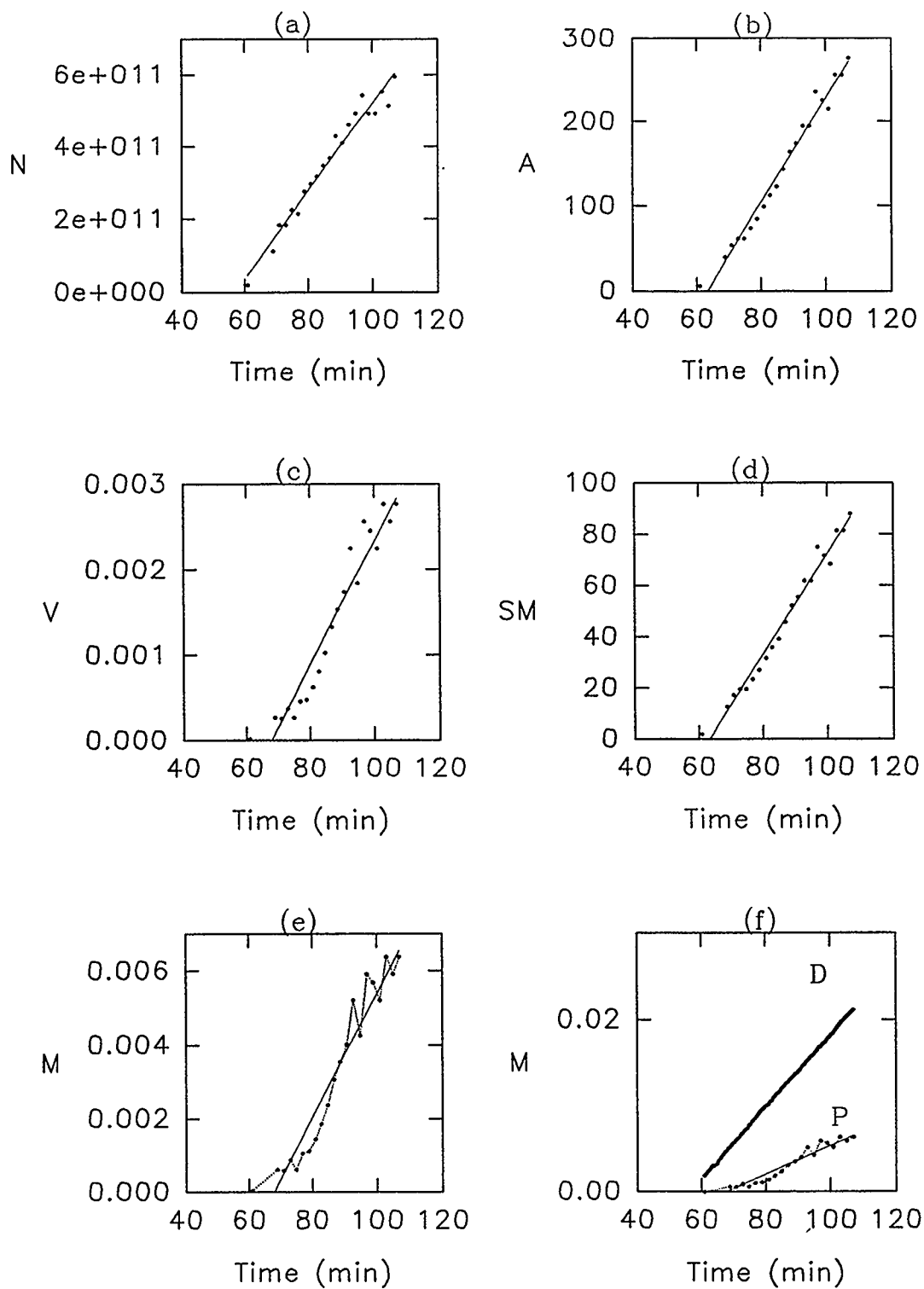


Figure B8 Experiment M012.

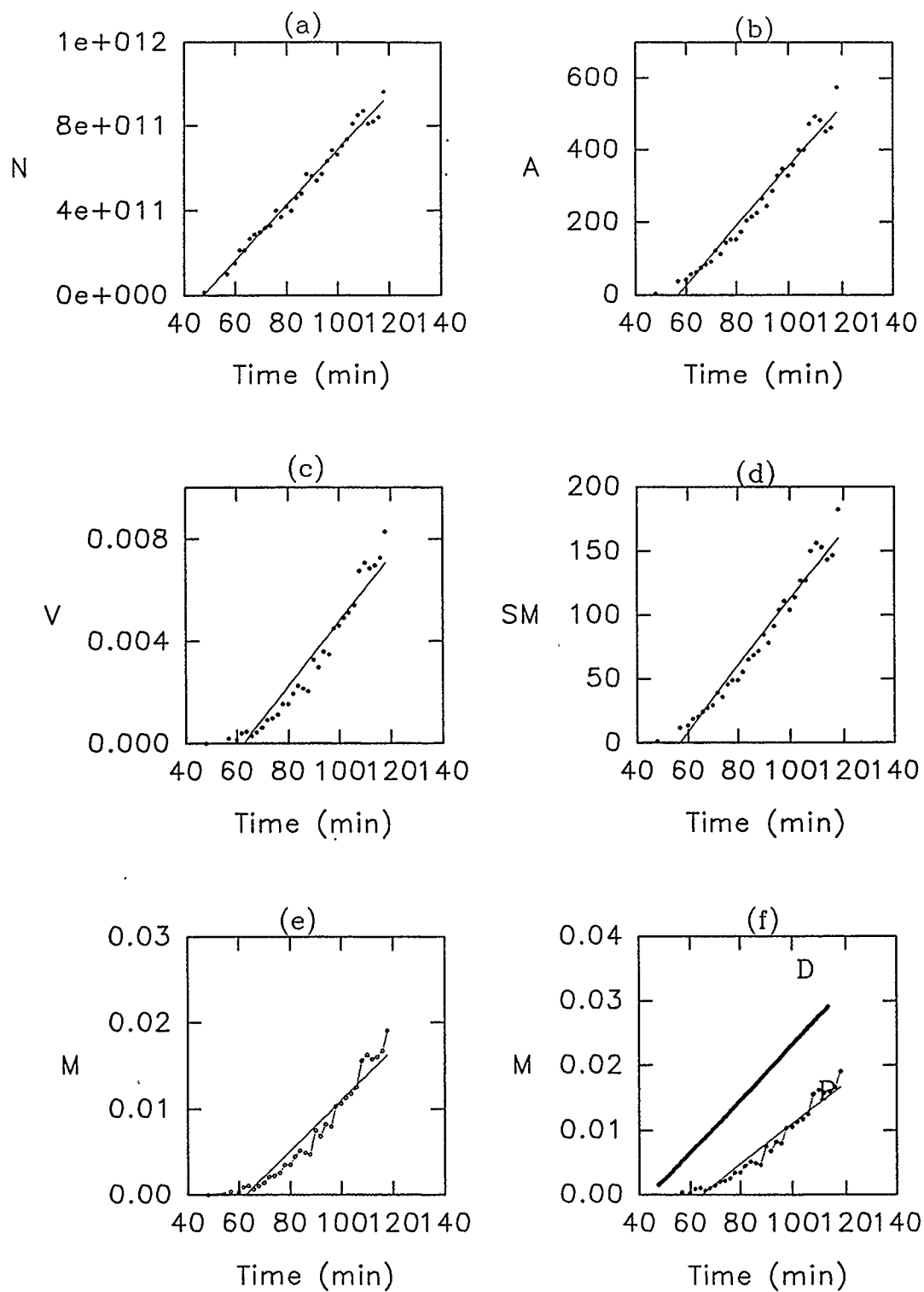


Figure B9 Experiment M014.

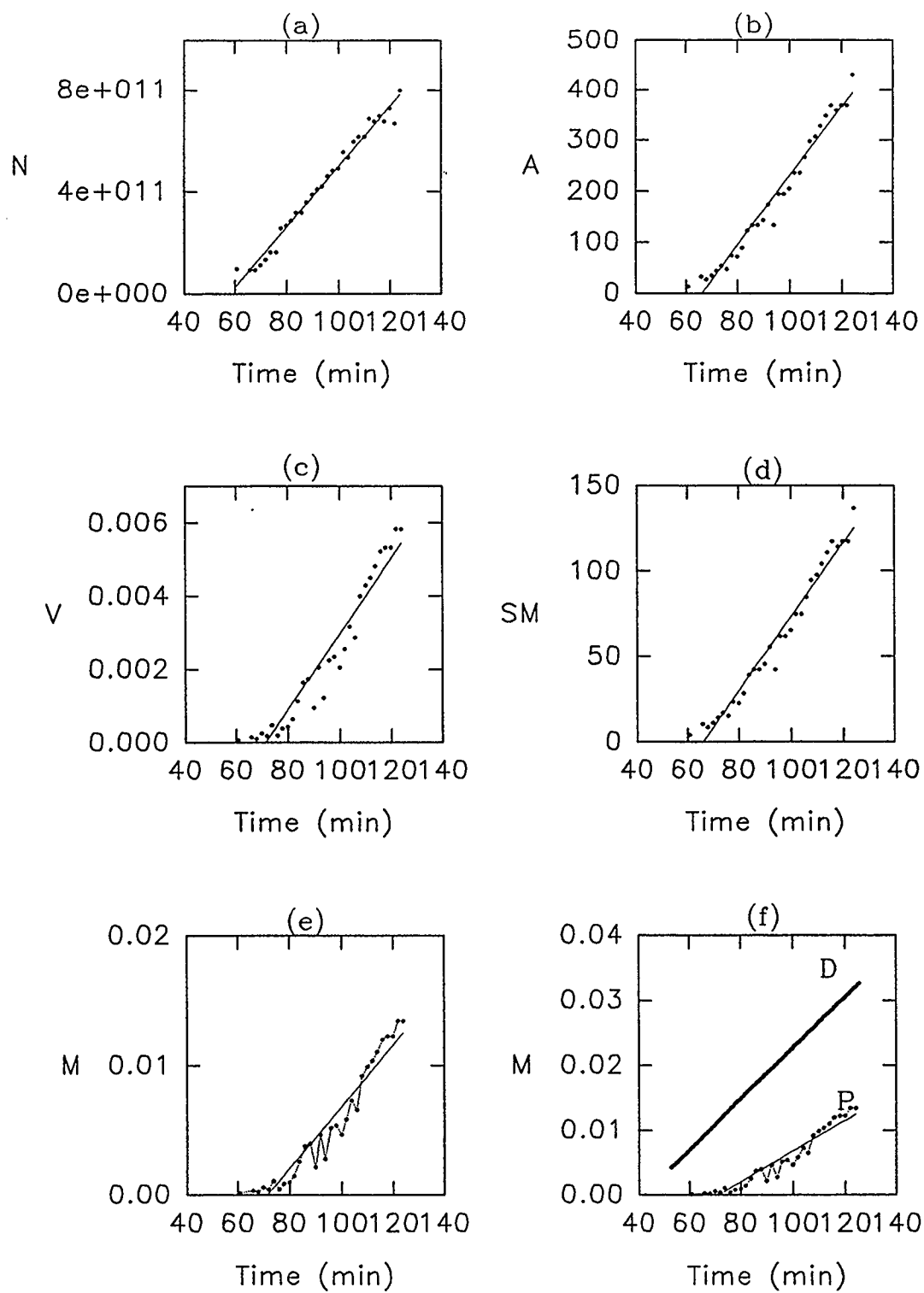


Figure B10 Experiment M015.

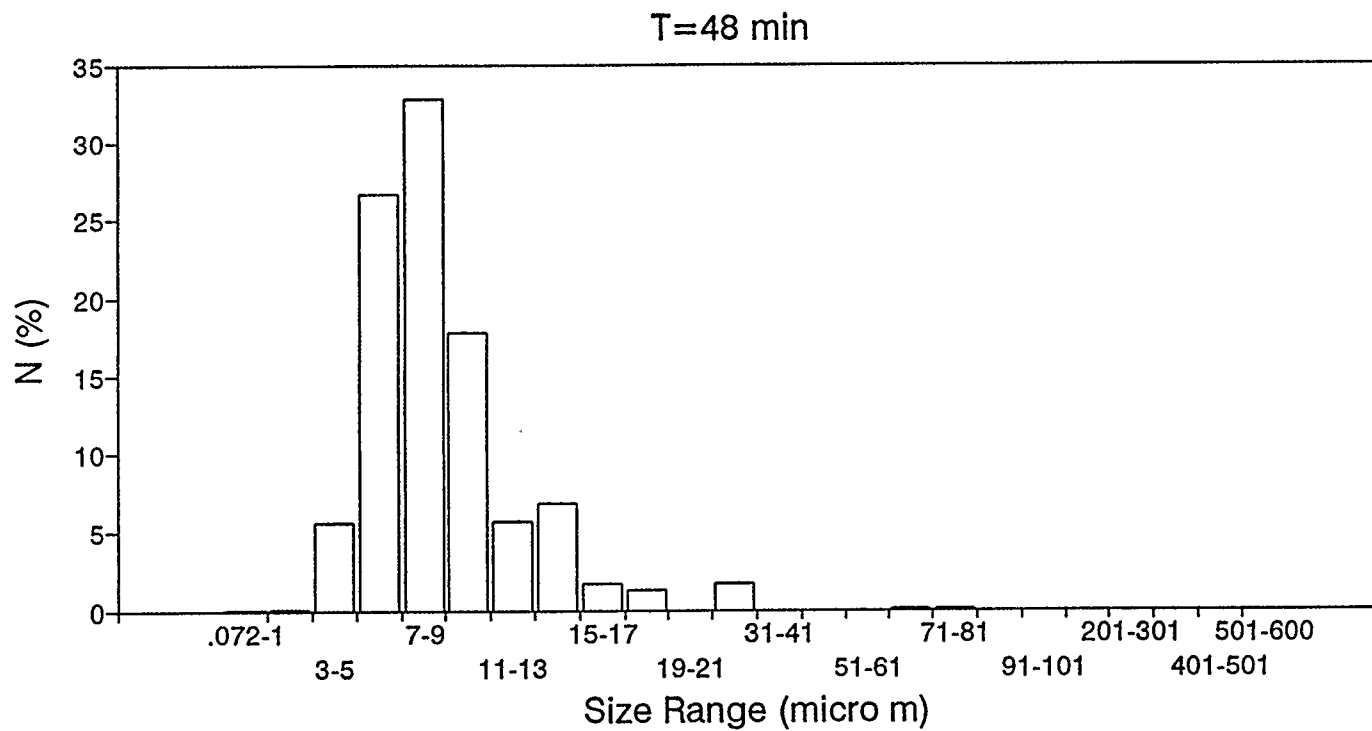


Figure B11 Distribution of Particle Number Density, N (%), with Size (μm).

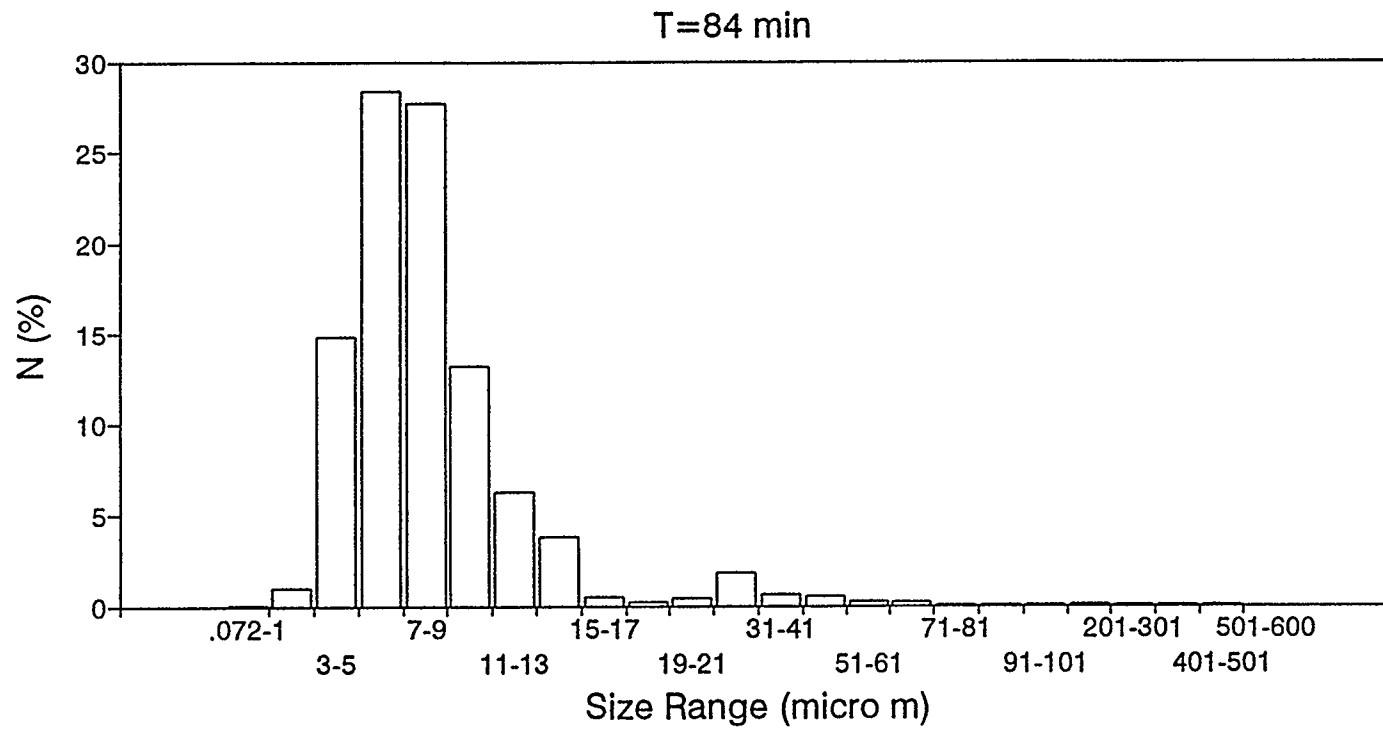


Figure B12 Distribution of Particle Number Density, N (%), with Size (μm).

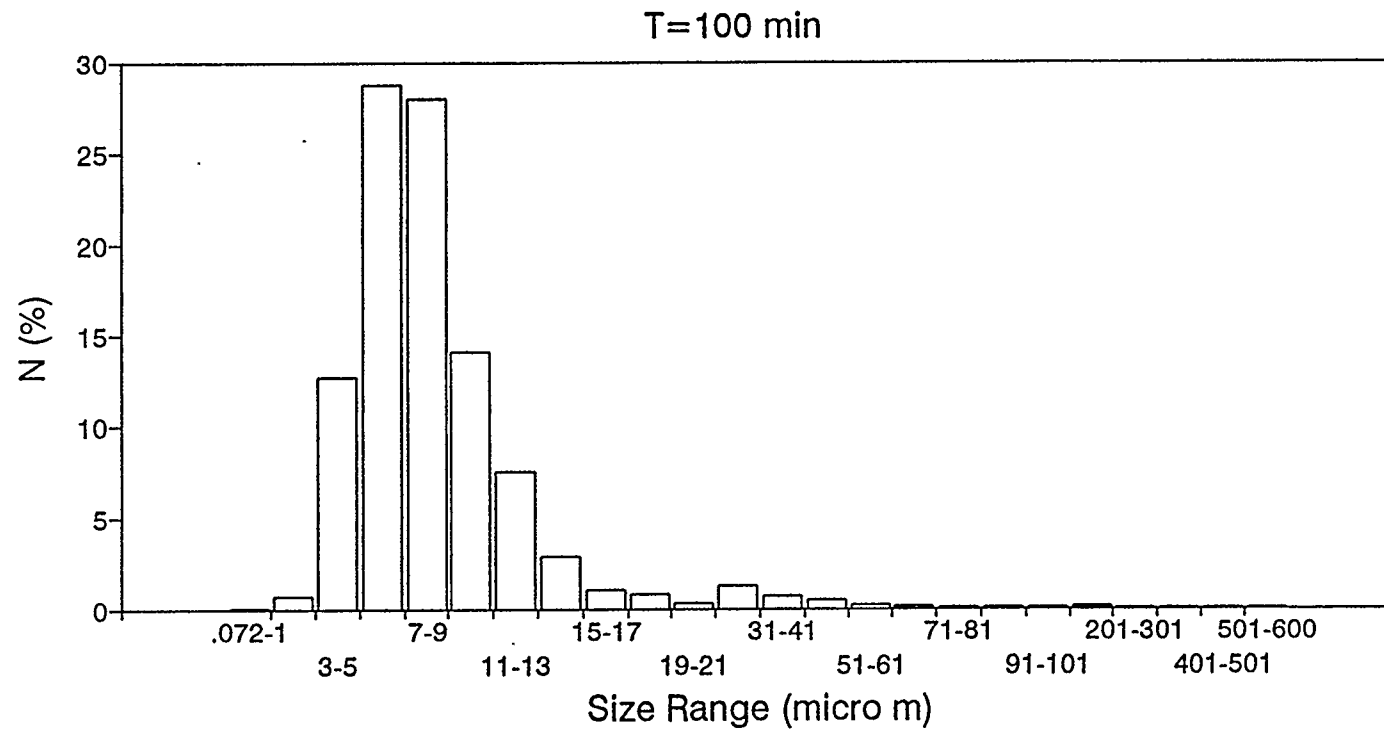


Figure B13 Distribution of Particle Number Density, N (%), with Size (μm).

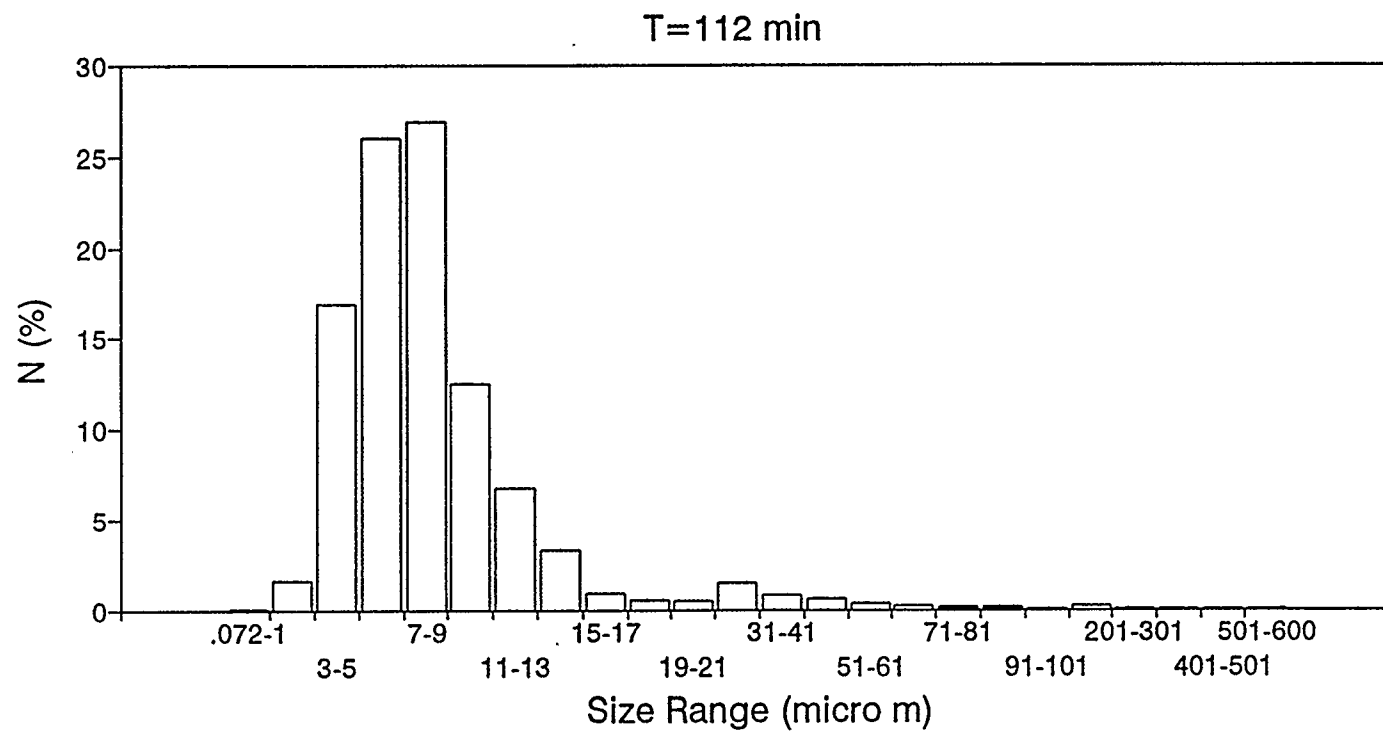


Figure B14 Distribution of Particle Number Density, N (%), with Size (μm).

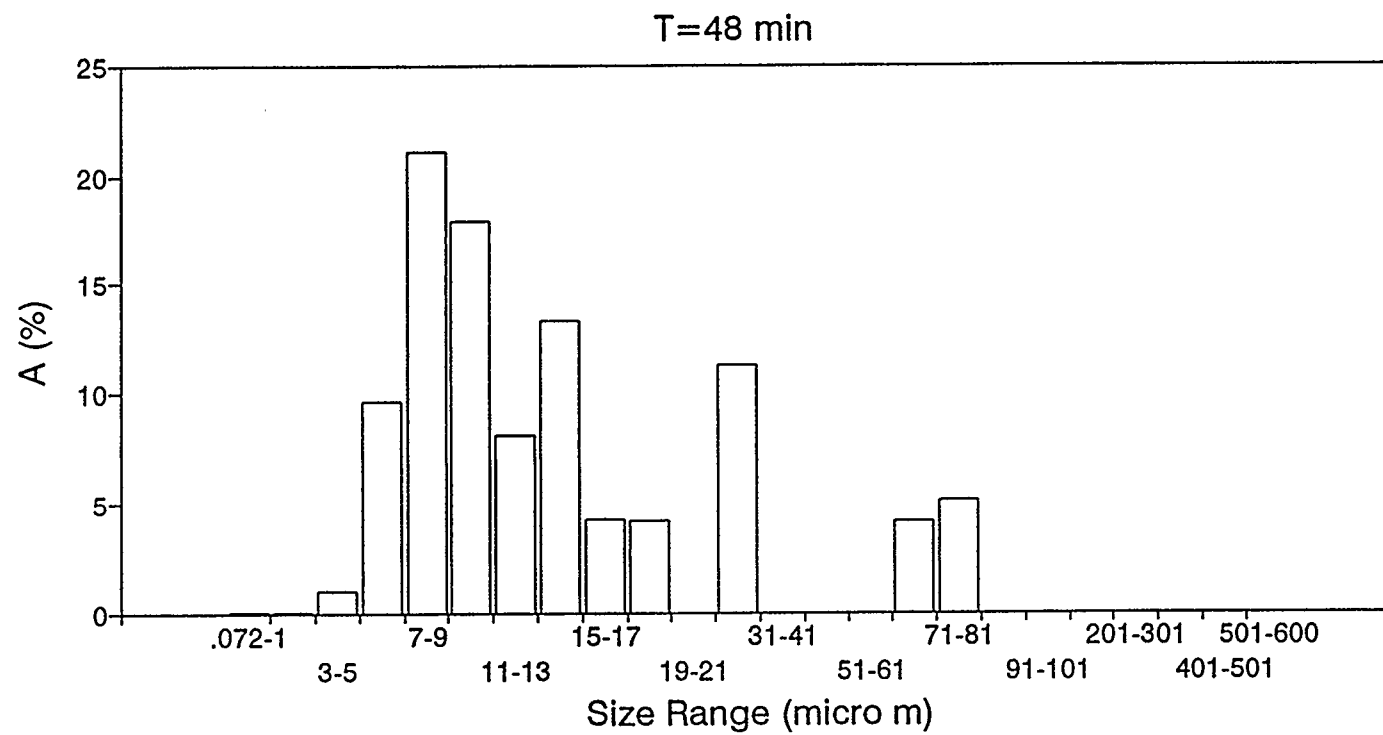


Figure B15 Distribution of Particle Area Density, A (%), with Size (μm).

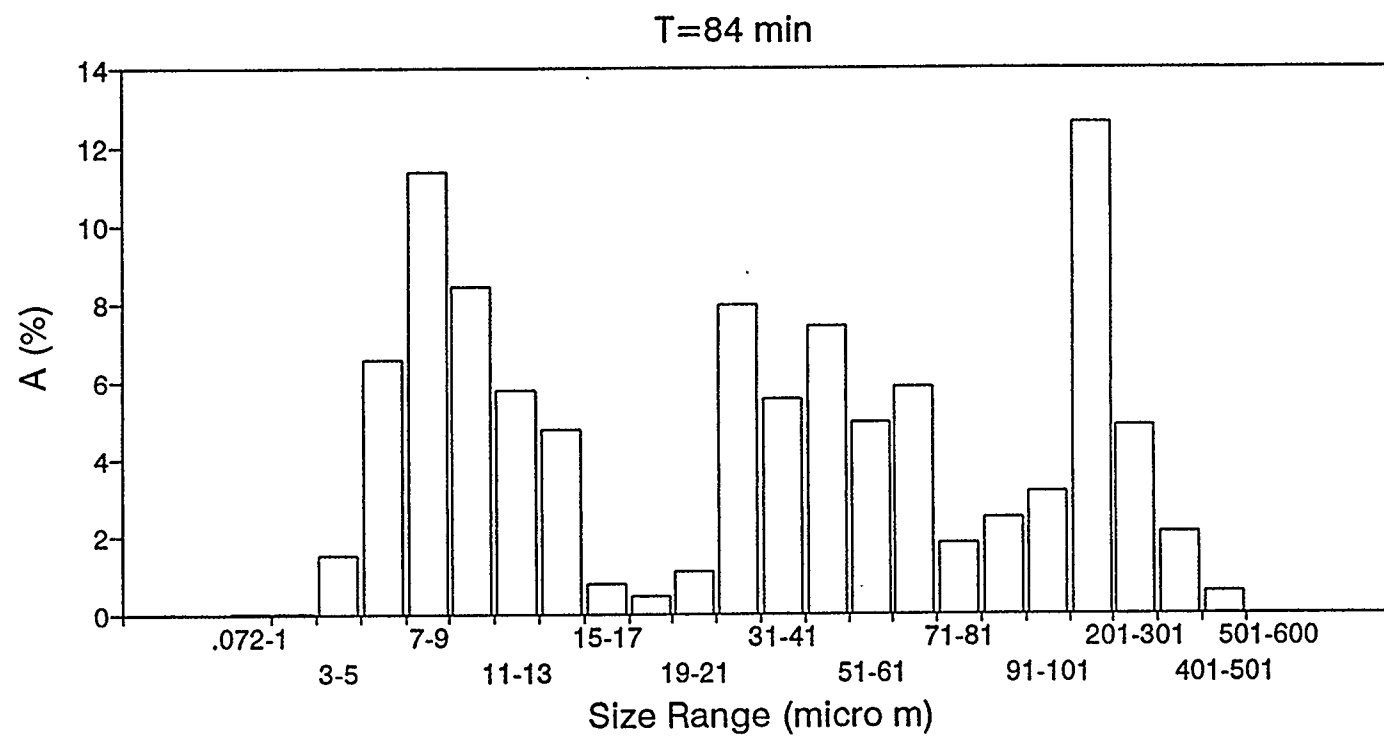


Figure B16 Distribution of Particle Area Density, A (%), with Size (μm).

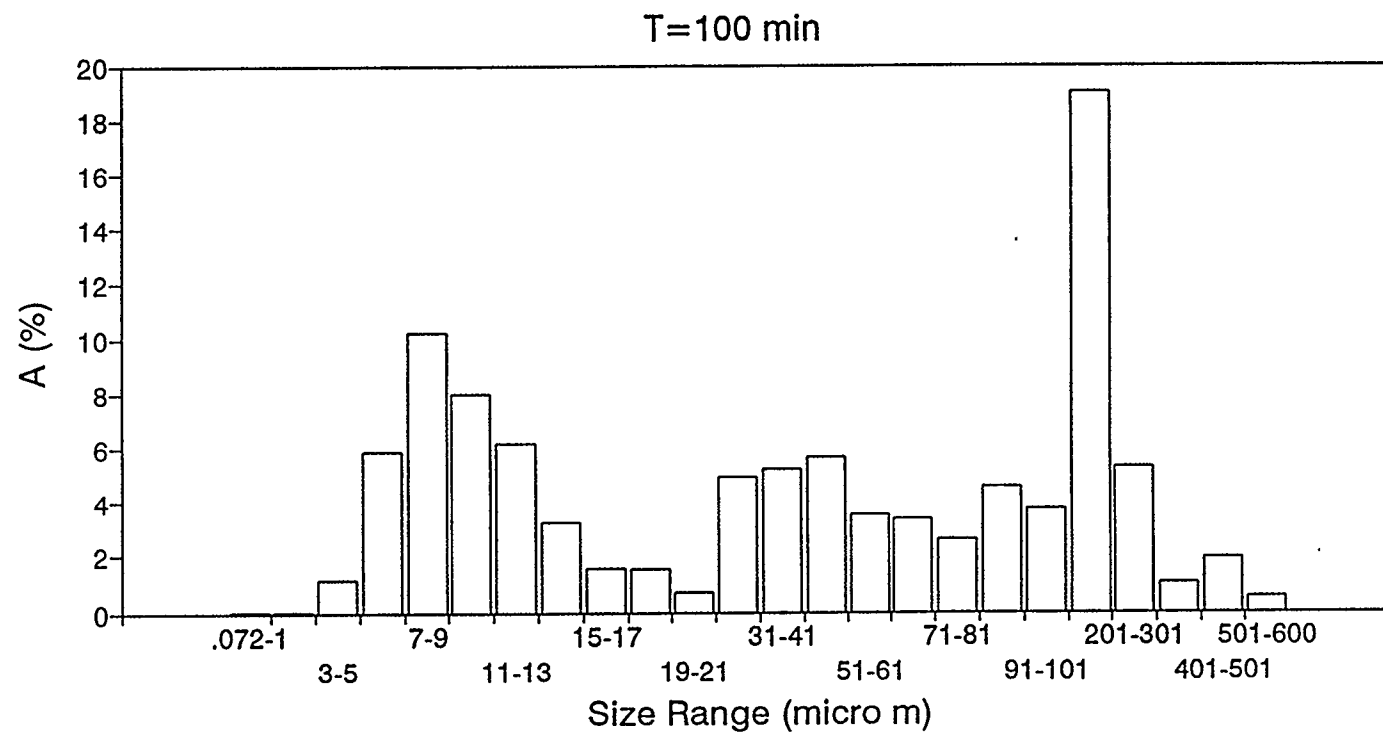


Figure B17 Distribution of Particle Area Density, A (%), with Size (μm).

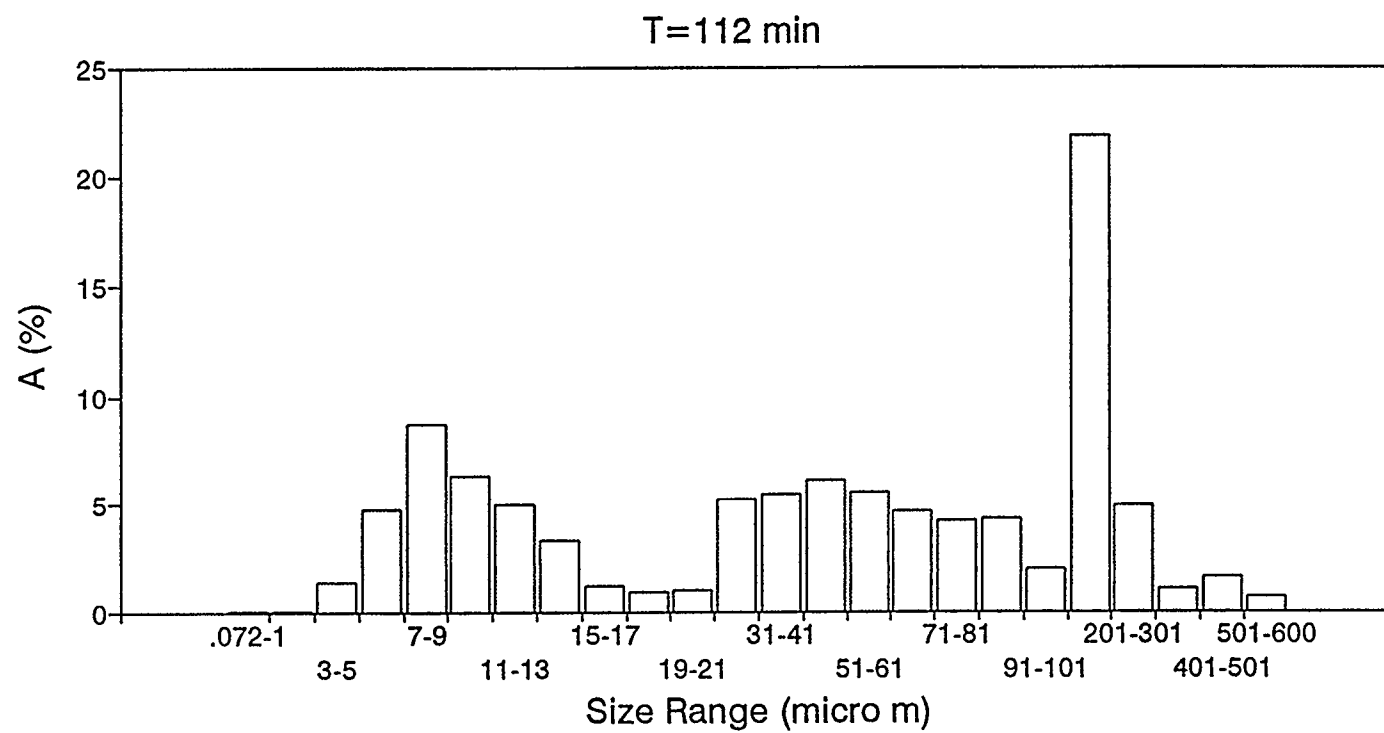


Figure B18 Distribution of Particle Area Density, A (%), with Size (μm).

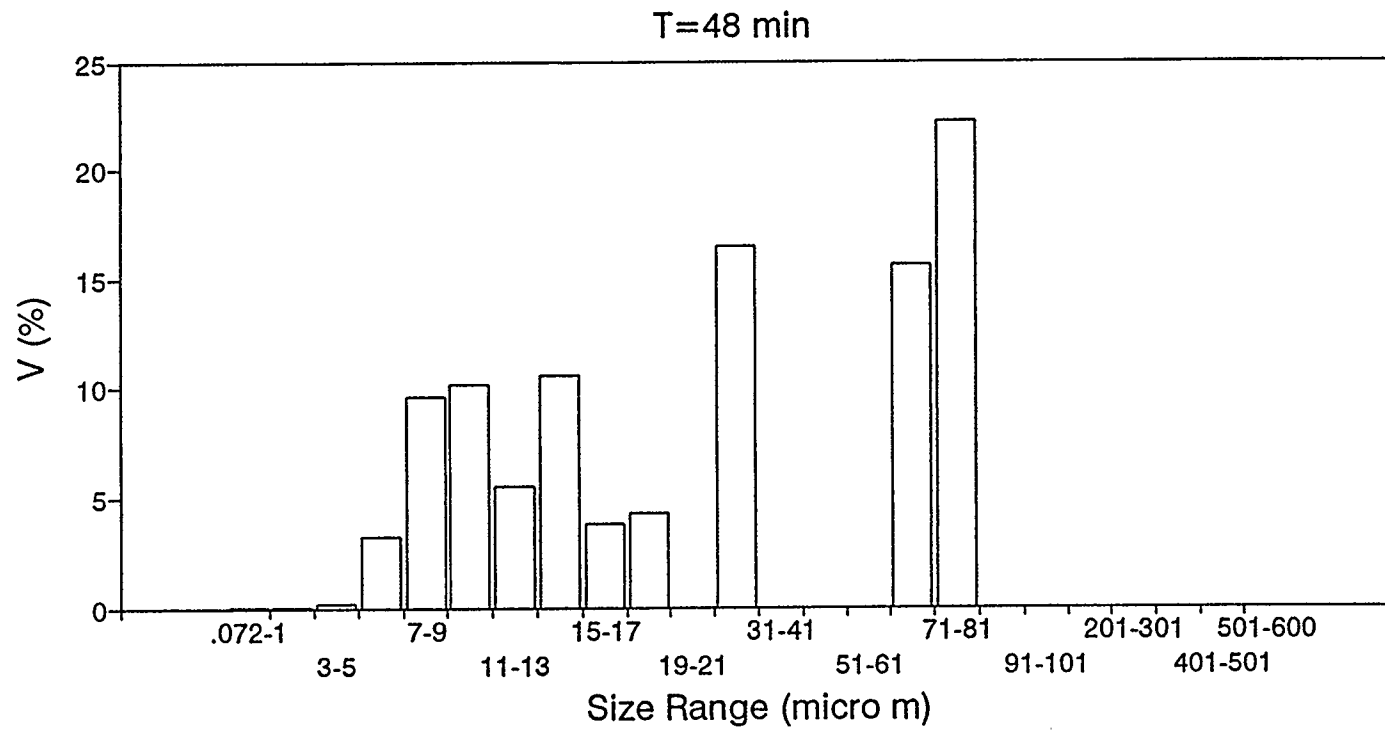


Figure B19 Distribution of Particle Volume Density, V (%), with Size (μm).

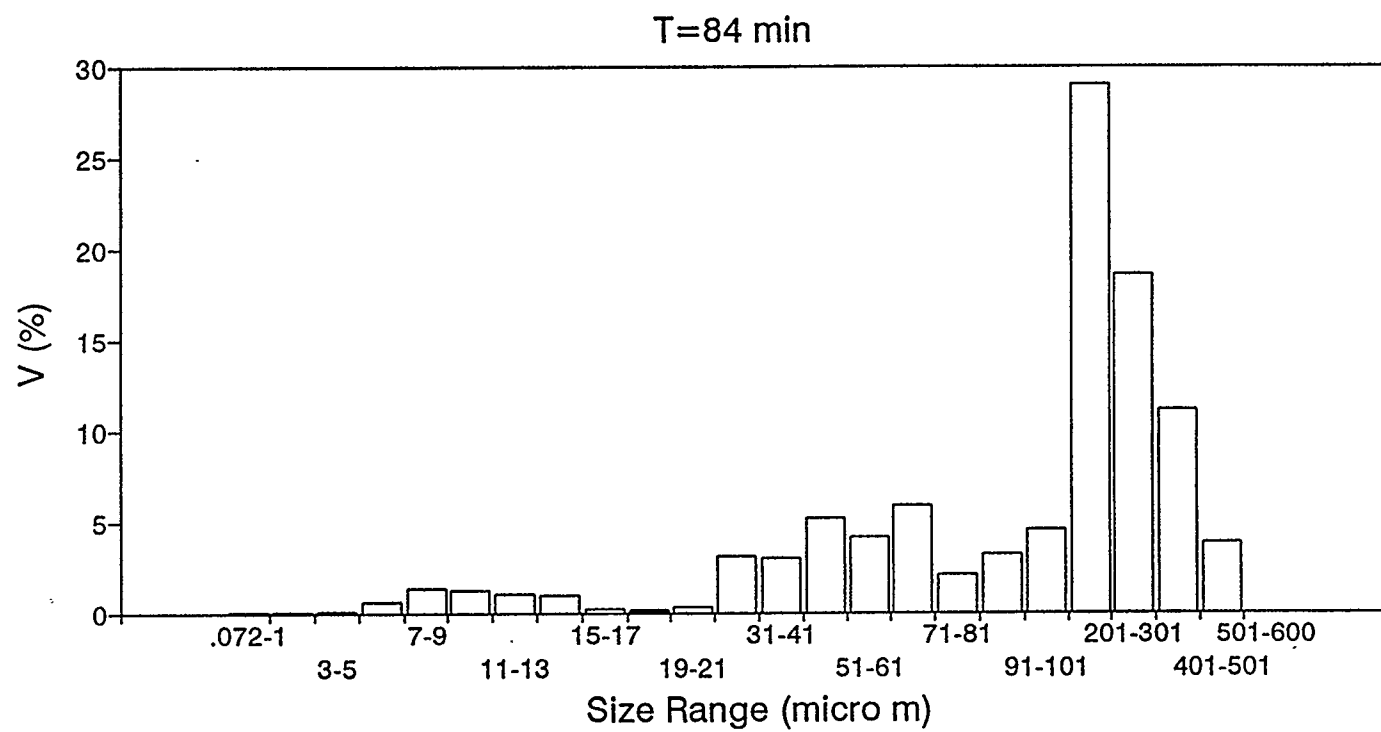


Figure B20 Distribution of Particle Volume Density, V (%), with Size (μm).

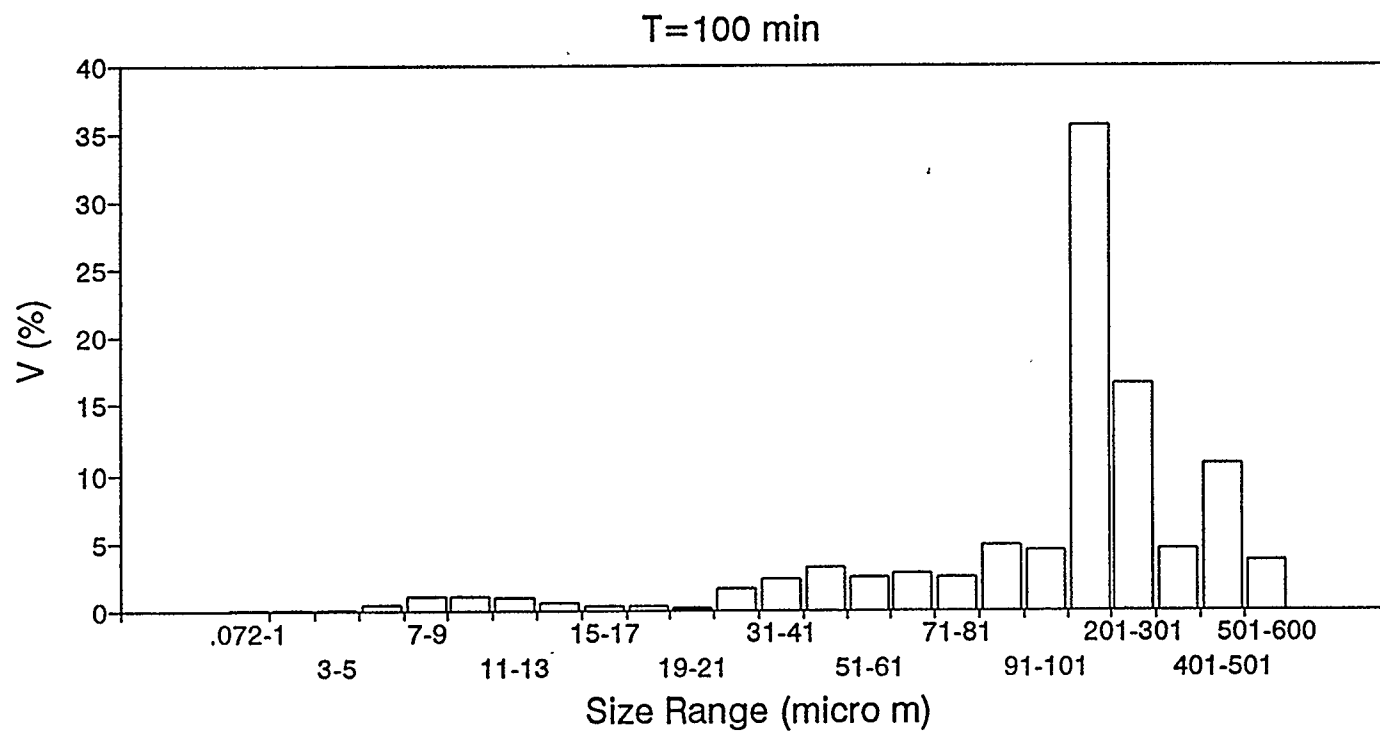


Figure B21 Distribution of Particle Volume Density, V (%), with Size (μm).

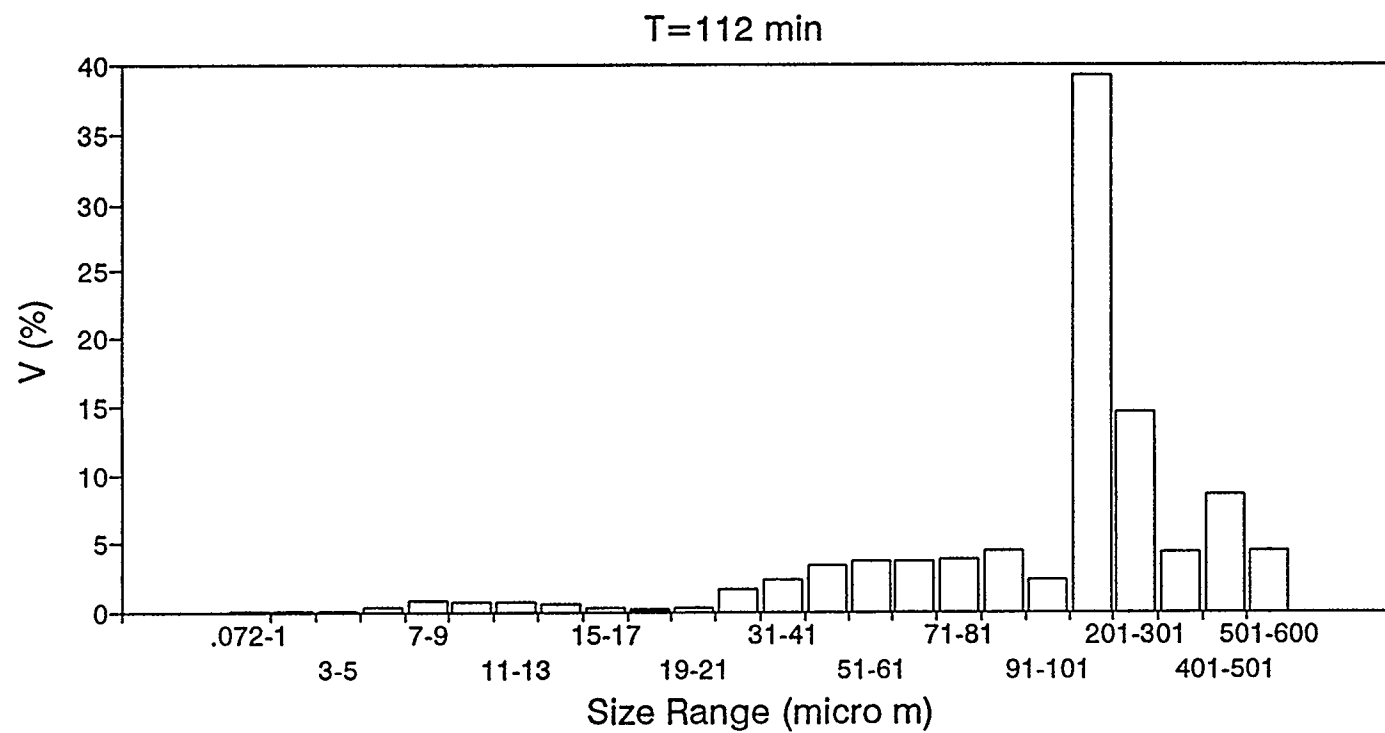


Figure B22 Distribution of Particle Volume Density, V (%), with Size (μm).

RUN #	a	b	c	2 σ
E007	-0.61988	0.02682	-0.00013	0.1422
E009	-1.33888	0.023005	-1.6e-05	0.1156
E011	-1.13312	0.034843	-6.7e-05	0.1269
E016	-2.34706	0.067493	-0.00022	0.0939
E019	-2.6057	0.075422	-0.00037	0.3216
M004	-3.5644	0.087113	-0.00014	0.1503
M005	-1.45581	0.033431	-0.00044	0.1866
M011	-0.55859	0.016328	-6.25e-05	0.0313
M012	-0.46524	0.003345	9.61e-05	0.0162
M014	0.595938	-0.02355	0.000284	0.1172
M015	0.791183	-0.02669	0.000254	0.09

Table B1 Second Moment , μ_2 (cm²/mL), as a
Function of Time, t (min)

$$\text{Function: } \mu_2 = a + bt + ct^2$$

APPENDIX-C

Particle Size Analysis

Particle Size Analysis

A particle size analysis can be plotted in terms of a cumulative number oversize or undersize in relation to the diameters of particles (cumulative analysis), or it can be plotted as the number present in each unit of diameter against the several diameters (differential analysis).

Cumulative Undersize:

It is obtained by adding, consecutively, the individual increments, starting with that containing the *smallest* particles, and plotting the cumulative sums against the *maximum* particle diameter in the increment. A function describing the cumulative undersize data is a cumulative (undersize) number distribution function.

Cumulative Oversize:

It is obtained by adding, consecutively, the individual increments, starting with that containing the *largest* particles, and plotting the cumulative sums against the *minimum* particle diameter in the increment. A function describing the cumulative oversize data is a cumulative (oversize) number distribution function.

Differential Analysis:

It is the number of particles present in each unit of diameter plotted against the several diameters and is called a *number distribution*. It is obtained as the slope of the cumulative (undersize or oversize) curve. A function describing the number distribution is called a "*Number Distribution Function*", $\phi(x)$. Between any two particle sizes, a and b , the number of particles per unit volume of sample, $N(\#/volume)$; the surface area of particles per unit volume of sample, A (area/volume); and the volume of particles per unit volume

of sample, V (volume/volume) are obtained from:

$$N = \int_a^b \phi(x) dx \quad \text{C-1}$$

$$A = \beta \int_a^b \phi(x) x^2 dx \quad \text{C-2}$$

$$V = \alpha \int_a^b \phi(x) x^3 dx \quad \text{C-3}$$

where,

x =Particle Diameter or Size

$\phi(x)$ =Number Distribution Function

β =Surface Shape Factor ($\beta=\pi$ for spherical particles)

α =Volume Shape Factor ($\alpha=\pi/6$ for spherical particles)

The Number Distribution Function, $\phi(x)$, can be obtained either from the cumulative undersize or the oversize plots. Figures C-1 and C-2 are plots of cumulative number undersize and oversize, respectively and figure C-3 is a number distribution plot, the number distribution being obtained from the cumulative oversize plot.

As described earlier, plotting the cumulative undersize requires data from the smallest particle size and onwards. The laser particle analyzer could measure particles only in the range 5-600 microns and the data clearly indicated the presence of particles below 5 microns. Therefore, plotting cumulative undersize was not possible. From the laser analyzer data it was observed that the largest particles were well below 600 microns. Therefore, a cumulative oversize could be plotted and the distribution function, $\phi(x)$, be

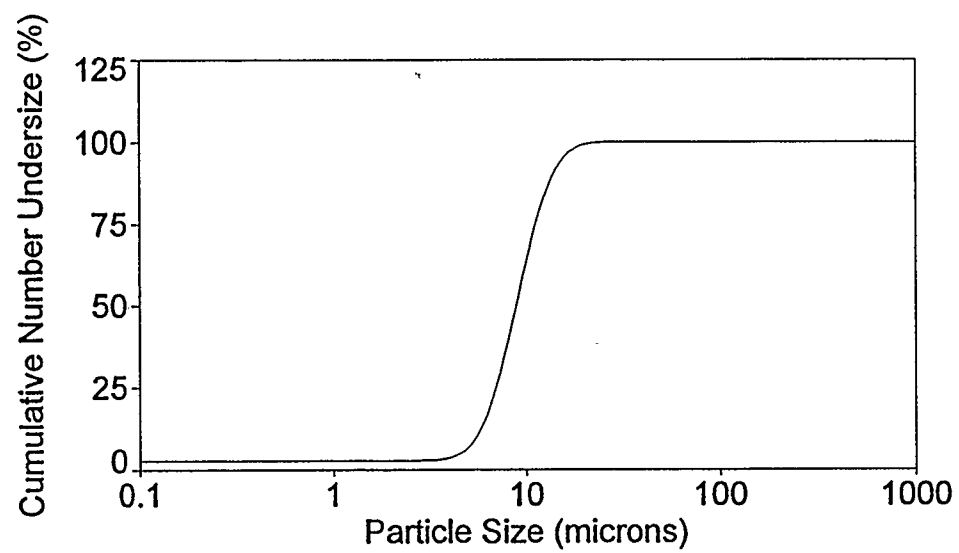


Figure C1 Cumulative Number Density Undersize Plot
Y axis: Cumulative Number Smaller than Stated
Size, %
X axis: Particle Diameter or Size.

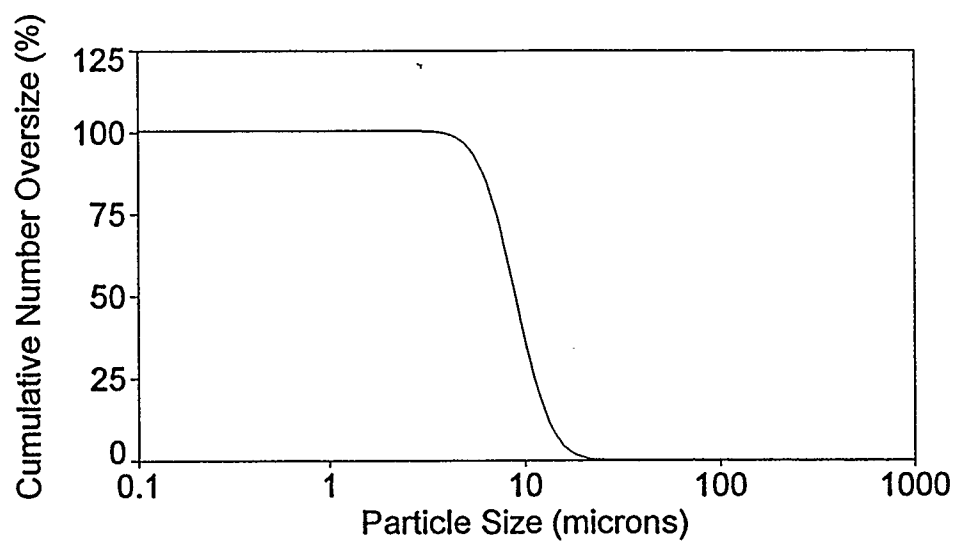


Figure C2 Cumulative Number Density Oversize Plot
Y axis: Cumulative Number Larger than Stated
Size, %
X axis: Particle Diameter or Size.

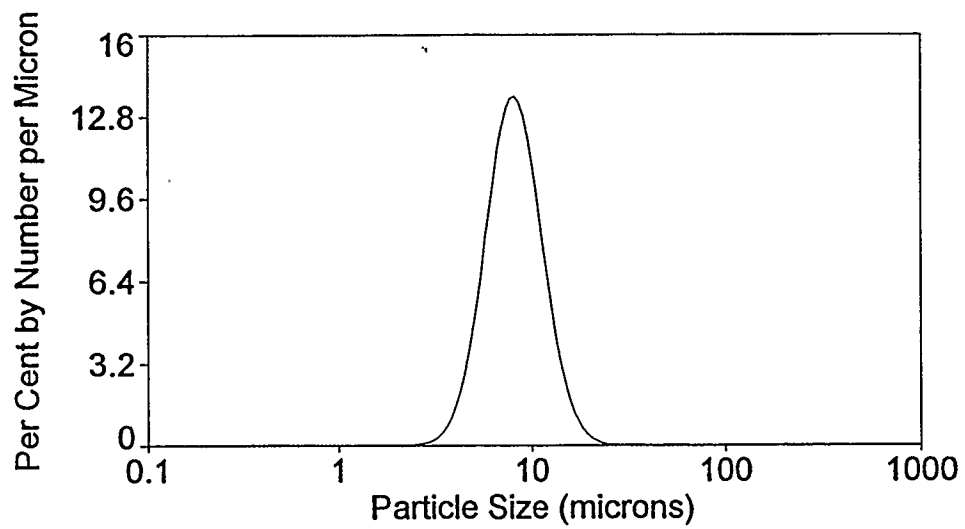


Figure C3 Number Density Distribution Plot
Y axis: Number Per cent per Micron
X axis: Particle Diameter or Size.

evaluated.

Discrete data obtained from the analyzer were that of particle size (6,8,10...600 microns, which were midpoints of ranges 5-7, 7-9, etc., microns) and the particle number density, N (#/mL), corresponding to each size. As discussed in Chapter 4, section 4.4.4, the data is clearly log-normal in distribution. Cumulative oversize plots were obtained for the raw data and cumulative log-normal distribution function (Equation C-4) regressed through the data. The number distribution function, $\phi(x)$, was obtained (Equation C-5) as the slope (first derivative wrt x) of the cumulative log-normal distribution function.

$$y = a + 0.5b(\operatorname{erfc})(-\ln(c/x)/(2^{0.5}d)) \quad \text{C-4}$$

where,

y =Cumulative Number Oversize

x =Particle Diameter or Size

a, b, c and d are constants obtained from the regression software.

$$\phi(x) = \left(-\frac{b}{\sqrt{(2\pi)d}}\right)\left(\frac{1}{x}\right)(\exp)\left(-0.5\left(\frac{\ln(c/x)}{d}\right)^2\right) \quad \text{C-5}$$

The number, area and volume densities were evaluated for particles not measured by the laser analyzer (i.e. < 5 microns) using equations C-1, C-2 and C-3.

Galai Analyzer Software Computations

The Galai analyzer software obtains raw data of the particle number density (#/mL) corresponding to the mean of each size range (size range 5-7, 7-9 μmcorresponding to mean size 6,8 μm).

Area density of each size range is computed by the software using the expression,

$$A_i = \pi N_i x_i^2 \quad \text{C-6}$$

where,

x_i = Mean Particle Size or Diameter

N_i = Particle Number Density (#/mL) Corresponding to the Size Range of Mean Size x_i .

A_i = Particle Area Density (cm²/mL) Corresponding to the Size Range of Mean Size x_i .

and the total area density (cm²/mL) of all particles measured is given by

$$A = \pi \sum N_i x_i^2 \quad \text{C-7}$$

for all the particles "i".

Similarly, the volume density of each size range is computed by the software using the expression

$$V_i = \frac{\pi}{6} N_i x_i^3 \quad \text{C-8}$$

where,

V_i = Particle Volume Density (cm³/mL) Corresponding to the Size Range of Mean Size x_i .

and the total volume density (cm³/mL) of all particles measured is given by

$$V = \frac{\pi}{6} \sum N_i x_i^3 \quad \text{C-9}$$

for all particles "i".

APPENDIX-D

Raw Particle Analyzer Data

The raw analyzer data is tabulated here as particle size or diameter (micro m), S, and the corresponding particle number density (#/mL), N. Each table is marked by a file name such as E7T70 which implies the ethane kinetic experiment E007 and the analyzer data obtained at time, T=70 minutes.

E7T33

S	N	S	N	S	N	S	N	S	N
6	26994.79	126	0	246	0	366	0	486	0
8	30723.51	128	0	248	0	368	0	488	0
10	19404.98	130	0	250	0	370	0	490	0
12	4064.594	132	0	252	0	372	0	492	0
14	7458.263	134	0	254	0	374	0	494	0
16	1513.689	136	0	256	0	376	0	496	0
18	0	138	0	258	0	378	0	498	0
20	0	140	0	260	0	380	0	500	0
22	984.7221	142	0	262	0	382	0	502	0
24	140.415	144	0	264	0	384	0	504	0
26	1786.444	146	0	266	0	386	0	506	0
28	0	148	0	268	0	388	0	508	0
30	279.4325	150	0	270	0	390	0	510	0
32	488.5919	152	0	272	0	392	0	512	0
34	0	154	0	274	0	394	0	514	0
36	0	156	0	276	0	396	0	516	0
38	213.6312	158	0	278	0	398	0	518	0
40	0	160	0	280	0	400	0	520	0
42	0	162	0	282	0	402	0	522	0
44	182.9664	164	0	284	0	404	0	524	0
46	0	166	0	286	0	406	0	526	0
48	0	168	0	288	0	408	0	528	0
50	0	170	0	290	0	410	0	530	0
52	0	172	0	292	0	412	0	532	0
54	0	174	0	294	0	414	0	534	0
56	0	176	0	296	0	416	0	536	0
58	0	178	0	298	0	418	0	538	0
60	0	180	0	300	0	420	0	540	0
62	0	182	0	302	0	422	0	542	0
64	0	184	0	304	0	424	0	544	0
66	0	186	0	306	0	426	0	546	0
68	0	188	0	308	0	428	0	548	0
70	0	190	0	310	0	430	0	550	0
72	0	192	0	312	0	432	0	552	0
74	0	194	0	314	0	434	0	554	0
76	0	196	0	316	0	436	0	556	0
78	0	198	0	318	0	438	0	558	0
80	0	200	0	320	0	440	0	560	0
82	0	202	0	322	0	442	0	562	0
84	0	204	0	324	0	444	0	564	0
86	0	206	0	326	0	446	0	566	0
88	0	208	0	328	0	448	0	568	0
90	0	210	0	330	0	450	0	570	0
92	0	212	0	332	0	452	0	572	0
94	0	214	0	334	0	454	0	574	0
96	0	216	0	336	0	456	0	576	0
98	0	218	0	338	0	458	0	578	0
100	0	220	0	340	0	460	0	580	0
102	0	222	0	342	0	462	0	582	0
104	0	224	0	344	0	464	0	584	0
106	0	226	0	346	0	466	0	586	0
108	0	228	0	348	0	468	0	588	0
110	0	230	0	350	0	470	0	590	0
112	0	232	0	352	0	472	0	592	0
114	0	234	0	354	0	474	0	594	0
116	0	236	0	356	0	476	0	596	0
118	49.55542	238	0	358	0	478	0	598	0
120	14.42585	240	0	360	0	480	0	600	0
122	0	242	0	362	0	482	0		
124	0	244	0	364	0	484	0		

S=Size (micro m); N=Particle Number Density (1/mL)

E7T39

S	N	S	N	S	N	S	N	S	N
6	71930.76	126	0	246	0	366	0	486	0
8	87188.22	128	0	248	0	368	0	488	0
10	30606.61	130	0	250	0	370	0	490	0
12	6738.743	132	0	252	0	372	0	492	0
14	7194.428	134	0	254	0	374	0	494	0
16	968.6058	136	0	256	0	376	0	496	0
18	0	138	0	258	16.10128	378	0	498	0
20	2356.077	140	0	260	0	380	0	500	0
22	1998.27	142	0	262	0	382	0	502	0
24	0	144	0	264	0	384	0	504	0
26	1282.658	146	0	266	0	386	0	506	0
28	924.8515	148	0	268	0	388	0	508	0
30	567.0449	150	0	270	0	390	0	510	0
32	0	152	0	272	0	392	0	512	0
34	314.7924	154	0	274	0	394	0	514	0
36	1061.729	156	0	276	0	396	0	516	0
38	433.5161	158	0	278	0	398	0	518	0
40	0	160	0	280	0	400	0	520	0
42	0	162	0	282	0	402	0	522	0
44	742.5776	164	0	284	0	404	0	524	0
46	0	166	0	286	0	406	0	526	0
48	0	168	0	288	0	408	0	528	0
50	0	170	0	290	0	410	0	530	0
52	288.3192	172	0	292	0	412	0	532	0
54	0	174	0	294	0	414	0	534	0
56	246.8345	176	0	296	0	416	0	536	0
58	0	178	0	298	0	418	0	538	0
60	191.8345	180	0	300	0	420	0	540	0
62	13.34522	182	0	302	0	422	0	542	0
64	0	184	0	304	0	424	0	544	0
66	0	186	0	306	0	426	0	546	0
68	0	188	0	308	0	428	0	548	0
70	0	190	0	310	0	430	0	550	0
72	0	192	0	312	0	432	0	552	0
74	0	194	0	314	0	434	0	554	0
76	0	196	26.06634	316	0	436	0	556	0
78	0	198	17.84825	318	0	438	0	558	0
80	0	200	0	320	0	440	0	560	0
82	0	202	0	322	0	442	0	562	0
84	0	204	0	324	0	444	0	564	0
86	0	206	0	326	0	446	0	566	0
88	0	208	0	328	0	448	0	568	0
90	0	210	0	330	0	450	0	570	0
92	0	212	0	332	0	452	0	572	0
94	0	214	0	334	0	454	0	574	0
96	0	216	0	336	0	456	0	576	0
98	0	218	0	338	0	458	0	578	0
100	0	220	0	340	0	460	0	580	0
102	0	222	0	342	0	462	0	582	0
104	0	224	0	344	0	464	0	584	0
106	0	226	0	346	0	466	0	586	0
108	0	228	0	348	0	468	0	588	0
110	140.7612	230	0	350	0	470	0	590	0
112	0	232	0	352	0	472	0	592	0
114	0	234	0	354	0	474	0	594	0
116	0	236	0	356	0	476	0	596	0
118	0	238	0	358	0	478	0	598	0
120	0	240	0	360	0	480	0	600	0
122	0	242	0	362	0	482	0		
124	0	244	0	364	0	484	0		

S=Size (micro m); N=Particle Number Density (1/mL)

E7T44

S	N	S	N	S	N	S	N	S	N
6	119077.6	126	0	246	0	366	0	486	0
8	117736.4	128	0	248	0	368	0	488	0
10	22538.96	130	0	250	0	370	0	490	0
12	12365.44	132	0	252	0	372	0	492	0
14	13721.55	134	0	254	0	374	0	494	0
16	6021.373	136	0	256	0	376	0	496	0
18	0	138	0	258	0	378	0	498	0
20	0	140	0	260	0	380	0	500	0
22	2978.082	142	0	262	0	382	0	502	0
24	5314.32	144	0	264	0	384	0	504	0
26	3491.134	146	0	266	0	386	0	506	0
28	1378.334	148	0	268	0	388	0	508	0
30	0	150	0	270	0	390	0	510	0
32	0	152	0	272	0	392	0	512	0
34	0	154	0	274	0	394	0	514	0
36	0	156	0	276	0	396	0	516	0
38	0	158	0	278	0	398	0	518	0
40	0	160	0	280	0	400	0	520	0
42	584.2562	162	0	282	0	402	0	522	0
44	553.3432	164	0	284	0	404	0	524	0
46	130.3721	166	0	286	0	406	0	526	0
48	368.8592	168	0	288	0	408	0	528	0
50	205.0421	170	0	290	0	410	0	530	0
52	238.41	172	0	292	0	412	0	532	0
54	0	174	0	294	0	414	0	534	0
56	0	176	0	296	0	416	0	536	0
58	0	178	0	298	0	418	0	538	0
60	0	180	0	300	0	420	0	540	0
62	0	182	0	302	0	422	0	542	0
64	0	184	0	304	0	424	0	544	0
66	0	186	0	306	0	426	0	546	0
68	0	188	0	308	0	428	0	548	0
70	0	190	0	310	0	430	0	550	0
72	147.4333	192	0	312	0	432	0	552	0
74	412.7462	194	0	314	0	434	0	554	0
76	0	196	0	316	0	436	0	556	0
78	0	198	0	318	0	438	0	558	0
80	0	200	0	320	0	440	0	560	0
82	0	202	0	322	0	442	0	562	1.681994
84	0	204	0	324	0	444	0	564	1.821169
86	0	206	0	326	0	446	0	566	0
88	0	208	0	328	0	448	0	568	0
90	0	210	0	330	0	450	0	570	0
92	0	212	0	332	0	452	0	572	0
94	0	214	0	334	0	454	0	574	0
96	0	216	0	336	0	456	0	576	0
98	232.8827	218	0	338	0	458	0	578	0
100	0	220	0	340	0	460	0	580	0
102	0	222	0	342	0	462	0	582	0
104	0	224	0	344	0	464	0	584	0
106	0	226	0	346	0	466	0	586	0
108	0	228	0	348	0	468	0	588	0
110	0	230	0	350	0	470	0	590	0
112	0	232	0	352	0	472	0	592	0
114	0	234	0	354	0	474	0	594	0
116	0	236	0	356	0	476	0	596	0
118	0	238	0	358	0	478	0	598	0
120	0	240	0	360	0	480	0	600	0
122	0	242	0	362	0	482	0		
124	0	244	0	364	0	484	0		

S=Size (micro m); N=Particle Number Density (1/mL)

E7T53

S	N	S	N	S	N	S	N	S	N
6	161514.2	126	0	246	0	366	0	486	0
8	133795.7	128	0	248	0	368	0	488	0
10	43230.18	130	0	250	0	370	0	490	0
12	4007.148	132	0	252	0	372	0	492	0
14	10478.75	134	0	254	0	374	0	494	0
16	10193.64	136	0	256	0	376	0	496	0
18	0	138	111.1122	258	0	378	0	498	0
20	5005.922	140	0	260	0	380	0	500	0
22	2122.849	142	0	262	0	382	0	502	0
24	1742.735	144	0	264	0	384	0	504	0
26	2549.581	146	0	266	0	386	0	506	0
28	126.6613	148	0	268	0	388	0	508	0
30	602.3965	150	0	270	0	390	0	510	0
32	0	152	91.90001	272	0	392	0	512	0
34	0	154	0	274	0	394	0	514	0
36	482.5782	156	19.59892	276	0	396	0	516	0
38	0	158	64.68977	278	0	398	0	518	0
40	438.5071	160	0	280	0	400	0	520	0
42	0	162	0	282	0	402	0	522	0
44	0	164	0	284	0	404	0	524	0
46	0	166	0	286	0	406	0	526	0
48	0	168	0	288	0	408	0	528	0
50	328.3295	170	0	290	0	410	0	530	0
52	612.5881	172	0	292	0	412	0	532	0
54	284.2585	174	0	294	0	414	0	534	0
56	0	176	0	296	0	416	0	536	0
58	0	178	0	298	0	418	0	538	0
60	0	180	0	300	0	420	0	540	0
62	215.4072	182	0	302	0	422	0	542	0
64	212.6626	184	0	304	0	424	0	544	0
66	0	186	54.41593	306	0	426	0	546	0
68	0	188	0	308	0	428	0	548	0
70	0	190	0	310	0	430	0	550	0
72	83.12113	192	0	312	0	432	0	552	0
74	116.9496	194	24.34565	314	0	434	0	554	0
76	0	196	23.61741	316	0	436	0	556	0
78	193.4504	198	0	318	0	438	0	558	0
80	190.7057	200	0	320	0	440	0	560	0
82	0	202	0	322	0	442	0	562	0
84	0	204	0	324	0	444	0	564	0
86	0	206	0	326	0	446	0	566	0
88	179.7274	208	0	328	0	448	0	568	0
90	0	210	0	330	0	450	0	570	0
92	0	212	0	332	0	452	0	572	0
94	0	214	0	334	0	454	0	574	0
96	0	216	0	336	0	456	0	576	0
98	0	218	0	338	0	458	0	578	0
100	0	220	0	340	13.69646	460	0	580	0
102	0	222	0	342	0	462	0	582	0
104	0	224	0	344	0	464	0	584	0
106	0	226	0	346	0	466	0	586	0
108	0	228	0	348	0	468	0	588	0
110	0	230	0	350	0	470	0	590	0
112	0	232	0	352	0	472	0	592	0
114	0	234	0	354	0	474	0	594	0
116	0	236	0	356	0	476	0	596	0
118	138.5583	238	0	358	0	478	0	598	0
120	0	240	0	360	0	480	0	600	0
122	0	242	0	362	0	482	0		
124	0	244	0	364	0	484	0		

S=Size (micro m); N=Particle Number Density (1/mL)

E7T60

S	N	S	N	S	N	S	N	S	N
6	86014.76	126	0	246	0	366	0	486	0
8	52181.05	128	0	248	0	368	0	488	0
10	63626.77	130	0	250	0	370	0	490	0
12	19840.64	132	0	252	0	372	0	492	0
14	3408.195	134	0	254	0	374	0	494	0
16	0	136	99.1506	256	0	376	0	496	0
18	4510.346	138	77.06592	258	0	378	0	498	0
20	0	140	0	260	0	380	0	500	0
22	3321.03	142	0	262	0	382	0	502	0
24	2726.374	144	0	264	0	384	0	504	0
26	2131.716	146	0	266	0	386	0	506	0
28	0	148	0	268	0	388	0	508	0
30	0	150	0	270	0	390	0	510	0
32	0	152	0	272	0	392	0	512	0
34	789.4288	154	0	274	0	394	0	514	0
36	754.956	156	0	276	0	396	0	516	0
38	393.5272	158	0	278	0	398	0	518	0
40	1683.332	160	0	280	0	400	0	520	0
42	0	162	0	282	0	402	0	522	0
44	1234.129	164	0	284	0	404	0	524	0
46	0	166	0	286	0	406	0	526	0
48	0	168	0	288	0	408	0	528	0
50	513.6458	170	0	290	0	410	0	530	0
52	0	172	0	292	0	412	0	532	0
54	0	174	0	294	0	414	0	534	0
56	0	176	0	296	0	416	0	536	0
58	0	178	0	298	0	418	0	538	0
60	0	180	0	300	0	420	0	540	0
62	0	182	0	302	0	422	0	542	0
64	0	184	0	304	0	424	0	544	0
66	0	186	0	306	0	426	0	546	0
68	414.2416	188	0	308	0	428	13.50124	548	0
70	341.2455	190	0	310	0	430	0	550	0
72	206.6275	192	0	312	0	432	0	552	0
74	0	194	0	314	0	434	0	554	0
76	0	196	0	316	0	436	0	556	0
78	0	198	0	318	0	438	0	558	0
80	501.2779	200	0	320	0	440	0	560	0
82	94.03756	202	0	322	0	442	0	562	0
84	235.9292	204	0	324	0	444	0	564	0
86	53.03002	206	0	326	0	446	0	566	0
88	0	208	0	328	0	448	0	568	0
90	0	210	2.109819	330	1.280824	450	0	570	0
92	0	212	53.93688	332	20.93295	452	0	572	0
94	0	214	0	334	0	454	0	574	0
96	0	216	0	336	0	456	0	576	0
98	0	218	0	338	0	458	0	578	0
100	0	220	46.99183	340	0	460	0	580	0
102	0	222	0	342	0	462	0	582	0
104	246.8197	224	0	344	0	464	0	584	0
106	0	226	0	346	0	466	0	586	0
108	0	228	0	348	0	468	0	588	0
110	0	230	0	350	0	470	0	590	0
112	0	232	25.93403	352	0	472	0	592	0
114	184.6691	234	7.089179	354	0	474	0	594	0
116	39.90681	236	0	356	0	476	0	596	0
118	0	238	0	358	0	478	0	598	0
120	0	240	0	360	0	480	0	600	0
122	18.22321	242	0	362	0	482	0		
124	186.0351	244	0	364	0	484	0		

S=Size (micro m); N=Particle Number Density (1/mL)

E7T70

S	N	S	N	S	N	S	N	S	N
6	185401.5	126	0	246	0	366	0	486	0
8	137714.7	128	0	248	0	368	0	488	0
10	90130.81	130	0	250	0	370	0	490	0
12	25331.78	132	0	252	0	372	0	492	0
14	8336.012	134	0	254	0	374	0	494	0
16	7466.3	136	0	256	0	376	0	496	0
18	10574.69	138	0	258	0	378	0	498	0
20	8000.125	140	171.2542	260	0	380	0	500	0
22	18151.54	142	74.75264	262	0	382	0	502	0
24	4254.634	144	0	264	0	384	0	504	0
26	9160.179	146	0	266	0	386	0	506	0
28	579.6119	148	0	268	0	388	0	508	0
30	7.026785	150	0	270	0	390	0	510	0
32	2403.844	152	0	272	38.0027	392	0	512	0
34	1154.576	154	0	274	0	394	0	514	0
36	227.5684	156	0	276	37.67859	396	0	516	0
38	836.5625	158	0	278	0	398	0	518	0
40	0	160	0	280	0	400	0	520	0
42	0	162	0	282	0	402	0	522	0
44	0	164	0	284	0	404	0	524	0
46	0	166	0	286	0	406	0	526	0
48	487.4748	168	0	288	0	408	0	528	0
50	1045.645	170	0	290	0	410	0	530	0
52	0	172	0	292	0	412	0	532	0
54	0	174	0	294	0	414	0	534	0
56	0	176	0	296	0	416	0	536	0
58	0	178	0	298	0	418	0	538	0
60	0	180	0	300	0	420	0	540	0
62	0	182	0	302	0	422	0	542	0
64	0	184	0	304	0	424	0	544	0
66	0	186	0	306	0	426	0	546	0
68	0	188	0	308	0	428	0	548	0
70	467.741	190	0	310	0	430	0	550	0
72	0	192	0	312	0	432	0	552	0
74	0	194	0	314	0	434	0	554	0
76	245.1754	196	0	316	0	436	0	556	0
78	200.8763	198	0	318	0	438	0	558	0
80	0	200	0	320	0	440	0	560	0
82	0	202	0	322	0	442	0	562	0
84	0	204	0	324	0	444	0	564	0
86	0	206	0	326	0	446	0	566	0
88	0	208	0	328	0	448	0	568	0
90	0	210	0	330	0	450	0	570	0
92	0	212	0	332	0	452	0	572	0
94	0	214	0	334	0	454	0	574	0
96	0	216	0	336	0	456	0	576	0
98	0	218	0	338	0	458	0	578	0
100	0	220	0	340	0	460	0	580	0
102	0	222	0	342	0	462	0	582	0
104	0	224	0	344	0	464	0	584	0
106	0	226	0	346	0	466	0	586	0
108	0	228	0	348	0	468	0	588	0
110	0	230	0	350	0	470	0	590	0
112	0	232	0	352	0	472	0	592	0
114	0	234	0	354	0	474	0	594	0
116	0	236	0	356	0	476	0	596	0
118	0	238	0	358	0	478	0	598	0
120	0	240	0	360	0	480	0	600	0
122	0	242	0	362	0	482	0		
124	0	244	0	364	0	484	0		

S=Size (micro m); N=Particle Number Density (1/mL)

M14T48

S	N	S	N	S	N	S	N	S	N
6	4040.373	126	0	246	0	366	0	486	0
8	4993.193	128	0	248	0	368	0	488	0
10	2711.077	130	0	250	0	370	0	490	0
12	853.0466	132	0	252	0	372	0	492	0
14	1025.863	134	0	254	0	374	0	494	0
16	250.7439	136	0	256	0	376	0	496	0
18	196.8052	138	0	258	0	378	0	498	0
20	0	140	0	260	0	380	0	500	0
22	144.9105	142	0	262	0	382	0	502	0
24	59.34889	144	0	264	0	384	0	504	0
26	46.61151	146	0	266	0	386	0	506	0
28	0	148	0	268	0	388	0	508	0
30	0	150	0	270	0	390	0	510	0
32	0	152	0	272	0	392	0	512	0
34	0	154	0	274	0	394	0	514	0
36	0	156	0	276	0	396	0	516	0
38	0	158	0	278	0	398	0	518	0
40	0	160	0	280	0	400	0	520	0
42	0	162	0	282	0	402	0	522	0
44	0	164	0	284	0	404	0	524	0
46	0	166	0	286	0	406	0	526	0
48	0	168	0	288	0	408	0	528	0
50	0	170	0	290	0	410	0	530	0
52	0	172	0	292	0	412	0	532	0
54	0	174	0	294	0	414	0	534	0
56	0	176	0	296	0	416	0	536	0
58	0	178	0	298	0	418	0	538	0
60	0	180	0	300	0	420	0	540	0
62	0	182	0	302	0	422	0	542	0
64	14.47442	184	0	304	0	424	0	544	0
66	0.041902	186	0	306	0	426	0	546	0
68	0	188	0	308	0	428	0	548	0
70	0	190	0	310	0	430	0	550	0
72	0	192	0	312	0	432	0	552	0
74	8.440526	194	0	314	0	434	0	554	0
76	5.068708	196	0	316	0	436	0	556	0
78	0	198	0	318	0	438	0	558	0
80	0	200	0	320	0	440	0	560	0
82	0	202	0	322	0	442	0	562	0
84	0	204	0	324	0	444	0	564	0
86	0	206	0	326	0	446	0	566	0
88	0	208	0	328	0	448	0	568	0
90	0	210	0	330	0	450	0	570	0
92	0	212	0	332	0	452	0	572	0
94	0	214	0	334	0	454	0	574	0
96	0	216	0	336	0	456	0	576	0
98	0	218	0	338	0	458	0	578	0
100	0	220	0	340	0	460	0	580	0
102	0	222	0	342	0	462	0	582	0
104	0	224	0	344	0	464	0	584	0
106	0	226	0	346	0	466	0	586	0
108	0	228	0	348	0	468	0	588	0
110	0	230	0	350	0	470	0	590	0
112	0	232	0	352	0	472	0	592	0
114	0	234	0	354	0	474	0	594	0
116	0	236	0	356	0	476	0	596	0
118	0	238	0	358	0	478	0	598	0
120	0	240	0	360	0	480	0	600	0
122	0	242	0	362	0	482	0		
124	0	244	0	364	0	484	0		

S=Size (micro m); N=Particle Number Density (1/ml)

M14T84

S	N	S	N	S	N	S	N	S	N
6	157136	126	0	246	0	366	0	486	0
8	153261.7	128	0	248	2.912241	368	0	488	0
10	72831.38	130	41.61882	250	3.027047	370	0	490	0
12	34717.83	132	40.68322	252	0	372	0	492	0
14	20961.68	134	39.74762	254	0	374	0	494	0
16	2643.245	136	0	256	0	376	0	496	0
18	1227.576	138	0	258	0	378	0	498	0
20	2347.798	140	0	260	1.387163	380	0	500	0
22	270.626	142	36.00526	262	4.401156	382	0	502	0
24	2152.794	144	34.82554	264	0	384	0	504	0
26	3307.778	146	0.237636	266	0	386	0	506	0
28	1801.357	148	0	268	0	388	0	508	0
30	282.6003	150	0	270	0	390	0	510	0
32	381.4773	152	0	272	0	392	0	512	0
34	730.7787	154	0	274	0	394	0	514	0
36	781.9074	156	0	276	0	396	0	516	0
38	548.3736	158	28.52051	278	0	398	0	518	0
40	972.118	160	0	280	0	400	0	520	0
42	496.3175	162	0	282	3.39729	402	0	522	0
44	437.7517	164	0	284	2.134481	404	0	524	0
46	539.775	166	0	286	0	406	0	526	0
48	119.1714	168	0	288	0	408	0	528	0
50	461.6703	170	0	290	0	410	0	530	0
52	196.0094	172	16.30357	292	0	412	0	532	0
54	193.7986	174	5.541687	294	0	414	0	534	0
56	88.93005	176	0	296	0	416	0	536	0
58	82.29534	178	20.50487	298	0	418	0	538	0
60	334.2331	180	0	300	0	420	0	540	0
62	330.8329	182	0	302	0	422	0	542	0
64	144.9868	184	0	304	0	424	0	544	0
66	143.1156	186	18.54954	306	0	426	0	546	0
68	70.62222	188	0	308	0	428	0	548	0
70	139.3732	190	0	310	0	430	0	550	0
72	0	192	0	312	0	432	0	552	0
74	0	194	0	314	0	434	0	554	0
76	0	196	0	316	0	436	0	556	0
78	65.94423	198	0	318	0	438	0	558	0
80	65.00866	200	0	320	0	440	0	560	0
82	64.07305	202	0	322	0	442	0	562	0
84	0	204	0	324	5.006914	444	0	564	0
86	23.0696	206	0	326	4.964665	446	0	566	0
88	38.54366	208	0	328	0	448	0	568	0
90	97.77586	210	12.68359	330	0	450	0	570	0
92	81.9257	212	0	332	0	452	0	572	0
94	58.45946	214	0	334	0	454	0	574	0
96	57.52391	216	0	336	0	456	0	576	0
98	0	218	10.72826	338	0	458	0	578	0
100	0	220	0	340	0	460	0	580	0
102	0	222	0	342	4.626662	462	2.047397	582	0
104	0	224	0	344	0	464	0.337912	584	0
106	52.84593	226	0	346	0	466	0	586	0
108	0	228	0	348	0	468	0	588	0
110	0	230	0	350	0	470	0	590	0
112	50.03917	232	7.30643	352	0	472	0	592	0
114	0	234	4.19161	354	0	474	0	594	0
116	0	236	2.437706	356	0	476	0	596	0
118	47.23236	238	6.072311	358	0	478	0	598	0
120	0	240	0	360	0	480	0	600	0
122	45.36118	242	0.689938	362	0	482	0		
124	0	244	5.312678	364	0	484	0		

S=Size (micro m); N=Particle Number Density (1/mL)

M14T100

S	N	S	N	S	N	S	N	S	N
6	222562.6	126	56.17208	246	0	366	0	486	1.581878
8	216999.8	128	0	248	0	368	0	488	0
10	108866.6	130	5.072562	250	0	370	0	490	0
12	58511.17	132	36.87194	252	6.069737	372	0	492	0
14	22678.94	134	40.8685	254	0	374	0	494	0
16	8291.034	136	0	256	0	376	0	496	0
18	6316.269	138	0	258	0	378	0	498	0
20	2414.005	140	0	260	0	380	0	500	0
22	1766.363	142	0	262	0	382	0	502	0
24	2213.502	144	0	264	0	384	0	504	0
26	1731.774	146	0	266	0	386	0	506	0
28	818.2869	148	0	268	5.871194	388	0	508	0
30	1029.007	150	12.2017	270	0	390	0	510	0
32	761.4132	152	36.23475	272	0	392	0	512	0
34	1303.815	154	47.09961	274	0	394	0	514	0
36	1036.232	156	30.28678	276	0	396	0	516	0
38	625.752	158	58.64959	278	0	398	0	518	0
40	710.5463	160	28.14913	280	0	400	0	520	0
42	565.3346	162	0.206404	282	0	402	0	522	0
44	881.2989	164	0	284	0	404	0	524	1.422444
46	962.59	166	0	286	5.647733	406	0	526	0
48	292.4319	168	24.51487	288	0	408	0	528	0
50	230.1573	170	0	290	0	410	0	530	0
52	107.3553	172	0	292	0	412	0	532	0
54	435.6433	174	19.14982	294	2.012275	414	0	534	0
56	333.3951	176	24.28241	296	9.043943	416	0	536	0
58	0	178	21.25397	298	3.368161	418	0	538	0
60	420.1201	180	4.975356	300	2.121007	420	0	540	0
62	113.6633	182	35.30191	302	0	422	0	542	0
64	149.0754	184	0	304	0	424	0	544	0
66	147.1514	186	0	306	0	426	0	546	0
68	145.2275	188	13.76899	308	0	428	0	548	0
70	71.65179	190	20.32456	310	0	430	0	550	0.988449
72	105.7975	192	2.346799	312	0	432	0	552	0
74	104.8257	194	0	314	0	434	2.924705	554	0
76	68.76586	196	3.993835	316	0	436	0.672513	556	0
78	0	198	12.18438	318	0	438	2.193162	558	0
80	267.1141	200	0	320	0	440	0	560	0
82	66.12965	202	15.05172	322	0	442	0	562	0
84	31.93856	204	0	324	0	444	0	564	0
86	288.3145	206	0	326	0	446	0	566	0
88	62.99401	208	0	328	0	448	0	568	0
90	124.064	210	1.50859	330	0	450	0	570	0
92	61.07	212	14.10504	332	0	452	0	572	0
94	52.32096	214	9.140083	334	0	454	0	574	0
96	244.2468	216	11.53339	336	4.819852	456	2.557467	576	0
98	6.995492	218	0	338	0.066958	458	0	578	0
100	64.36867	220	0	340	0	460	0	580	0
102	42.46957	222	10.0256	342	0	462	0	582	0
104	55.29814	224	0	344	0	464	2.379312	584	0
106	33.67734	226	0	346	0	466	0.043973	586	0
108	73.66733	228	0	348	0	468	0	588	0
110	52.41221	230	0	350	4.583335	470	0	590	0
112	0	232	0	352	0	472	0	592	0
114	100.9766	234	0	354	0	474	0	594	0
116	49.52628	236	0	356	0	476	0	596	0
118	48.56431	238	5.398625	358	0	478	0	598	0
120	0	240	0.841541	360	0	480	0	600	0
122	0	242	6.903284	362	0	482	0		
124	79.65472	244	5.462516	364	0	484	0.482565		

S=Size (micro m); N=Particle Number Density (1/mL)

M14T112

S	N	S	N	S	N	S	N	S	N
6	261992.1	126	45.67378	246	12.55161	366	0	486	0
8	270575.4	128	89.09688	248	0	368	0	488	0
10	125042.1	130	43.98796	250	6.225116	370	0	490	0
12	68512.67	132	20.80483	252	0	372	0	492	0
14	33433.1	134	63.16067	254	0	374	0	494	0
16	9489.971	136	0	256	6.149	376	0	496	0
18	5547.502	138	0	258	0	378	0	498	0
20	5042.632	140	0	260	1.456821	380	4.015875	500	0
22	3324.15	142	0	262	4.622135	382	0	502	0
24	2573.54	144	36.83066	264	0	384	0	504	1.79392
26	1707.917	146	75.92499	266	0	386	0	506	0
28	1316.747	148	30.75252	268	0	388	1.798779	508	0
30	1294.752	150	58.80882	270	0	390	5.810038	510	0
32	1178.627	152	57.80934	272	5.877572	392	0	512	0
34	1331.73	154	16.19022	274	0.068343	394	0	514	1.623387
36	1489.755	156	0	276	0	396	0	516	0
38	1194.708	158	29.95266	278	0	398	0	518	0
40	1844.504	160	28.97002	280	0	400	0	520	0
42	727.6328	162	55.97495	282	0	402	0	522	0
44	758.959	164	27.00492	284	0	404	0	524	0
46	583.2391	166	45.13588	286	0	406	0	526	0
48	1050.729	168	44.01187	288	0	408	0	528	0
50	749.0431	170	12.2167	290	0	410	0	530	0
52	781.5143	172	0	292	0	412	0	532	0
54	534.248	174	67.68377	294	0	414	0	534	0
56	540.0116	176	22.04787	296	0	416	0	536	0
58	559.1386	178	0	298	0	418	0	538	0
60	351.0162	180	0	300	0	420	0	540	0
62	337.5876	182	0	302	0	422	0	542	0
64	542.0001	184	0	304	0	424	1.525326	544	0
66	226.1114	186	0	306	0	426	1.614884	546	0
68	333.2923	188	18.96758	308	0	428	0	548	0
70	329.7957	190	18.4542	310	0	430	0	550	1.009596
72	252.4692	192	0	312	0	432	0	552	0
74	178.2907	194	17.42752	314	0	434	0	554	0
76	263.142	196	0	316	0	436	0	556	0
78	225.328	198	0	318	0	438	0	558	0
80	204.819	200	0	320	0	440	0	560	0
82	218.169	202	0	322	0	442	0	562	0
84	165.4894	204	0	324	0	444	0	564	0
86	278.418	206	12.42213	326	1.885017	446	0	566	0
88	192.4843	208	1.85619	328	3.300622	448	2.748615	568	0
90	103.2211	210	0	330	0	450	0	570	0
92	23.66195	212	0	332	0	452	0	572	0
94	168.2772	214	0	334	0	454	0	574	0
96	76.0655	216	0	336	0	456	0	576	0
98	0	218	11.26694	338	0	458	2.578163	578	0
100	58.44727	220	10.75356	340	0	460	0	580	0
102	78.72737	222	10.24018	342	0	462	0	582	0
104	92.06508	224	19.45368	344	0	464	0	584	0
106	110.9991	226	0	346	0	466	2.44172	586	0
108	0	228	10.78838	348	0	468	2.40763	588	0
110	53.53436	230	6.221634	350	0	470	0.845865	590	0
112	52.55181	232	15.34671	352	0	472	1.50573	592	0
114	6.155313	234	4.402043	354	0	474	0	594	0
116	145.722	236	9.206697	356	0	476	0	596	0
118	49.60407	238	0	358	0	478	0	598	0
120	169.8852	240	6.351842	360	0	480	0	600	0
122	167.0206	242	0	362	0	482	0		
124	0	244	0	364	0	484	0		

S=Size (micro m); N=Particle Number Density (1/mL)

APPENDIX-E

Error Analysis

Error Analysis

Error analysis was done on K^* in order to estimate the error in K^* due to the error in approximating the experimental data, μ_2 , as a function of time.

$$R_y(t) = \pi K^* \mu_2 (f - f_{eq}) \quad \text{E-1}$$

$$K^* = \frac{R_y(t)}{\pi (f - f_{eq}) \mu_2} \quad \text{E-2}$$

Assuming negligible errors in the terms $R_y(t)$ and $(f - f_{eq})$ we can substitute

$$G = \frac{R_y(t)}{\pi (f - f_{eq})} = \text{Const.} \quad \text{E-3}$$

Therefore,

$$K^* = \frac{G}{\mu_2} = \frac{G^1}{\mu_2^1} \quad \text{E-4}$$

For a function

$$x = \frac{a^k}{c^m} \quad \text{E-5}$$

The relative error in “x” is given by the equation

$$\left(\frac{W_x}{x_0}\right)^2 = \left(\frac{kW_a}{a_0}\right)^2 + \left(\frac{mW_c}{c_0}\right)^2 \quad \text{E-6}$$

where, $\pm W = \pm 2\sigma$ (σ = Standard Deviation) and x_0 , a_0 and c_0 are average values of x , a and c .

Therefore, relative error in K^* from Equation E-4 is

$$\left(\frac{W_{K^*}}{K_0^*}\right)^2 = \left(\frac{1.W_G}{G_0}\right)^2 + \left(\frac{-1.W_{\mu_{20}}}{\mu_{20}}\right)^2 \quad \text{E-7}$$

Since the error in G is assumed to be negligible, we have

$$\left(\frac{W_{K^*}}{K_0^*}\right)^2 = \left(\frac{W_{\mu_{20}}}{\mu_{20}}\right)^2 \quad \text{E-8}$$

$$\frac{W_{K^*}}{K_0^*} = \frac{W_{\mu_{20}}}{\mu_{20}} \quad \text{E-9}$$

Therefore, the relative error in the estimation of K^* is approximately equal to the relative error in the measurement of μ_2 . It can be seen from Equation E-9 that the value of μ_{20} from the experimental data will influence W_{K^*} .

Sample Calculation

For ethane kinetic experiment E007, $K^*=0.21 \text{ mol/m}^2\cdot\text{s}\cdot\text{MPa}$ and standard deviation $\sigma=0.0711 \text{ cm}^2/\text{cm}^3$.

Taking $\mu_{20} = 0.38 \text{ cm}^2/\text{cm}^3$, the value of μ_2 approximately midway through the experiment and since units cancel out in relative errors, from Equation E-9 we have,

$$\frac{W_{K^*}}{0.21} = \frac{2.0 * 0.0711}{0.38}$$

$$W_{K^*} = 0.08 \text{ mol/m}^2\cdot\text{s}\cdot\text{MPa}$$

Therefore, $K^* = 0.21 \pm 0.08 \text{ mol/m}^2\cdot\text{s}\cdot\text{MPa}$ (95 % Confidence)

$$\text{At } -W_{K^*}, K^* = 0.13 \text{ mol/m}^2\cdot\text{s}\cdot\text{MPa}$$

$$\text{At } +W_{K^*}, K^* = 0.29 \text{ mol/m}^2\cdot\text{s}\cdot\text{MPa}$$